CHEMICAL REVIEWS

pubs.acs.org/CR

Review

Assembly and Applications of Macrocyclic-Confinement-Derived Supramolecular Organic Luminescent Emissions from Cucurbiturils

Haigen Nie, Zhen Wei, Xin-Long Ni,* and Yu Liu*

Cite This: https://doi.org/10.1021/acs.chemrev.1c01050

Read Online

ACCESS | Metrics & More | Article Recommendations

ABSTRACT: Cucurbit[*n*]urils (Q[*n*]s or CB[*n*]s), as a classical of artificial organic macrocyclic hosts, were found to have excellent advantages in the fabricating of tunable and smart organic luminescent materials in aqueous media and the solid state with high emitting efficiency under the rigid pumpkin-shaped structure-derived macrocyclic-confinement effect in recent years. This review aims to give a systematically up-to-date overview of the Q[*n*]-based supramolecular organic luminescent emissions from the confined spaces triggered host−guest complexes, including the assembly fashions and the mechanisms of the macrocycle-based luminescent complexes, as well as their applications. Finally, challenges and outlook are provided. Since this class of Q[*n*]-based supramolecular organic luminescent emissions, which have essentially derived from the cavity-dependent confinement effect and the resulting assembly fashions, emerged only a few years ago, we hope this review will provide valuable information for the further development of macrocycle-based light-emitting materials and other related research fields.

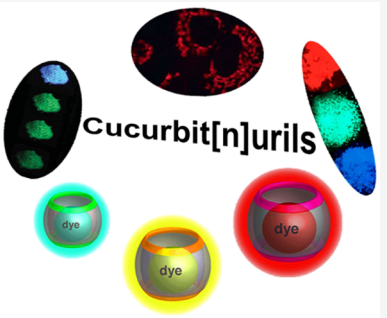

CONTENTS

Received: December 27, 2021

1. INTRODUCTION

Luminescent emissions, such as fluorescence and phosphorescence, play important roles in our daily colorful world. Inspired by nature, researchers began studying this phenomenon in the early 19th century.[1] Following rapid scientific and technological development, luminescent materials and, in particular, fluorescence-based techniques have been broadly applied in fields including biology,[2] medicine,[3] optoelectronics,[4] and mechanical engineering.[5] Indeed, the Nobel prizes for Chemistry in 2008 and 2014 were for the discovery of green fluorescent protein and super-resolved fluorescence microscopy, respectively. So, the design of highly efficient luminescence systems is an important issue for scientists.

In comparison with inorganic luminescent materials,[6−12] organic luminescent materials have attracted much attention because of their accurate molecular structures, variety, and tunable emissions with high quality via chemical modification.[12−26] It is believed that the development of highly efficient fluorophores relies on a high degree of electronic conjugation resulting from covalent bonding. Their preparation, however, often involves difficult and tedious organic synthesis with multiple steps and high cost. Notably, π-extended aromatic chromophores, which usually exhibit strong intra-/intermolecular $\pi-\pi$ stacking, suffer from aggregation-caused quenching (ACQ) of light emission in the condensed phase (Figure 1a).[27] The ACQ effect has long prevented many lead luminogens, identified by laboratory solution-screening, from finding real-world applications. In 2001, however, Tang et al. discovered a system in which luminogen aggregation played a constructive, rather than destructive, role in the light-emitting process: a series of silole derivatives were found to be nonluminescent in the solution state but strongly emissive in the aggregated state (Figure 1b).[28,29] The concept of aggregation-induced emission (AIE) was proposed for this novel phenomenon, which has provided an efficient approach for the construction of various advanced luminescent materials for use as sensors, as light-emitting diodes, and in environmental and biological systems during the last two decades.[30,31] As shown in Figure 1, ACQ is often self-quenching at high concentrations, and AIE is inhibited when aggregation is disrupted. Thus, there is a challenge to be overcome in constructing efficient luminogens with bright-light emission at both low and high concentrations.

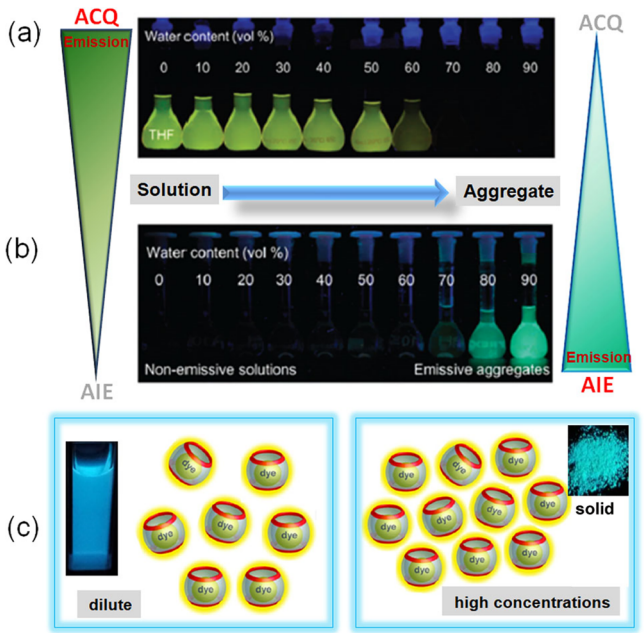

Figure 1. Fluorescence photographs: (a) ACQ emission of *N*,*N*-dicyclohexyl-1,7-dibromo-3,4,9,10-perylenetetracarboxylic diimide and (b) AIE phenomenon of hexaphenylsilole in THF−water mixtures with different water contents. Reproduced with permission from ref 31. Copyright 2014 Royal Society of Chemistry. (c) Q[*n*]-based supramolecular luminescent emissions: example from Q[7] complex with guest dye 4,4′-[(1E,1′E)-1,4-phenylenebis(ethene-2,1-diyl)]bis(1-carboxyethylpyridinium) (1:1) in dilute water (478 nm) and in solid (487 nm). Reproduced with permission from ref 57. Copyright 2018 American Chemical Society.

Cucurbit[*n*]urils (Q[*n*]s or CB[*n*]s, n = 5−8, 10, and 13−15)[32−36] are classical macrocyclic hosts formed by acid-catalyzed condensation of glycoluril and formaldehyde (Figure 2) with cavity size of 2.4−11.0 Å and a common depth (9.1 Å). Compared with other macrocycles, such as crown ethers, cryptands, cyclodextrins, calixarenes, and pillararenes,[37,38] Q[*n*]s distinguish themselves by their excellent ability to form inclusion complexes with various guest molecules, especially cationic guests, with high selectivity and high affinity in aqueous solution attributed to their rigid pumpkin-shaped structures[39−50] and the corresponding macrocyclic-confinement effect.[51,52] Notably, early host−guest studies on cucurbiturils have already revealed that the Q[*n*]-derived confined spaces generally result in profound changes of the physicochemical properties of the encapsulated dye guests such as absorption/emission wavelengths and quantum yields, which has been reviewed and discussed with other macrocycles by Nau and co-workers in 2011.[53] However, the size-dependent macrocyclic confinement[52,54] is commonly regarded as the hydrophobic effect in Q[*n*]-based supramolecular luminescent assemblies in aqueous solution and has received little attention so far.[55]

In 2016, Ni et al. discovered that a wide variation in the emission color of a single fluorophore guest from blue to cyan, white, yellow, or green could be achieved by a addition of different amounts of Q[8] hosts to the aqueous solution with a facile operation.[56] Furthermore, the dynamic properties of the noncovalent interactions led to switchable fluorescent emissions due to the reversibility of the host−guest inclusion. Importantly, the Q[8]-based host−guest complex exhibited long fluorescence lifetime and high quantum yield (QY) in both dilute and high concentrations of the complexes. This result indicated that the macrocycle triggered host−guest-induced emission,[56,57] or so-called supramolecular-assembly-induced luminescence,[58] could possibly be utilized as a new type of chromophoric dye in light-emitting materials.

From a structural viewpoint, the rigid-cavity-derived Q[*n*] units can be expected to advantageously prevent dye aggregation and ACQ at high concentrations, and even in the solid state, by providing a regular macrocyclic fence for each of the encapsulated fluorophore dye molecules via noncovalent interactions. Meanwhile, the inclusion of guest dyes inside the Q[*n*] confined cavity in aqueous solution not only suppresses quenching of the triplet state by oxygen or other quenchers but also restricts the molecular motions under the cavity-dependent confinement effect. All of these factors eventually lead to bright fluorescence of the Q[*n*]-dye complexes in both dilute and high concentration solution including in the solid state (Figure 1c).[56,57] For example, Park

https://doi.org/10.1021/acs.chemrev.1c01050
Chem. Rev. XXXX, XXX, XXX−XXX

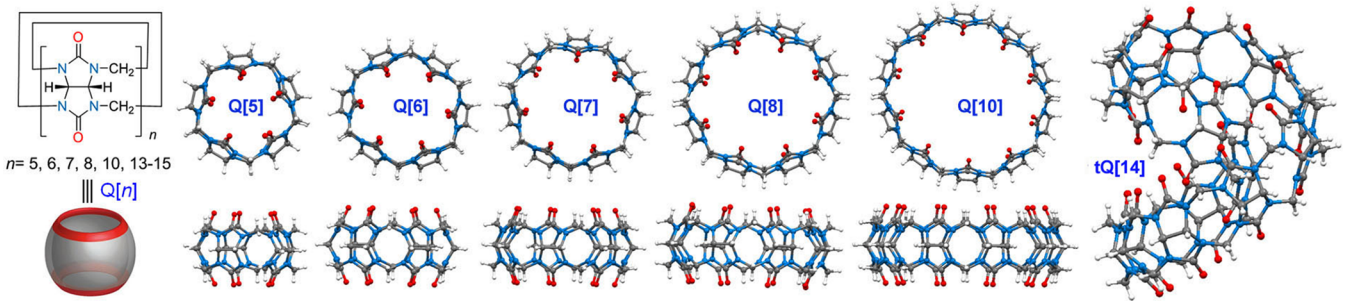

Figure 2. Chemical and X-ray crystal structures of Q[*n*]s.

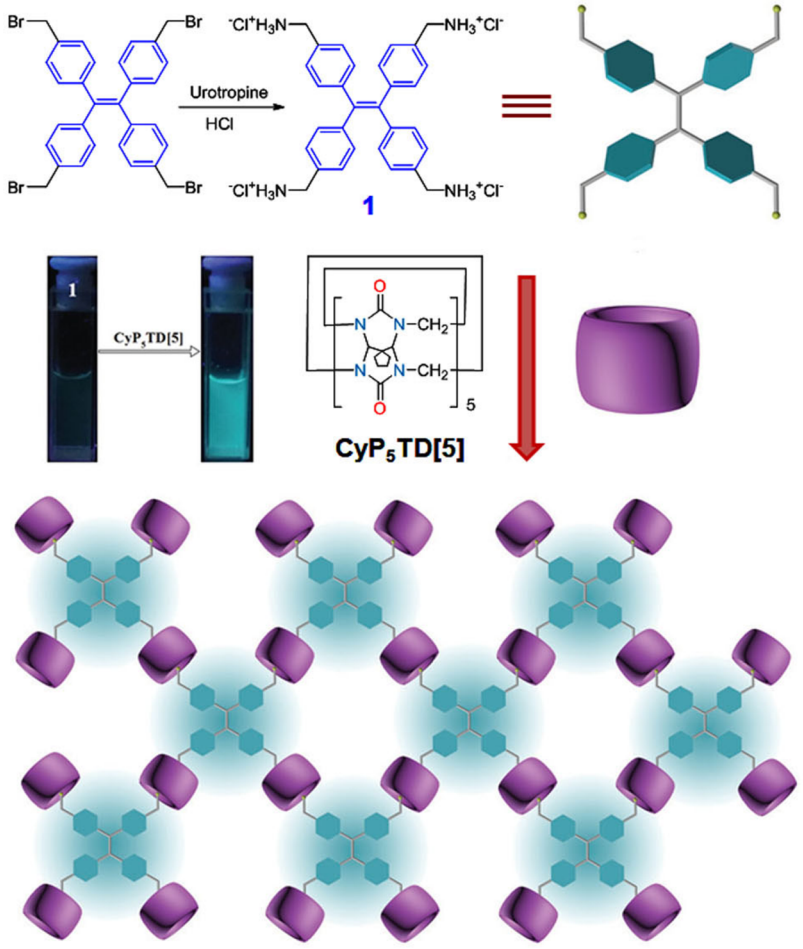

Figure 3. Structure of **1** and graphical representation for the supramolecular self-assembly of monomers in aqueous solution. Reproduced with permission from ref 66. Copyright 2018 Royal Society of Chemistry.

et al. recently reported that the QY of cyanostilbene derivatives in the Q[8] cavity can be dramatically enhanced up to 91% in aqueous media.[59]

More recently, it was found that macrocyclic Q[*n*] hosts can enhance intersystem crossing under the cavity-dependent confinement effect and consequently increase the yield of the triplet state, leading to increased phosphorescence, and some publications have revealed inspiring results. For instance, Liu et al. reported that the host−guest interaction of Q[6] with 4-(4-bromophenyl)-*N*-methylpyridinium exhibited strong room temperature phosphorescence (RTP) properties (QY was determined to be 81%) in the solid state.[60] At the same time, Ma and co-workers demonstrated an example of multicolor luminescence through combined fluorescence and RTP in both aqueous solution and the solid state, attributed to a 2:2 quaternary complex being formed between a Q[8] host and a triazine core-derived 4-(4-bromophenyl)pyridinium guest.[61]

Therefore, as evidenced by the reports presented above, the classical rigid macrocyclic Q[*n*] hosts have exhibited excellent properties for fabrication of tunable and smart organic luminescent materials in both solution and the solid state with high emission efficiency under the corresponding macrocyclic-confinement effect. In particular, because of their high selectivity for binding guests in water, they are exceptionally useful for constructing water-soluble luminescent systems, making them suitable for environmentally friendly applications in the materials field. Remarkably, the Q[*n*]-based multiple organic luminescent emissions are mainly derived

https://doi.org/10.1021/acs.chemrev.1c01050
Chem. Rev. XXXX, XXX, XXX−XXX

from the confined spaces triggered noncovalent interactions in the host−guest complexes, which greatly reduces synthesis costs compared to tuning emission performance by covalent modification of π-conjugated aromatic ring substituents. As yet, the topic of Q[n]-based luminescence has not been systematically reviewed;[62,63] in particular, little attention has been attracted to the role of the macrocyclic-confinement effect in these systems. Accordingly, this review aims to provide an up-to-date overview of noncovalent interactions and strategies used for the preparation of Q[n]-based luminescent materials in different host−guest assemblies, as well as their various applications over the past decade. Since this class of macrocyclic complex-based smart supramolecular organic luminescent materials, which have essentially derived from the cavity-dependent confinement effect and the resulting assembly fashions, emerged only a few years ago, we hope to cover all research developments in the field. Because the host−guest interaction of Q[n]s is mostly dependent on the cavity, thus, we start with a discussion of the smallest member, Q[5], and then review each of the larger homologues in turn. Selected examples are highlighted, especially the latest developments in this field. Finally, an outlook on future developments is given.

2. SUPRAMOLECULAR ORGANIC LUMINESCENT EMISSIONS FROM THE Q[5] HOST

Unsubstituted Q[5] and its substituted analogues are the smallest members of their respective homologous families. The smaller portal size of Q[5]s inhibits the entry of most organic molecules into the cavity, reducing the possible range of Q[5]-based inclusion complexes.[64,65] In the literature, one can find only two examples of supramolecular luminescent systems incorporating the Q[5] host. One is the fluorescence emission triggered by a Q[5] analogue, $CyP_5TD[5]$, through portal interaction triggered confinement of a fluorophore guest in a supramolecular polymer structure.[66] The other is RTP emission derived from the Q[5]-outer-surface-complex-induced confinement effect for naphthol derivatives in aqueous media.[67]

2.1. Fluorescent Emission from $CyP_5TD[5]$-Based Polymer

As shown in Figure 3, characterization including ^1H nuclear magnetic resonance (NMR) spectroscopy, isothermal titration calorimetry (ITC), transmission electron microscopy (TEM), and 2D DOSY ^1H NMR indicated that a supramolecular polymer was formed via the portal interaction between tetraphenylethylene (TPE) derivative **1** and $CyP_5TD[5]$ in pure water at room temperature.[66] Fluorescence spectra revealed a very weak fluorescence peak at 480 nm due to free **1**, the intensity of which was gradually enhanced upon addition of increasing concentrations of $CyP_5TD[5]$ to the solution. The QY increased from 0.27% to 16.2%, and the $CyP_5TD[5]$-induced change in fluorescence of **1** could be clearly observed by the naked eye. Essentially, the host-enhanced light emission can be attributed to the AIE phenomenon. The ion−dipole interaction between the ammonium group of **1** and the carbonyl groups on the $CyP_5TD[5]$ portal efficiently restricts intramolecular rotation of the TPE moiety (which can be defined as the portal interaction triggered confinement effect). Consequently, the supramolecular polymer exhibits much higher fluorescence than the monomer due to the AIE properties of TPE in dilute solution. In fact, TPE core-derived guests and the corresponding AIE properties have been fully exploited in the construction of various Q[8]-based supramolecular fluorescent systems under the cavity-dependent macrocyclic confinement, which will be discussed in detail in the Q[8] section.

2.2. Q[5]-Outer-Surface-Complex-Induced RTP Emission

Tao et al. found that Q[5]-outer-surface-complex-induced RTP of α-naphthol (**2**) and β-naphthol (**3**) via weak noncovalent interactions between the convex outer walls of Q[5] and the aromatic plane of naphthol combined with the affinity of Q[5] for metal ions.[67] X-ray crystallography showed that the naphthol luminophore was always arranged between two Q[5] molecules and the aromatic plane of the luminophore was roughly parallel to one of the five-membered rings of glycoluril in the adjacent Q[5]. This parallel orientation appears to reflect the presence of π−π stacking and C−H−π interactions. In addition, the authors proposed that hydrogen bonding between naphthol hydroxyl groups and portal carbonyls in Q[5] persisted in solution and thereby maintained a degree of aggregation between Q[5], naphthol, and the heavy atom (I^- or Tl^+). To confirm the formation of such aggregates by Q[5]-naphthol-heavy atom systems in the solution state, NMR diffusion experiments were performed. Furthermore, the increasing RTP intensity of the naphthol luminophore in the presence of increasing amounts of Q[5]-metal complex indicated that the luminophore is likely surrounded by a number of metal-bound Q[5] molecules, involving π−π stacking and C−H−π interactions as presented in Figure 4a. Such a sandwich arrangement not only would assist in protecting the luminophore from oxygen but also would confine the luminophore and the heavy atom to set positions in a luminophore-Q[5]-heavy atom exclusion complex (confinement effect like in MOFs),[52] which in turn gives rise to the observed RTP.

To verify the role of the convex outer wall of Q[5] in the Q[5]-induced RTP, two fully alkyl-substituted Q[5] hosts, pentacyclohexano-Q[5] ($CyH_5Q[5]$) and decamethyl-Q[5] ($Me_{10}Q[5]$), were used in additional RTP experiments. The authors proposed that if the convex outer walls of unsubstituted Q[5] contributed to the formation of a confinement environment containing the luminophore and heavy atom, the presence of alkyl substituents on the outer walls of Q[5] would be expected to seriously perturb the formation of such a microenvironment and inhibit π−π stacking and C−H−π interactions. Phosphorescence emission spectra indicated very low or completely quenched emission in the fully alkyl-substituted Q[5] systems (Figure 4b). Actually, this study not only fabricated a novel Q[5]-outer-surface-complex-induced RTP system but also provided new insight into the convex outer walls of cucurbiturils, leading to the proposal of the "outer-surface interactions" of Q[n]s concept[68] and its potential application in the field of energy research.[69]

3. SUPRAMOLECULAR ORGANIC LUMINESCENT EMISSIONS FROM THE Q[6] HOST

The first synthesized homologue in the Q[n] family, Q[6],[70] was fully investigated during early Q[n] chemistry by Mock,[71,72] Buschmann et al.,[73] and Kim et al.[74] However, the insolubility of Q[6] in organic solvents and its poor water solubility have seriously limited its applications. In particular, the portal diameter is only 3.9 Å, so Q[6] is only able to form stable inclusion complexes with aliphatic amines and small neutral heterocyclic molecules such as 1,4-dioxane and furan.

https://doi.org/10.1021/acs.chemrev.1c01050
Chem. Rev. XXXX, XXX, XXX−XXX

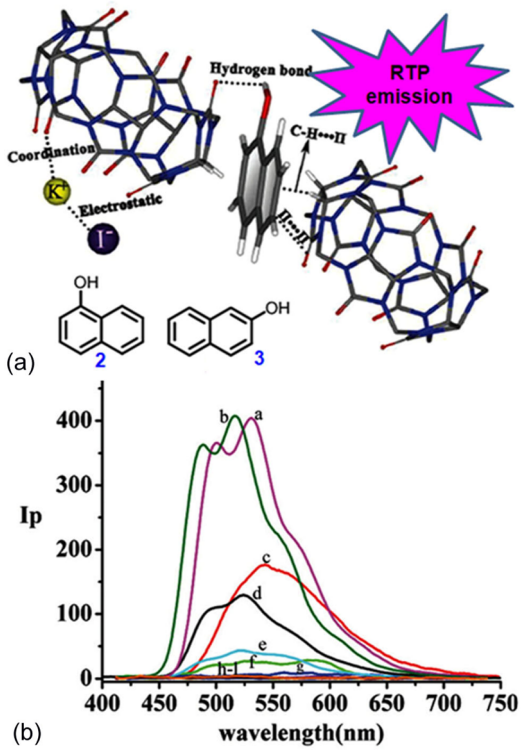

Figure 4. (a) Chemical structures of **2** and **3**, and the formation of $\pi\cdots\pi$ stacking and C−H$\cdots\pi$ interactions between naphthol and the outer surface of Q[5]. (b) RTP spectra of Q[5], Me_{10}Q[5], and CyH_5Q[5]: (a) **1**-Q[5]-$TINO_3$; (b) **2**-Q[5]-$TINO_3$; (c) **1**-Q[5]-KI-Na_2SO_3; (d) **2**-Q[5]−KI-Na_2SO_3; (e) **1**-Me_{10}Q[5]-KI-Na_2SO_3; (f) **2**-Me_{10}Q[5]-KI-Na_2SO_3; (g) **1**-CyH_5Q[5]-KI-Na_2SO_3; (h) **2**-CyH_5Q-[5]-KI-Na_2SO_3; (i) **1**-Me_{10}Q[5]-$TINO_3$; (j) **1**-CyH_5Q[5]-$TINO_3$; (k) **2**-Me_{10}Q[5]-$TINO_3$; and (l) **2**-CyH_5Q[5]-$TINO_3$. Reproduced with permission from ref 67. Copyright 2013 Royal Society of Chemistry.

Poor binding affinity is observed with aromatic guests (commonly in the range 10^2−10^3 M^{-1}).[39] Consequently, like the Q[5] homologue, the Q[6] host has mainly been used in the field of metal coordination chemistry in recent publications.[64] In fact, the rigid distinctive inner confined cavities and the resulting macrocyclic-confinement effect of Q[*n*]s enable potential applications for control and catalysis of chemical reactions with high efficiency. For example, the Q[6] host was first used to catalyze dipolar [3 + 2] cycloaddition between azides and acetylenes by Mock and co-workers in the early 1980s.[75] To some extent, this paved the way to a class of catalytic reactions that later became popular as in situ "click chemistry".[76,77] Meanwhile, fluorescent enhancement of dyes upon complexation with cucurbiturils was also first observed with the Q[6] host. For example, Wagner and Buschmann have shown that Q[6] enhances the fluorescence of guest dyes in solution and the solid state.[78,79] Kim et al.[80] and Tian et al.[81] used the Q[6] host as a molecular "bead" to construct a rotaxane-based molecular switch with fluorescent signals in response to pH and metal coordination. It is worth noting that Nau and co-workers have demonstrated that Q[6]-dye complex fluorescent signals can be exploited to monitor the enzymatic activity of lysine decarboxylase due to the macrocyclic-confinement-assisted pK_a shift,[82−84] which is selected as a representative example in this section.

3.1. Fluorescent Emission from Q[6]-Based Complexes

Fluorescent dye **4** was synthesized from 3-amino-9-ethyl-carbazole, which acts as the fluorescent signal moiety, and a diamino-alkyl moiety that acts as an anchor in the confined Q[6] cavity (Figure 5a).[82] A titration experiment indicated

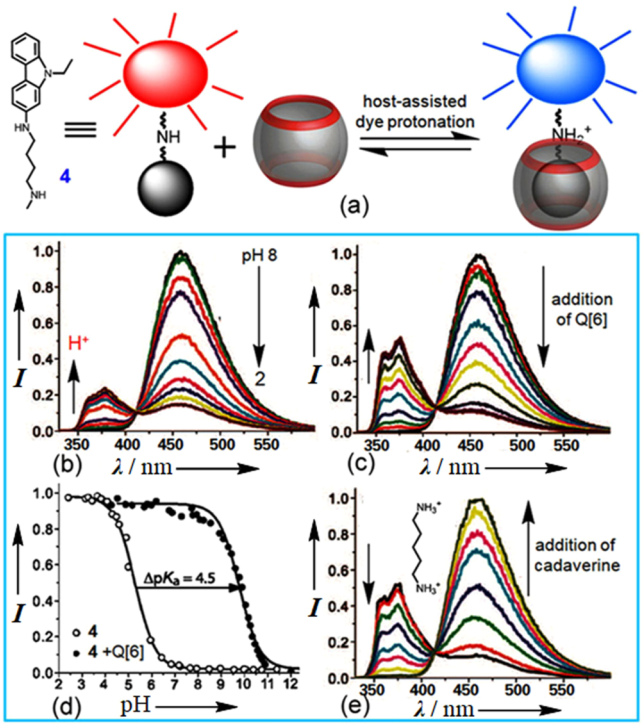

Figure 5. (a) Chemical structure of **4** and the proposed sensing mechanism of lysine decarboxylase, and fluorescence spectra of **4** (b) upon lowering the pH in water and (c) upon addition of increasing concentrations of Q[6] in NH_4OAc buffer, pH 7. (d) pK_a shift of **4** upon complexation with Q[6]. (e) Fluorescence titration for the competitive displacement of **4** from Q[6] by cadaverine in NH_4OAc buffer at pH 7. Reproduced with permission from ref 82. Copyright 2008 American Chemical Society.

that the fluorescence of **4** is pH-sensitive (Figure 5b). At pH ≥ 7, strong fluorescence emission with a maximum at 458 nm was observed due to the unprotonated form of **4**. At acidic pH (e.g., pH 3), the peak at 458 nm was strongly decreased and was accompanied by increased emission around 375 nm due to protonation of **4.** The pK_a of **4** was determined to be 5.3. Upon addition of increasing concentrations of Q[6] to the solution of **4** (pH 7), a similar change in fluorescence was observed (Figure 5c). This result suggested that the Q[6] host promoted protonation of **4** in neutral buffer solution, which can be attributed the cooperation of the confinement effect of the confined Q[6] cavity and the ion−dipole interactions of the Q[6] portals. The binding constant of Q[6] with **4** was determined to be $(2.22 \pm 0.16) \times 10^7$ M^{-1}. The corresponding pK_a of the host−guest complex was found to be 9.8, one of the largest supramolecular pK_a shifts in the literature (Figure 5d). The largest fluorescence response associated with the host-assisted pK_a shift of the dye is expected in the region between the pK_a values of the uncomplexed free dye (unprotonated form) and the complexed form (protonation occurs in the cavity of Q[6]), i.e., between pH 5.3 and 9.8. In other words, the host-assisted dye protonation can be fully survived in neutral aqueous solution. Interestingly, it was found that the

https://doi.org/10.1021/acs.chemrev.1c01050
Chem. Rev. XXXX, XXX, XXX−XXX

binding constant of Q[6] with 1,5-diaminopentane (cadaverine) in the same buffer solution was (9.5 ± 1.1) × 10^9 M^{-1}, much higher than the host–guest complex of Q[6] with dye **4**. Therefore, a novel fluorescent indicator displacement (FID) chemosensor was constructed by typical displacement titration of cadaverine with the solution of the Q[6]-**4** complex (Figure 5e). Most importantly, this displacement model is ideal for operation in the physiologically relevant neutral pH region (7 ± 2) to monitor the enzymatic decarboxylation of lysine to form cadaverine. Therefore, this study demonstrates an innovative use of Q[*n*]-derived host–guest chemistry and luminescent emission to fabricate an advanced stimuli-responsive biological probe. Undoubtedly, one of the key factors in this sensing system is the pK_a shift of the dye under the confinement effect of the Q[6] host. Indeed, supramolecular pK_a shifts induced by host–guest complexation are particularly attractive for chemists because this approach provides a simple but useful way to modify the acidity or basicity of the substrate in the confined space of artificial macrocycles.[85]

Motivated by the the FID sensing mechanism of Q[6]-**4**, Ni and co-workers developed Q[6]-assisted competitive recognition of lysine and methionine in aqueous solution with a distinct ratiometric fluorescent signal.[86] As shown in Figure 6,

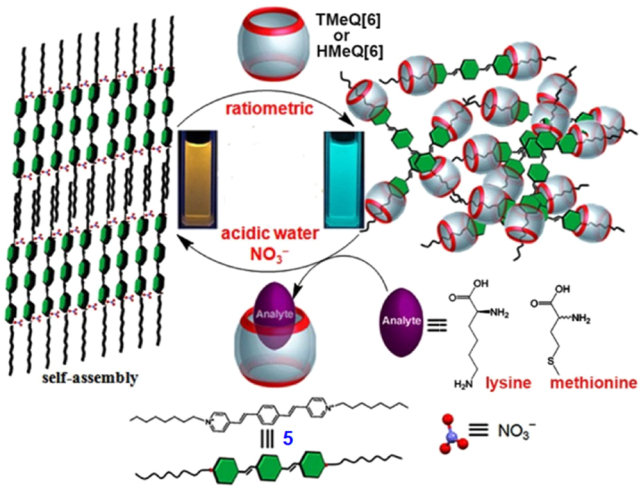

Figure 6. Illustration of the plausible FID process for lysine and methionine recognition in water based on the host–guest interactions of Q[6] analogues. Reproduced with permission from ref 86. Copyright 2017 Wiley-VCH.

two Q[6] analogues, tetramethylcucurbit[6]uril (TMeQ[6]) and hemimethyl-substituted cucurbit[6]uril (HMeQ[6]), both of which were previously found to exhibit better solubility in aqueous media than the parent Q[6], were exploited as hosts to construct FID chemosensors. In weak acidic aqueous solution, the cationic dye guest **5** self-assembled to nanoribbon-like aggregates in the presence of NO_3^- anions, which was accompanied by a significant ratiometric fluorescence signal from green (470 nm) to yellow (605 nm). The aggregates of **5**-NO_3^- could be disturbed by the TMeQ[6] or HMeQ[6] hosts through formation of stable host–guest inclusion complexes (TMeQ[6]-**5** or HMeQ[6]-**5**) with a reversible fluorescent emission from 605 to 485 nm. FID experiments suggested that TMeQ[6]-**5** was sensitive to both lysine and methionine, while HMeQ[6]-**5** appeared to interact only with lysine. This is attributed to the ellipsoidal cavity of TMeQ[6] and the resulting confinement effect being more suitable for inclusion of guests containing alkyl chain moieties than the rounder cavity present in HMeQ[6]. Indeed, the ellipsoidal cavity of TMeQ[6] also exhibited high binding affinity to aromatic molecules compared with unsubstituted Q[6].[49]

In 2015, Stoddart and co-workers reported a hetero[4]-rotaxane system (**6**) (Figure 7a),[87] which was isolated as an unexpected byproduct during synthesis of heterorotaxane **7** from Q[6], γ-cyclodextrin (γ-CD), and two fluorescent precursors (pyrene-based acetylene ammonium derivative **8** and diazaperopyrenium (DAPP), **9**). However, there was no complexation between **8** and γ-CD in aqueous solution (Figure 7b). Herein, the Q[6] host plays a crucial role in the construction of heterorotaxane **6**. Two Q[6] molecules are fixed at the periphery of DAPP due to ion–dipole interaction, which helps to outweigh the unfavorable energetics of threading γ-CD onto the dumbbell of the heterorotaxane by hydrogen bonding with the neighboring γ-CD and releasing high energy water molecules from its cavity. Furthermore, as part of a mechanically interlocked molecule, the confined cavity of Q[6] provides highly efficient catalysis of the dipolar [3 + 2] cycloaddition between **8** and **9** with the macrocyclic-confinement effect.

Heterorotaxane **7** is poorly soluble and undergoes aggregation in water, whereas heterorotaxane **6** exhibits significant water solubility. ^{1}H NMR spectroscopy reveals that **6** undergoes aggregation at room temperature and disaggregation to its monomeric form upon heating to 80 °C. The fluorescence emission of **6** can, therefore, be tuned and is reversible over a wide range (∼100 nm) of wavelengths as a result of stimuli-responsive aggregation and disaggregation processes (Figure 7c). Furthermore, hetero[4]rotaxane **6** underwent increased aggregation at high concentrations and in the solid state to form supramolecular polymers. Its narrow emission band at 510 nm, triggered by Förster resonance energy transfer (FRET) from pyrene to DAPP, attributed to hydrogen bonding between Q[6] and γ-CD, was gradually replaced by a broad, featureless band around 610 nm. This indicated that either DAPP homodimers (excimers) or pyrenyl-DAPP heterodimers (exciplexes) were being formed in the excited state. The process was reversed when the aggregated state was heated (Figure 7c). This study provides a new insight into construct tunable fluorescent materials for encryption by utilizing of the Q[6]-derived macrocyclic-confinement effect.

3.2. RTP Emission from Q[6] Host-Based Encapsulation

Pure organic RTP emission systems constitute an exciting class of materials because of their ultralong lifetimes, diverse molecular design, low cost, and lack of toxicity. However, it is well-known that purely organic molecules usually suffer from inefficient RTP, attributed to inherently feeble spin–orbit coupling and vulnerable triplet excitations. The key points to construct highly efficient RTP systems are to promote intersystem crossing to triplet excitations, minimize vibrational dissipation to restrict nonradiative relaxation, and isolate triplet excitons from triplet oxygen to prevent quenching. To date, much effort has been devoted to achieving efficient RTP by developing new methods, such as crystal engineering,[88−93] *H*-aggregation,[94−96] halogen bonding,[97−99] polymers,[100−106] and host–guest complexation.[107] Fortunately, the inclusion of organic dye guests inside the rigid confined cavities of Q[*n*]s

https://doi.org/10.1021/acs.chemrev.1c01050
Chem. Rev. XXXX, XXX, XXX−XXX

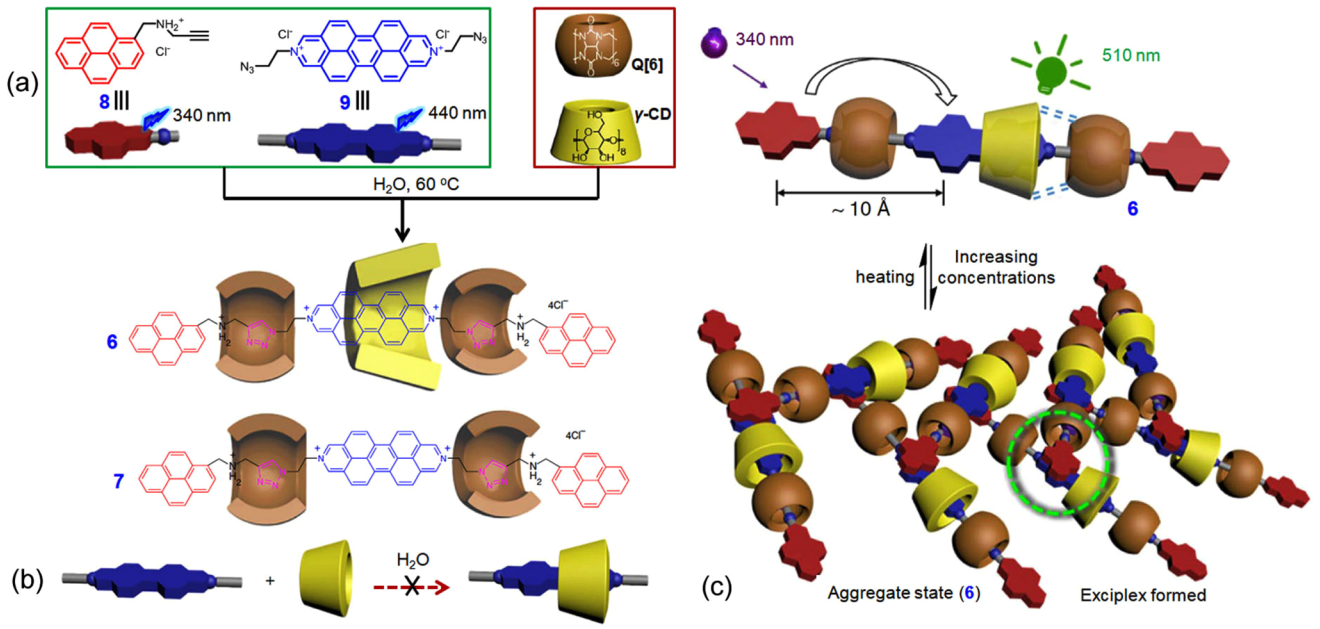

Figure 7. (a) Synthesis of heterorotaxanes **6** and **7** from stopper **8** and dumbbell precursor **9** and graphical representation of Q[6] and γ-CD. (b) No complexation was observed between **7** and γ-CD. (c) Graphical representation of the aggregation of **6** monomers in response to changes in concentration or temperature. Reproduced with permission from ref 87. Copyright 2015 Nature Publishing Group.

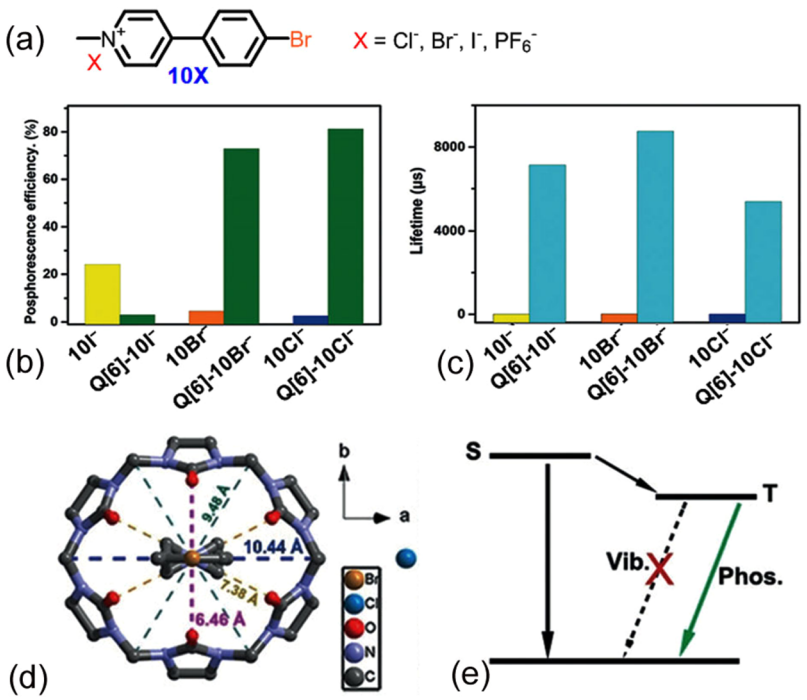

Figure 8. (a) Chemical structure of **10X**. (b) Phosphorescence quantum efficiencies of **10X** and Q[6]-**10X** complexes. (c) Lifetimes of **10X** and Q[6]-**10X** complexes. (d) Crystal structure of Q[6]-**10Cl**$^-$. (e) Mechanism of efficient phosphorescence emission of Q[6]-**10Cl**$^-$. Reproduced with permission from ref 60. Copyright 2019 Wiley-VCH.

generally suppresses quenching of the triplet state by oxygen or other quenchers and further restricts molecular motion due to the cavity-dependent confinement effect. All of these factors ultimately promote enhancement of intersystem crossing and efficiently increase the QY of RTP.

For example, Liu and co-workers demonstrated the modulation of solid-state RTP emission in a series of 4-(4-bromophenyl)-*N*-methylpyridinium salts with various counter-anions (**10X**, X = Cl^-, Br^-, I^-, and PF_6^-) in the presence of Q[6]. Remarkably increased QY was achieved (e.g., the QY of **10Cl**$^-$ increased from to 2.6% to 81.2%).[60] As shown in Figure 8, the salts of **10X** themselves exhibited RTP in their crystalline states, but poor quantum yields were observed for **10Cl**$^-$ (λ_{max} = 426 nm, QY = 2.6%), **10Br**$^-$ (λ_{max} = 470 nm, QY = 4.6%), and **10PF$_6$**$^-$ (λ_{max} = 510 nm, QY = 0.4%). In comparison, the iodide salt **10I**$^-$ had the best profile with yellow emission at 575 nm (Figure 8b), a lifetime of 5.61 μs, and QY of 24.1%. The high efficiency of RTP emission by **10I**$^-$ was attributed to

https://doi.org/10.1021/acs.chemrev.1c01050
Chem. Rev. XXXX, XXX, XXX−XXX

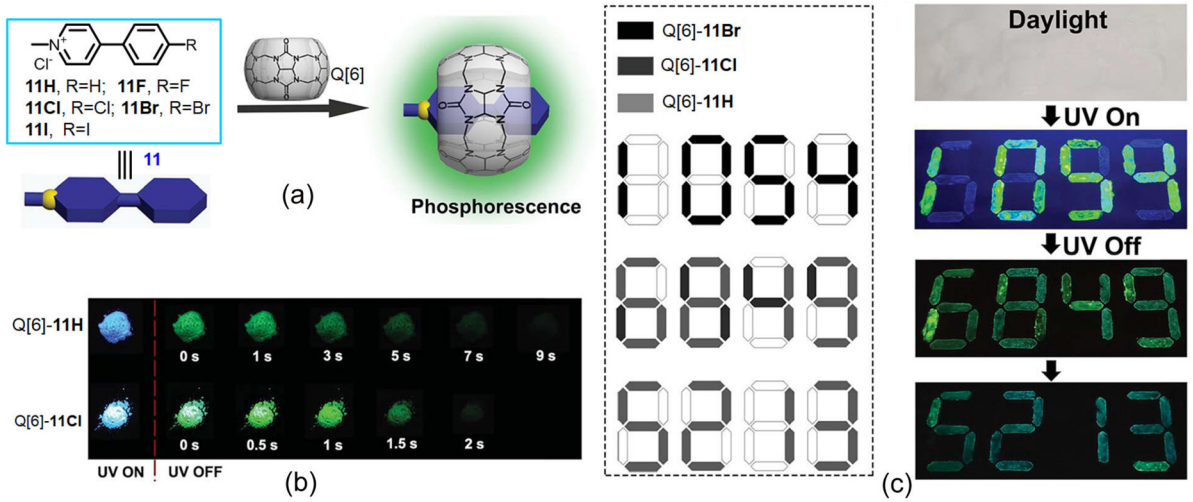

Figure 9. (a) Chemical structures of **11** derivatives and schematic representation of solid-state phosphorescence using Q[6]-based supramolecular complexes. (b) Luminescence photographs of Q[6]-**11H** and Q[6]-**11Cl** powder under 365 nm UV irradiation and at different time intervals after removal of the ultraviolet lamp. (c) Schematic illustration of lifetime encoding for security applications using Q[6]-based supramolecular complexes. Reproduced with permission from ref 108. Copyright 2019 Royal Society of Chemistry.

the formation of C−Br···I^- halogen bonds in the crystal lattice, promoting spin−orbit coupling.

Complexes were prepared by grinding the **10X** and Q[6] solids in a mortar in the presence of a small amount of deionized water, followed by drying in vacuum. ^{1}H NMR analysis and X-ray crystallography confirmed the formation of the inclusion host−guest complexes (Figure 8d). Notably, among the complexes, Q[6]-**10Cl**$^-$ was found to be the most promising. Its spectrum displayed two peaks at 388 and 500 nm having lifetimes of 3.62 ns and 5.40 ms, respectively. The green emission at 500 nm exhibited a 930-fold longer lifetime compared to uncomplexed **10Cl**$^-$ (Figure 8c), and there was a dramatic increase of QY (81.2%). Q[6]-**10Br**$^-$ also exhibited a high RTP QY of 72.9%, whereas the QY of Q[6]-**10I**$^-$ was only 3.0%.

Herein, the highly enhanced RTP emissions of Q[6]-**10Cl**$^-$ and Q[6]-**10Br**$^-$ can be attributed to the strong cavity-derived confinement effect, which not only suppresses vibrational relaxation by tight enclosure of the guest in the Q[6] host but also boosts intersystem crossing by the short distance between the inclusion guest and the carbonyl group of Q[6], resulting in greatly improved phosphorescent efficiency and lifetime of **10Cl**$^-$ and **10Br**$^-$. In contrast, the low QY of the RTP emission for Q[6]-**10I**$^-$ was ascribed to strong charge transfer between the parent pyridinium cation and I^- counterion.

Although appended heavy atoms are known to facilitate intersystem crossing of the parent organic molecules, a major shortcoming of this approach is the shorter lifetimes of the triplet states. In order to achieve a longer lifetime, the same research group described a modified method utilizing host−guest inclusion of Q[6] with similar phenyl-methyl-pyridinium guests (**11H**, **11F**, **11Cl**, and **11I**, Figure 9a)[108] with Cl^- as the counteranion. The compound **11H** in the solid state emitted only blue fluorescence (λ_{max} = 441 nm) with a lifetime of 2.25 ns. However, the Q[6]-**11H** solid-state complex emitted green phosphorescence (λ_{max} = 510 nm) (Figure 9b) with an ultralong lifetime of 2.62 s, together with fluorescence at λ_{max} = 427 nm. The phosphorescence QY was determined to be 9.7%, and the afterglow of the ultralong phosphorescence lasted more than 9 s after turning off the UV lamp (Figure 9b). The other complexes, Q[6]-**11F**, Q[6]-**11Cl**, and Q[6]-**11I**, also exhibited phosphorescence with variable lifetimes at 520 nm (τ = 0.0095 ms), 500 nm (τ = 275 ms), and 575 nm (τ = 1.40 ms), respectively. The diverse lifetimes of these complexes were further utilized for triple lifetime encoding for anticounterfeiting and information encryption (Figure 9c).

4. SUPRAMOLECULAR ORGANIC LUMINESCENT EMISSIONS FROM THE Q[7] HOST

Q[7] is the most attractive homologue in the Q[n] family because it exhibits sufficient water solubility (20−30 mM). It has a portal size of 5.4 Å, which is close to that of β-CD, and has attracted much attention in host−guest chemistry because of its ability to form 1:1 complexes with a variety of organic guest molecules in aqueous solution.[109] In contrast to other synthetic macrocycles, Q[7] commonly displays high binding affinities to its guests (such as aromatic derivatives) between 10^6 and 10^{17} M^{-1}, attributed to the confined rigid molecular space and the corresponding size matching effect. Consequently, Q[7] was widely used in early Q[n]-based supramolecular chemistry studies to explore the effects of cucurbituril encapsulation on the photophysical and photochemical properties of fluorophore guest molecules[62] and to evaluate potential applications in water-based dye laser systems,[110,111] supramolecular pK_a shift,[112,113] photostabilization,[114−117] and FID.[118,119] Subsequently, assisted emission of luminogens by strong host−guest interactions of the Q[7] host and its functionalized derivatives has been utilized for fluorescent markers and imaging, photodynamic therapy, and RTP emission in solution, among others, as detailed in the following sections.

4.1. Fluorescence Emission from Q[7]-Assisted Disaggregation of Dyes

Inspired by the ability of macrocyclic host molecules such as cyclodextrins to increase the solubility of poorly water-soluble molecules by forming inclusion complexes, numerous drug-related applications of Q[7] have been based on this desirable supramolecular approach in the development of Q[n] chemistry.[120,121] The effectiveness of Q[7] complexation to

https://doi.org/10.1021/acs.chemrev.1c01050
Chem. Rev. XXXX, XXX, XXX−XXX

control dye aggregation and the corresponding emission in water was demonstrated by Halterman and co-workers through study of the conversion of *H*-dimer to *J*-dimer emission of a tethered rhodamine B dyad in the presence of the Q[7] host.[122]

Kaifer et al. demonstrated the disruption of *H*- and *J*-aggregates of two cyanine dyes via Q[7] inclusion complexes.[123] As shown in Figure 10, cationic pinacyanol (**12**) and

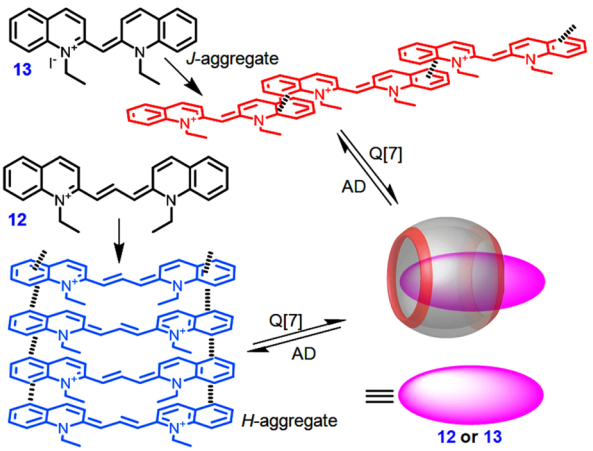

Figure 10. Schematic representation of Q[7]-assited disaggregation of dyes in water.

pseudoisocyanine (**13**) exhibit *H*- and *J*-aggregate emissions in water via ionic interactions at high concentrations. Upon addition of Q[7] to the solution, the *J*-aggregate of **12** and the *H*-aggregate of **13** undergo disaggregation attributed to encapsulation of the monomeric cyanine dyes in the cavity of Q[7]. Furthermore, aggregate emission can be controlled by introducing a strong competitive guest/Q[7] binder, such as adamantylamine (AD).

More recently, Banerjee and co-workers constructed a tunable fluorescence emissive system in aqueous solution and as a solid film by combining the host–guest complex of a Q[7]-derived disaggregate and the aggregate of an amphiphilic cyanostilbene derivative (**14**) (Figure 11).[124] Compound **14** underwent self-assembly in water, and the aggregate displayed a greenish-yellow excimer emission (λ_{em} = 539 nm). When Q[7] was added to the aggregated solution of **14**, the emission peak at 539 nm gradually diminished, accompanied by the appearance of a blue-shifted peak at 460 nm that was assigned to the formation of a monomer Q[7]-**14** complex (Figure 11b). Therefore, by simple variation of the Q[7] concentration (approximately 1.5 equiv), the emission color changed from yellow to blue including a near white light. Such luminescent color tuning could be reversed using adamantylamine as a competitive guest. In the solid film state, multiple emissions were obtained by drop casting aqueous solutions of Q[7]-**14** (Figure 11c). Essentially, the Q[7]-assisted disaggregation of dyes can be attributed to the strong confinement effect of the Q[7] cavity in aqueous solution, which leads to the high binding constant of the host–guest complexes.

Using the strategy of Q[7]-complex-assisted disaggregation of dyes, Zhang et al. developed a series of radical-generating supramolecular photosensitizers with enhanced antibacterial efficiency rather than simply focusing on the monomeric emission of dyes.[125−131] For example, a porphyrin derivative with four positive charges (**15**) was selected as the photosensitizer and used as the building block to construct a supramolecular photosensitizer with Q[7] (Figure 12) attributed to the high binding constant (6.6×10^7 M^{-1}) in aqueous solution.[125] The positively charged porphyrin favored adsorption of the photosensitizer onto the negatively charged bacterial surface via electrostatic attraction. Due to the strong host–guest interaction, the distance between porphyrins was greatly increased and an enhanced porphyrin monomer emission was observed. Therefore, a low porphyrin concentration and brief light irradiation resulted in improved antibacterial photodynamic therapy efficacy.

Later, the same group discovered that the radical yield and near-infrared (NIR) photothermal conversion were significantly improved by Q[7]-complex-induced disaggregation of dye.[128] As shown in Figure 13a, free bola-form amphiphile (**16**) with a perylene diimide core (PDI) as radical anions (**16a**) was obtained in lower yield upon chemical reduction ($Na_2S_2O_4$), attributed to radical anion reactivity and aggregation of PDI causing **16a** to dimerize and quench in aqueous solution. After encapsulating the two end groups of **16** in the Q[7] cavity to form a dumbbell-shaped supramolecular

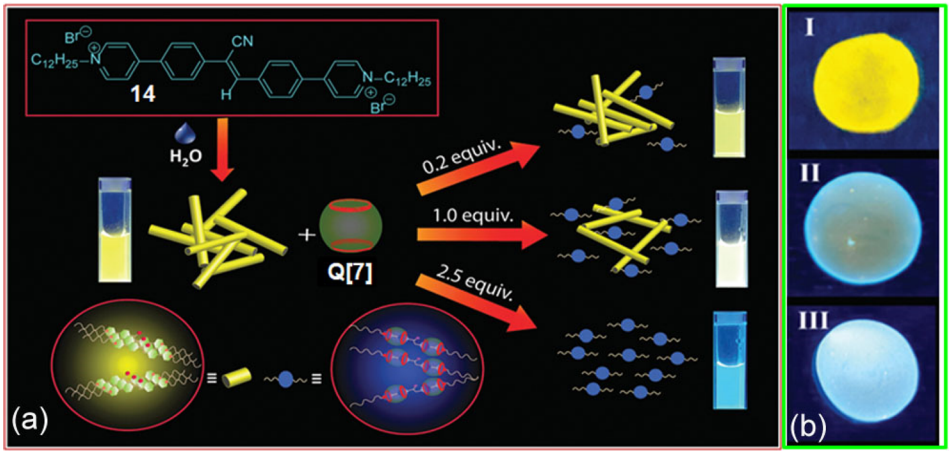

Figure 11. (a) Schematic representation of the generation of multicolor fluorescence from amphiphilic guest **14** and the Q[7] host. (b) Solid films of **14** (10 mM) and Q[7]: (I) without Q[7]; (II) with 20 equiv of Q[7]; and (III) with 40 of equiv Q[7]. Reproduced with permission from ref 124. Copyright 2020 Royal Society of Chemistry.

https://doi.org/10.1021/acs.chemrev.1c01050
Chem. Rev. XXXX, XXX, XXX−XXX

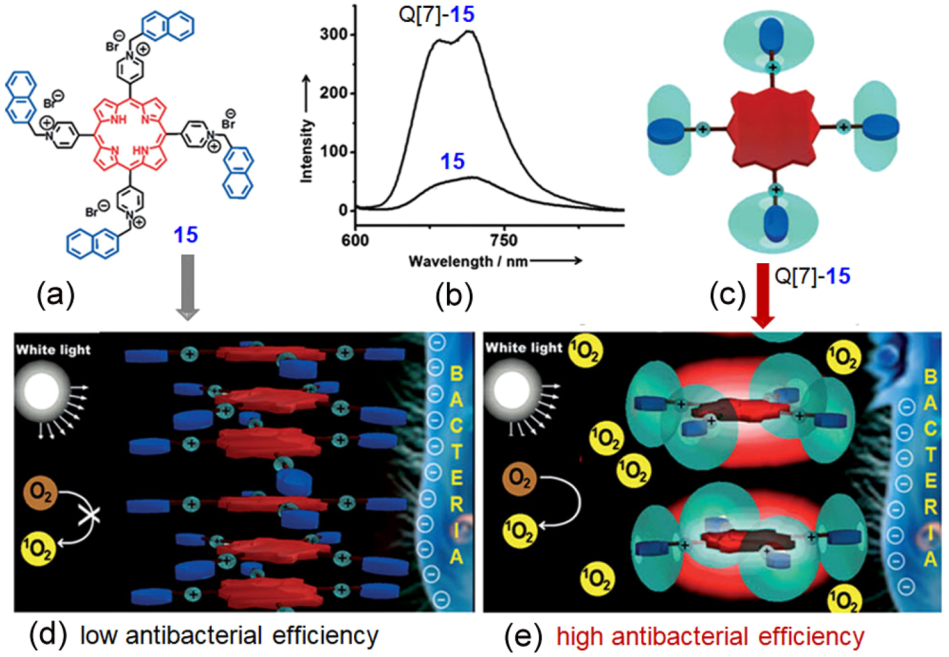

Figure 12. (a) Chemical structure of **15**. (b) Fluorescecnce spectra of **15** in the absence and presence of Q[7] in water. (c) Schematic representation of the Q[7]-**15** complex and the mechanism of the enhanced antibacterial efficiency of Q[7]-**15** (e) compared with that of **15** (d). Reproduced with permission from ref 125. Copyright 2013 Wiley-VCH.

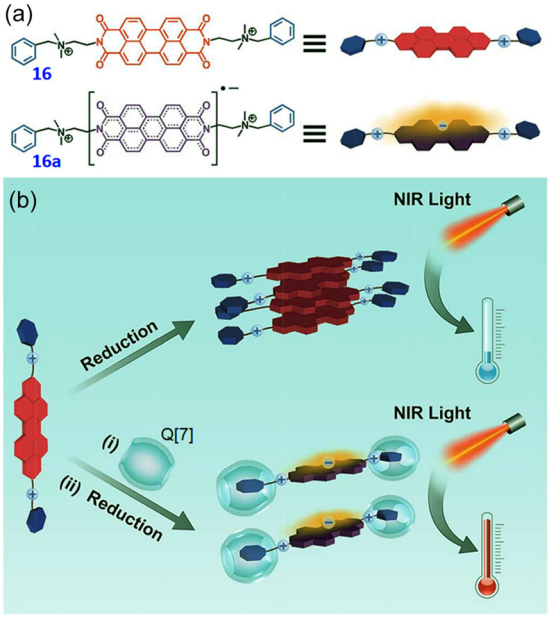

Figure 13. (a) Chemical structures of **16** and **16a**. (b) Radical anions (**16a**) generated by chemical reduction, leading to low NIR photothermal conversion efficiency (top); Q[7] stabilized **16a** via host–guest interactions, leading to improved NIR photothermal conversion efficiency (bottom). Reproduced with permission from ref 128. Copyright 2015 Royal Society of Chemistry.

complex with stable binding constant (2.9×10^{12} M^{-2}), the aggregation of PDI and the dimerization of **16a** in aqueous solution were hindered and suppressed (Figure 13b). As a result, efficient NIR photothermal conversion was easily achieved due to the increased concentration of **16a** and its absorption above 800 nm in water.

To demonstrate the applicability of Q[7]-complex-promoted supramolecular radicals, a new kind of bacterial-responsive supramolecular complex was further designed by the same group for photothermal therapy with high selectivity toward facultative anaerobic bacteria.[130] Perylene diimide derivative **17** (Figure 14a) has a similar molecular structure to that of **16**, and complexation by the Q[7] host formed the supramolecular complex **18** with expected high binding constant. It was found that facultative anaerobic bacteria such as *Escherichia coli* (*E. coli*) reductively converted **18** into radical anion **19** in situ and could, therefore, be used for photothermal therapy under NIR irradiation, leading to the death of *E. coli*. It was proposed that complex **18** was reduced by the hydrogenase on the surface of facultative anaerobic bacteria (Figure 14b). As a comparative study, aerobic bacteria such as *Bacillus subtilis* (*B. subtilis*) did not induce the formation of radical anion **19** in situ due to the weaker reductive ability. Herein, the macrocyclic-confinement effect of the Q[7] host plays a key role in the reduction process of the host–guest complex of **18** by narrowing in the energy gaps of guest **17** to match the reductive ability of *E. coli*.[127] Accordingly, the selective responses of supramolecular complex **18** to different bacteria could be employed to selectively and effectively inhibit bacteria by photothermal therapy. The results thus provide new insight into development of macrocycle-based supramolecular complexes and the corresponding macrocyclic confinement to regulate microbial balance.

4.2. Fluorescence Emission from Q[7]-Based Rotaxanes

The modest water solubility of Q[7] and the ideal size of its confined rigid cavity to accommodate most aromatic molecules to form 1:1 complexes with high affinity with the suitable macrocyclic-confinement effect have made the Q[7] host a popular macrocycle to construct various supramolecular rotaxanes. However, because of the intrinsic hydrophobic effect of organic chromophores in aqueous solution and the limitations of organic reaction in water, there is still much

https://doi.org/10.1021/acs.chemrev.1c01050
Chem. Rev. XXXX, XXX, XXX–XXX

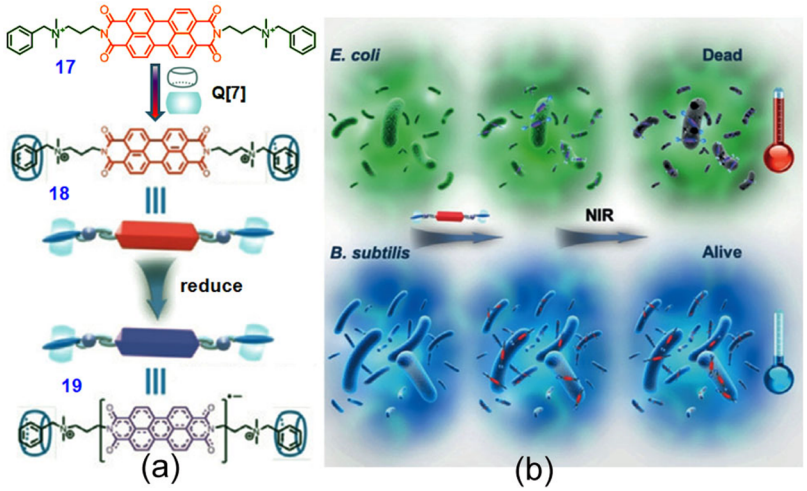

Figure 14. (a) Chemical structure of **17** and schematic representation of the supramolecular complex (**18**) and radical anions (**19**). (b) Diagram of photothermal therapy for **18** with high selectivity toward *E. coli* over *B. subtilis*. Reproduced with permission from ref 130. Copyright 2017 Wiley-VCH.

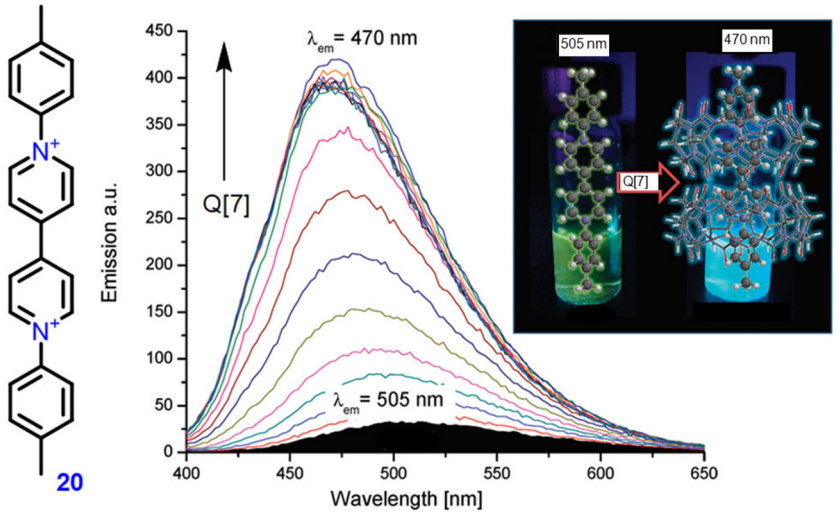

Figure 15. Chemical structure of **20** and fluorescence spectral changes of **20** in the presence of increasing concentrations of Q[7] in water. Reproduced with permission from ref 132. Copyright 2012 American Chemical Society.

room for improvement in the development of Q[7]-based fluorescent rotaxanes. In 2012, Galoppini et al. described fluorescence enhancement of di-*p*-tolyl viologen (**20**) by complexation in the Q[7] host.[132] Aqueous solutions of **20** exhibited weak fluorescence around 505 nm (QY = 0.01%, τ < 20 ps). Upon encapsulation by Q[7] to form the [3]-pseudorotaxane (Figure 15), **20** exhibited dramatically enhanced fluorescence (QY = 0.12%, τ = 0.7 ns) that was blue-shifted by 35 nm. Density functional theory and configuration interaction singles calculations indicated that hindrance of rotational relaxation of the S1 state of **20** caused by the macrocyclic-confinement effect of the Q[7] host is the key factor in that enhancement emission.

Akkaya and co-workers reported a Q[7]-BODIPY-based fluorescent [2]pseudorotaxane through autonomous shuttling driven by an oscillating reaction.[133] As shown in Figure 16, a water-soluble fluorophore axle guest (**21**) was synthesized from bipyridinium dication-substituted BODIPY with a terminal carboxylic acid, which contained two alternative stations for Q[7] with moderate binding constant (1.34×10^5 M^{-1}). Changing the pH from acidic to basic resulted in shuttling of Q[7] from one station to another, and this shuttling was accompanied by enhanced fluorescence of the BODIPY dye. A reverse shuttling motion and weak emission could be triggered by changing the pH from basic to acidic. As a result, this study constructed an autonomous shuttling of the Q[7]-based pseudorotaxane system in an oscillating pH system with distinct fluorescent signals. Notably, the higher emission intensity at neutral/alkaline pH can be attributed to Q[7] encapsulation of the bipyridinium dication with a strong macrocyclic-confinement effect, which may partially neutralize the positive charge on the bipyridinium. In other words, the Q[7] inclusion complex of bipyridinium efficiently inhibited the reverse photoinduced electron transfer (PET) between the BODIPY dye and bipyridinium moiety.

A very similar Q[7]-BODIPY-based fluorescent [2]-pseudorotaxane was fabricated by Halterman and co-workers (Figure 17).[134] In this work, the BODIPY fluorophore and bipyridinium were linked with a more flexible structure in guest **22**. In aqueous solution of free guest **22**, very weak

https://doi.org/10.1021/acs.chemrev.1c01050
Chem. Rev. XXXX, XXX, XXX−XXX

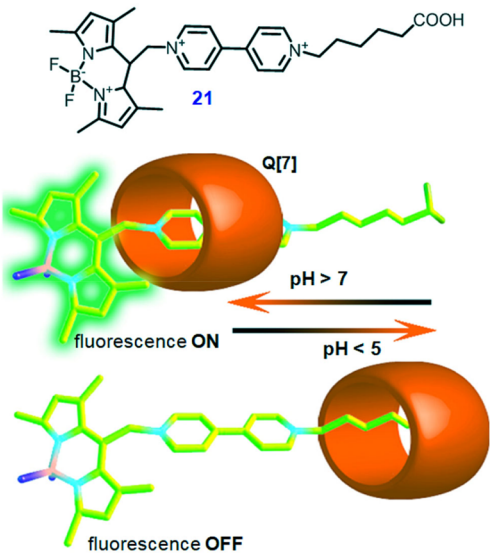

Figure 16. Chemical structure of **21** and graphical representation of the pH-dependent fluorescent pseudorotaxane of Q[7]-**21**. Reproduced with permission from ref 133. Copyright 2013 American Chemical Society.

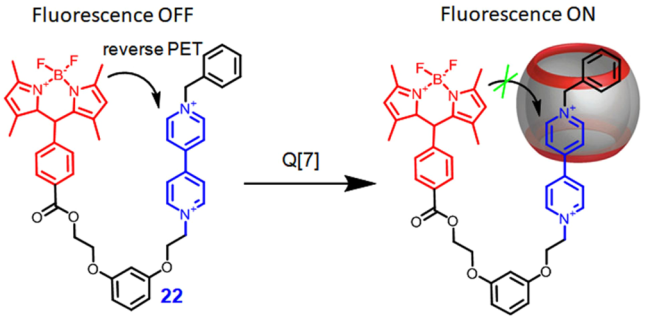

Figure 17. Mechanisms to Q[7] encapsulation disrupt fluorescence quenching.

fluorescence of BODIPY was observed, which was ascribed to electron transfer from the BODIPY fluorophore (electron donor) to the positively charged appended bipyridinium (electron acceptor) in the excited state (reverse PET). When the bipyridinium moiety was encapsulated by Q[7], the reverse PET process from BODIPY to bipyridinium was strongly inhibited as described in the case of **21**. As a result, when the bipyridinium moiety of guest **22** was encapsulated by the Q[7] host, the fluorescence emission of BODIPY was recovered.

Subsequently, Scherman, Nau, and co-workers fabricated an efficient host−guest energy transfer triggered emission in Q[7]-assisted polycationic cyclophane (ExBox)-perylene diimide (PDI) 3-polypseudorotaxane in water (Figure 18).[135] Derivatives of dicationic perylene diimides (PDI-**23**-**25**) underwent aggregation in water, and the aggregates were disturbed by addition of ExBox to the solution to form [2]pseudorotaxanes of ExBox-PDIs. In most cases, ExBox acts as a strong electron acceptor within the host−guest complexes (E_{red} ca. −0.72 eV), and remarkable charge transfer bands are generally observed in their visible absorption spectra. However, the PDI guests (**23**−**25**) in this work also acted as electron-deficient (E_{red} ca. −0.70 eV) in the pseudorotaxane system. As a result, no charge transfer bands were observed in the UV/vis spectra during titrations of the PDI solutions with ExBox. Instead, enhanced fluorescence of the PDIs and increased fluorescence lifetime were observed in this work. Furthermore, the overlap around 450 nm between the emission of ExBox and the absorption of the PDI indicated that energy transfer from ExBox (as donor) to PDI (as acceptor) should outcompete PET in water. In other words, ExBox serves as an antenna to transfer photonic energy to the PDI dyes through FRET, which is efficient because of the small spatial separation of the two chromophores in the host−guest-based [2]pseudorotaxane. This hypothesis was unequivocally confirmed by much larger fluorescence enhancements for a particular PDI dye upon ExBox excitation at 319 nm (ca. 17−92-fold) than those observed upon direct excitation at 520 nm (ca. 2.1−12.6-fold).[135]

Interestingly, the hexacationic-based [2]pseudorotaxane complexes are capable of further complexation with Q[7] with high binding constant to form a 3-polypseudorotaxane via self-assembly in orthogonal fashion (Figure 18). The ExBox serves as the central ring, sliding onto the PDI core; then two Q[7] molecules act as terminal stoppers, binding to the two outer quaternary ammonium motifs of PDI. Fluorescence

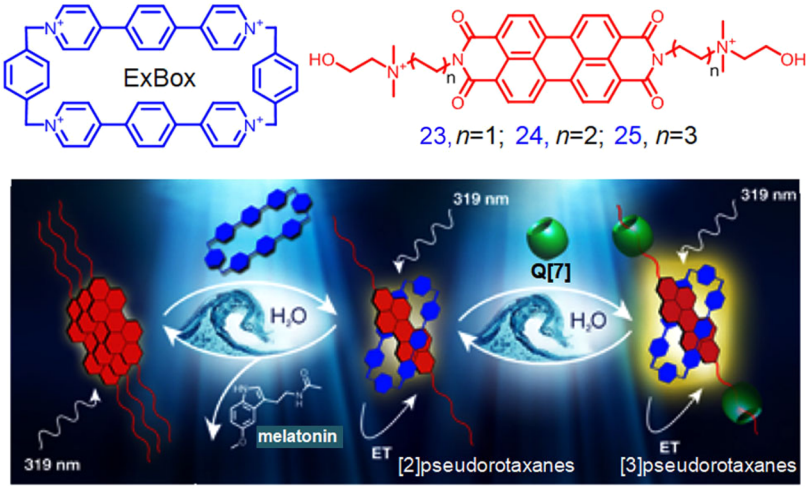

Figure 18. Chemical structures of ExBox and PDI derivatives (**23**−**25**) and the schematic representation of ExBox- and Q[7]-derived pseudorotaxane promoted energy transfer (ET) for PDIs. Reproduced with permission from ref 135. Copyright 2014 American Chemical Society.

https://doi.org/10.1021/acs.chemrev.1c01050
Chem. Rev. XXXX, XXX, XXX−XXX

titrations of Q[7] into ExBox:PDI-**24** (1:1, 10 μM) and Q[7]:ExBox (2:1) into PDI-**24** (10 μM) gave average fluorescence enhancements of 30 ± 3 (λ_{ex} = 520 nm, direct excitation) and 250 ± 10 (λ_{ex} = 319 nm, indirect excitation) fold relative to bare PDI-**24**. Very small enhancements of monomeric PDI-**24** fluorescence (2.7-fold, λ_{ex} = 520 nm, and 2.6-fold, λ_{ex} = 319 nm) were observed in the presence of 2 equiv of Q[7]. This result suggested that the Q[7] complex enhanced the fluorescence of PDI-**24** by promoting the electron transfer efficiency of the ExBox chromophore to the PDI chromophore, rather than by inhibiting the reverse PET between the PDI fluorophore and the positively charged quaternary ammonium group. Overall, the large fluorescence enhancement of PDI-**24** is partly due to disaggregation complexation of both ExBox and Q[7] and partly due to Q[7]-complex-promoted efficient FRET from ExBox to the PDI fluorophore. In addition, 3-polypseudorotaxane has also been used as an FID chemosensor for selective recognition of the neurotransmitter melatonin in water. Evidently, this work provides an excellent example of the design of a macrocycle-based advanced rotaxane with superior photophysical properties.[135] In addition, the confinement effect of ExBox and the Q[7] host should be conducive to formation of polypseudorotaxane.

In 2015, Wang et al. reported a supramolecular antibiotic switch based on the Q[7] triggered polypseudorotaxane with poly(*p*-phenylenevinylene) (PPV) derivative **26** (Figure 19a).[136] A quaternary ammonium group side chain was appended to the PPV parent because the biocidal activity of PPV is dependent on penetration of the quaternary ammonium cationic groups into the cell membrane (*E. coli*). The Q[7] host formed a polypseudorotaxane with **26** by encapsulating the cationic quaternary ammonium moiety in the cavity through ion−dipole interaction and the corresponding macrocyclic confinement, which resulted in remarkably increased emission intensity of PPV combined with a blue-shift. This can be attributed to aggregation of the positively charged conjugated polymer **26** in water. Interactions between the quaternary ammonium groups increase the nonradiative energy consumption, and fluorescence intensity decreases due to self-quenching. Upon complexation with Q[7], the interactions between the quaternary ammonium groups are disturbed and nonradiative energy consumption is inhibited, leading to bright emission (Figure 19b). However, assembly of the Q[7]-**26** polypseudorotaxane reduces the biocidal activity of PPV because of inclusion of the quaternary ammonium groups, which decreased the penetration of PPV into the cell membrane and led to the inhibition of the antibacterial activity of **26** (switch off). Addition of adamantylamine (AD) induces disassembly of the Q[7]-**26** polypseudorotaxane to form a more stable Q[7]-AD complex accompanied by release of **26** through competitive replacement, which is conveniently monitored by the decreased fluorescence emission. Consequently, the antibacterial activity of **26** is recovered (switch on). Furthermore, it was found that the free cationic PPV **26** efficiently generates reactive oxygen species (ROS) upon light illumination to kill bacteria, while the Q[7]-**26** polypseudorotaxane produces less ROS because the PPV core is prevented by the Q[7] host from contacting the surrounding oxygen (Figure 19c). Accordingly, this study develops a new approach to monitor and switch antimicrobial activity using a Q[7]-based supramolecular rotaxane.

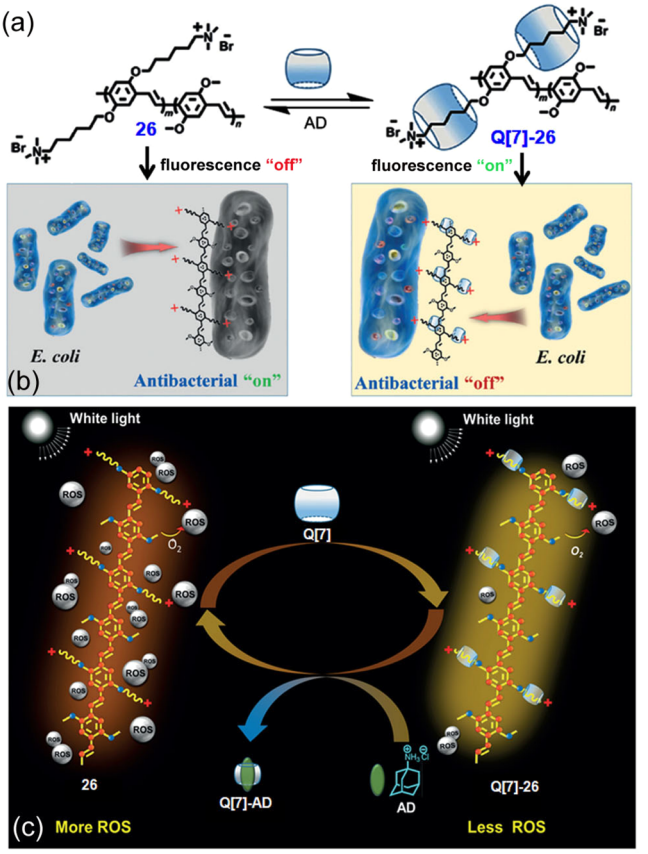

Figure 19. (a) Chemical structure of **26**. (b) Pseudorotaxane assembly of **26** with Q[7] and disassembly of **26** with Q[7] mediated by the adamantylamine (AD) molecule for reversible control of the fluorescence emission and antibacterial activity of **26**. (c) Pseudorotaxane assembly and disassembly of **26** with Q[7] for reversible control of the ROS generation of **26**. Reproduced with permission from ref 136. Copyright 2017 Wiley-VCH.

4.3. Fluorescent Markers and Imaging Using Q[7]-Assisted Emissions

Fluorescence sensing and imaging approaches based on various fluorophore emissions are particularly useful for monitoring environmental and biological substances in living systems because they are highly sensitive, exhibit good spatial resolution, are noninvasive, and can be employed in situ.[137] Inspired by the advantages of Q[*n*] confined cavity-assisted fluorescence emission for highly selective FID chemosensors of neutral and cationic molecules,[138] a series of pioneering works have been reported by Nau and co-workers.[139−144] For example, Nau, Urbach, and co-workers described a supramolecular tandem assay for continuous monitoring of protease activity on unlabeled peptides in real time by utilizing the host−guest complex of Q[7] with acridine orange (**27**) as the FID sensor.[143] The weak fluorescence of **27** in aqueous solution was strongly enhanced under the confinement effect Q[7] cavity (the binding constant of Q[7]-**27** was determined to be 2.9 × 10^5 M^{-1}). The experimental results indicated that this binding constant was in between the binding strengths of Q[7] with the substrate and the proteolytic products of some peptides. In the example provided in Figure 20, when thermolysin is added to the solution containing an enkephalin-based substrate and Q[7]-**27**, the enzymatic product, containing an *N*-terminal phenylalanine residue

https://doi.org/10.1021/acs.chemrev.1c01050
Chem. Rev. XXXX, XXX, XXX−XXX

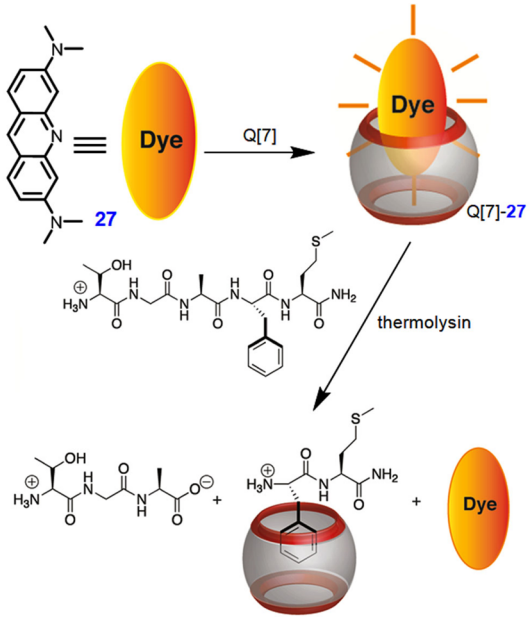

Figure 20. Product-selective fluorescence switch-off tandem assay using Q[7]-**27** as the FID sensor. Reproduced with permission from ref 143. Copyright 2011 American Chemical Society.

(having 3 orders of magnitude higher affinity for Q[7] compared to **27**), should rapidly and competitively displace **27** from the Q[7] cavity. This results in decreased fluorescence intensity that reports the protease activity continuously and in real time. Affinity is reduced for the simple amino acid, *N*-terminal phenylalanine, accompanied by restored fluorescence emission of Q[7]-**27**. The fluorescence changes of the Q[7]-**27** complex were further exploited as fluorescent markers to monitor the stepwise proteolytic degradation of an entire peptide by leucine amino peptidase.[144]

In 2013, a NIR cationic fluorescent dye **28** (Figure 21a) was synthesized by Peng and co-workers.[145] Fluorescence spectra indicated that the dye **28** exhibited emission at 682 nm with a large Stokes shift (224 nm) in water, which was attributed to the combination of intramolecular charge transfer (ICT) and internal conversion. Compound **28** displayed remarkably enhanced fluorescent responses to RNA compared with DNA. Essentially, the fluorescence enhancement can be ascribed to the restriction of the twist of benzothiazolium vinyl groups, which was caused by interactions between the cationic benzothiazolium unit and the anionic phosphate of the nucleic acid. The imaging properties of **28** in fixed cells suggested that it mainly stained RNA in nucleoli and cytoplasm, with little staining of DNA in the nucleus. However, the confocal laser scanning microscopy (CLSM) image indicated that **28** did not permeate into the live cell nucleus but aggregated at the cell membrane (Figure 21b). Interestingly, **28** can be delivered into live cell nuclei by the Q[7] host via formation of a 1:2 complex with further enhanced fluorescence emission, since Q[7] is taken up by the cell and cell nucleus through endocytosis. Herein, the increased fluorescence of **28** can be attributed to the macrocyclic-confinement effect of the Q[7] host, which restricts benzothiazolium group torsional motion through the host-inclusion interaction (Figure 21c). In cells, the higher binding affinity of RNA-**28** compared with that of the 2Q[7]-**28** complex means that RNA can bind with **28** on one of the benzothiazolium moieties; meanwhile, Q[7] can interact with the other benzothiazolium moiety to form the RNA-**28**-Q[7] ternary complex. Both interactions contribute to the strong fluorescence of **28**. Overall, these studies suggest the possibility of transporting cell-impermeant dyes into living cells as fluorescent markers and imaging by Q[7] through host–guest interaction.[145]

Utilizing the high binding ability of Q[7] with a cationic guest under the macrocyclic-confinement effect, Ni et al. recently demonstrated that novel vesicles of Q[7]-anchored polymers enhanced photosensitization of porphyrin derivative **29** in the cell nucleus.[146] As shown in Figure 22, the poly(acrylic acid) (PAA) chain spacer triggered Q[7] polymers on the surfaces of the vesicles at a regular distance, which not only inhibited aggregation-induced self-quenching of the porphyrin derivative **29** in aqueous solution but also fixed **29** at high concentration on the nanoscale as a supramolecular photosensitizer via host–guest interactions. The CLSM image indicated that **29** was highly penetrant, entering the nuclei of cancer cells, enabling its use as a fluorescent marker in nuclei.

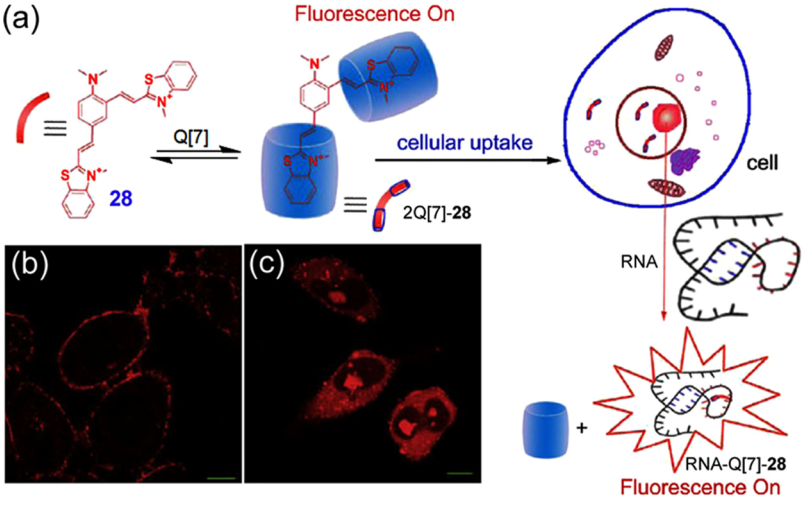

Figure 21. (a) Chemical structure of **28** and the probable staining mechanism of **28** in the presence of Q[7]. CLSM images of HeLa cells stained with **28** for 10 h in the absence (b) and presence of Q[7] (c). Reproduced with permission from ref 145. Copyright 2013 Elsevier Inc.

https://doi.org/10.1021/acs.chemrev.1c01050
Chem. Rev. XXXX, XXX, XXX−XXX

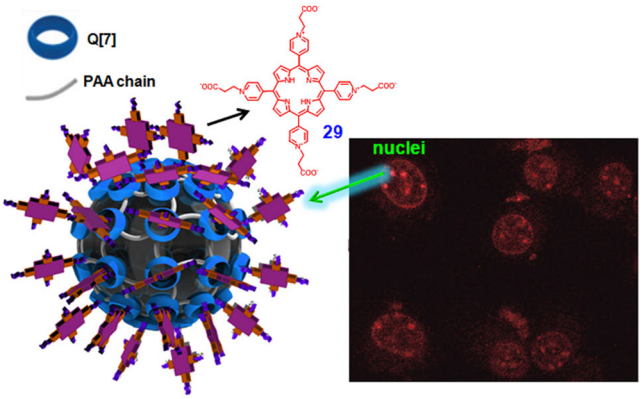

Figure 22. Schematic representation of Q[7]-**29** nanoparticles and CLSM images of Q[7]-**29** nanoparticles in SH-SY5Y cells. Reproduced with permission from ref 146. Copyright 2019 Royal Society of Chemistry.

The compound also exhibited efficient anticancer effects via highly enhanced photosensitization.

Urbach and co-workers reported another example of a Q[7] covalent conjugate fluorescent dye (**30**) as a marker for direct cellular imaging.[147] As shown in Figure 23a, **30** was synthesized in two steps from monofunctionalized azidobutyl-Q[7] and the *N*-hydroxysuccinimide-activated fluorescent dye tetramethylrhodamine (**31**). Compound **30** has better solubility in pure water at room temperature and exhibits significantly higher fluorescence intensity compared with the free monomer **31**. The CLSM images of live and fixed HT22 neurons demonstrated cellular uptake of **30** and its punctate localization in the cytoplasm (Figure 23b). Cell growth was not altered by **30** at concentrations up to 2.2 μM over 4 days because Q[7] has no intrinsic cytotoxicity. Herein, the hydrophobic effect from the macrocyclic confinement of the Q[7] rigid structure may play an important role in inproving the cellular uptake of **30**.

Utilizing a monofunctionalized Q[7] scaffold, Kim and co-workers fabricated a novel host–guest FRET pair to study SNARE (soluble *N*-ethylmaleimide-sensitive factor attachment protein receptor)-mediated membrane fusion, combining the advantages of small molecular probes and the high signal-to-noise ratio benefits of FRET-based techniques (Figure 24a).[148] Monofunctionalized Q[7]-derived dyes **32** and adamantylamine-derived **33** were first encapsulated in SNARE protein as donor (**32**-*v*-vesicle) and acceptor (**33**-*t*-vesicle) vesicles, respectively (Figure 24b). A single-vesicle content mixing assay was then performed using a total internal reflection fluorescence microscope. The acceptor vesicle, **33**-*t*-vesicle, was immobilized on a quartz surface, and the **32**-*v*-vesicle donor was injected into the flow chamber of the analysis setup. Docking of the donor vesicle onto the acceptor vesicle was monitored by the sudden appearance of **32** emission in the time trace. Pore opening led to mixing of the two opposite vesicles to form a strong host–guest complex, which generated the **33** emission FRET signal. The high stability of the Q[7]-AD complex makes the technique compatible with a wide range of reaction conditions during both vesicle preparation and fusion. Consequently, the strategy of the "host–guest FRET pair" with extremely strong binding affinity under the confinement effect of the Q[7] host is expected to be useful in various chemical and biological studies as a supramolecular beacon (Figure 24c).

4.4. RTP Emission from Q[7]-Based Complexes

Solid-state materials with efficient RTP emissions have been widely investigated in the latest decade, but liquid- or solution-phase pure organic RTP systems have rarely been reported because of nonradiative decay and quenchers from the liquid medium. Ma and co-workers demonstrated that the Q[*n*] host had advantages for fabrication of a pure organic RTP system in aqueous solution via host–guest interaction.[61,149−151] For example, they described controllable RTP emission through pH-stimuli-responsive molecular shuttling between Q[7] and bromo-isoquinoline guest derivatives **34**, **35**, and **36** (Figure 25a) in aqueous solution.[149] The different behaviors of the guests were determined by the presence of variable length carboxyl-terminated N-substituted alkyl chains. The RTP intensity of **34** was almost unchanged in aqueous solutions at different pH in the presence of the Q[7] host, which was attributed to the short aliphatic docking site inhibiting the threading motion of Q[7]. Guest **36** showed weak RTP even under nonacidic conditions due to the longer length of the alkyl chain. The optimal chain length of the aliphatic docking site in **35** allowed Q[7] to shuttle through the molecule in acidic media but was retained at the bromo-isoquinoline moiety after the addition of base. Therefore, **35** exhibited weak RTP emission in acidic solution and strong RTP emission when the pH was raised (Figure 25b). Very similar RTP emission has been reported by the same group through inclusion of a bromo-naphthalimide derivative in the cavity of

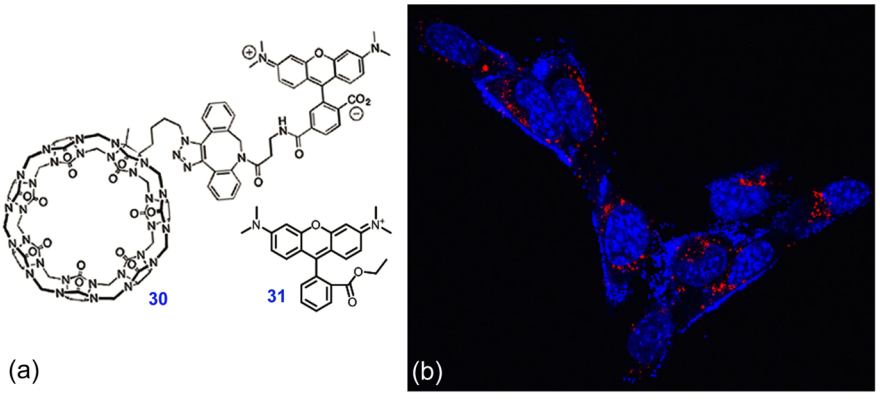

Figure 23. (a) Chemical structures of **30** and **31**. (b) CLSM images of live HT22 cells treated with 91 μM **30** (red) and Hoechst 33342 (blue). Reproduced with permission from ref 147. Copyright 2016 American Chemical Society.

https://doi.org/10.1021/acs.chemrev.1c01050
Chem. Rev. XXXX, XXX, XXX−XXX

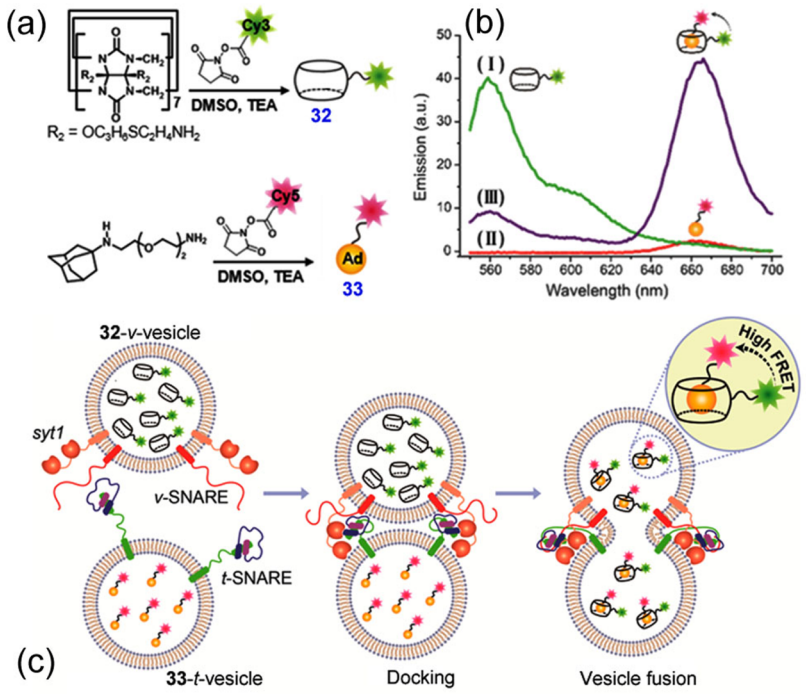

Figure 24. (a) Chemical structures of **32** and **33**. (b) Fluorescence emission spectra of **32** and **33** and FRET between **32** and **33**. (c) Schematic illustration of the SNARE-mediated content mixing using a high affinity host−guest binding FRET pair. Reproduced with permission from ref 148. Copyright 2015 American Chemical Society.

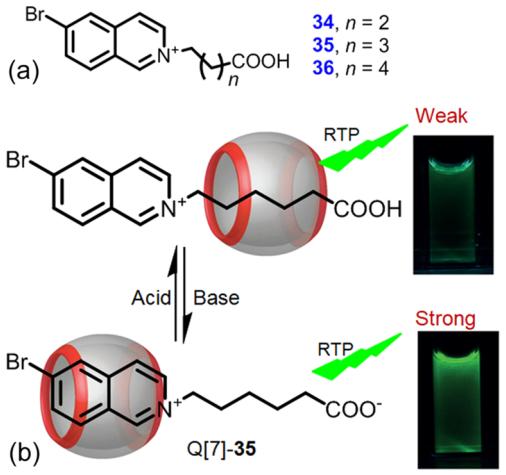

Figure 25. (a) Chemical structures of **34**−**36**. (b) pH switched RTP emission of Q[7]-**35** and photographs of the solution under UV light at 254 nm. Reproduced with permission from ref 149. Copyright 2016 Wiley-VCH.

Q[7].[150] These studies suggest that inclusion of a heavy-atom-substituted fluorogen into the confined cavity of Q[7] is the key factor for enhancing RTP emission in solution. In other words, these studies revealed that the confinement effect in the Q[7] cavity played the crucial role in improving the RTP emission of the phosphors.

Very recently, Liu and co-workers systematically investigated the effect of Q[*n*] cavity size (in which different macrocyclic-confinement effects are expected to be induced due to the different confined cavity sizes) on the fabrication of efficient RTP materials.[152] As shown in Figure 26a, monomer phosphors of 4-phenyl-1-(4-vinylbenzyl)pyridinium chloride (**37**) and 4-(4-bromophenyl)-1-(4-vinylbenzyl)pyridinium chloride (**38**) were copolymerized with acrylamide to produce the corresponding polymers **39** and **40**, respectively. The authors discovered that the ratio of phosphors had a large influence on the photoluminescence of the polymers. A lower ratio of phosphors resulted in a better distribution and, therefore, a longer lifetime, but less phosphor also meant weak emission. In contrast, a higher ratio produces stronger phosphorescence but causes ACQ or, worse, embeddedness, together with less restriction of the phosphors, which combine to shorten lifetime sharply. Host interactions of Q[6,7,8] could further enhance the phosphorescence of those polymers by blocking ACQ and encapsulating phosphors in the cavity. For example, complexation by Q[6,7] prolonged the lifetime of **39(1)** (copolymer **39** containing 1% phosphors) from 1.46 to 2.37 and 2.33 s, respectively. In particular, the luminescence of Q[7]-**39(1)** lasted 12 s after removing the UV irradiation (Figure 26b). The shorter lifetime of Q[8]-**39(1)** (t = 1.17 s) indicated that the presence of two phosphors in one host cavity did not favor prolongation of lifetime. In the case of **40(1)**, complexation with Q[6,7,8] prolonged its lifetime to 10.9 ms (Q[6]-**40(1)**), 9.02 ms (Q[7]-**40(1)**), and 9.30 ms (Q[8]-**40(1)**) with phosphorescence quantum yields changed from 56.7% (**40**) to 76.0% (Q[6]-**40(1)**), 52.7% (Q[7]-**40(1)**), and 65.3% (Q[8]-**40(1)**). For comparison, a short lifetime was observed in the complexes of **37** and **38** monomers with Q[6,7,8]. Therefore, it is believed that copolymerization between phosphors and acrylamide provides plenty of hydrogen bonds and carbonyl groups to lock the phosphors and promote intersystem crossing. After encapsulation by Q[6,7,8], the nonradiative decay of phosphors is further suppressed under the corresponding macrocyclic confinement, ACQ is blocked and quenchers are shielded more effectively, resulting in further enhancement of RTP. Obviously, this work provides a convenient synergistic strategy for fabrication of

https://doi.org/10.1021/acs.chemrev.1c01050
Chem. Rev. XXXX, XXX, XXX−XXX

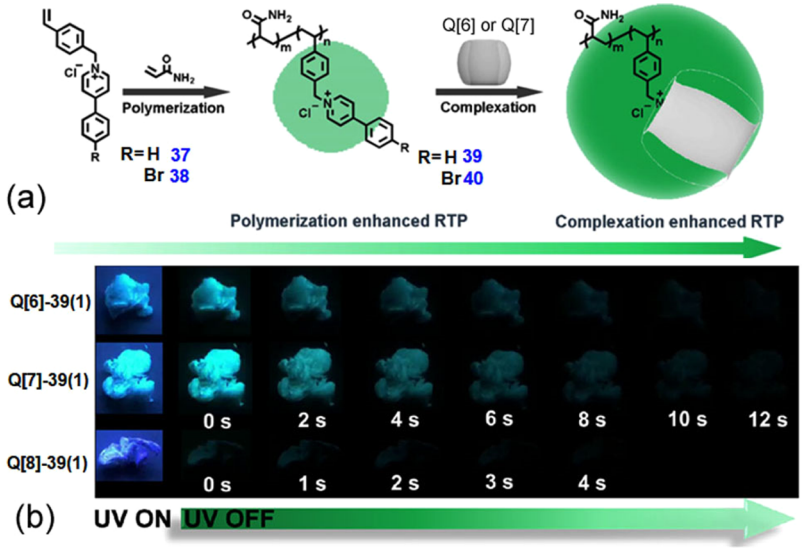

Figure 26. (a) Schematic representation of **37**−**40** and the synergistic enhancement strategy for ultralong and efficient RTP. (b) Luminescence photographs of Q[6,7,8]-**39**(**1**) under UV light and at different time intervals after ceasing irradiation. Reproduced with permission from ref 152. Copyright 2020 Wiley-VCH.

ultralong and efficient RTP by utilizing the different strength of the macrocyclic-confinement effect of Q[*n*]s

5. SUPRAMOLECULAR ORGANIC LUMINESCENT EMISSIONS FROM THE Q[8] HOST

With a cavity comparable to that of γ-cyclodextrin, Q[8] is unique because of its ability to bind two hetero- or homoguests in its cavity with high affinity in water. In early studies of Q[8], its confined cavity was used to mediate chemical reactions such as stereospecific [2 + 2] cycloadditions,[153−158] which belong to typical artificial molecular containers that alter chemical reactivity through the macrocyclic-confinement effect. Meanwhile, it was found that the confined space of the Q[8] host could stabilize otherwise unstable species, such as methyl viologen cation radicals or tetrathiafulvalene cation radicals, to form stable π-dimers by encapsulation.[159,160] Subsequently, the ability of Q[8] to accommodate two different guest molecules, an electron-deficient molecule (often 4,4′-bipyridinium dications, also called viologens) and an electron-rich molecule (generally aromatic molecules), to form a stable 1:1:1 ternary complex (the driving force for host-stabilized charge transfer, HSCT),[161,162] has captured the imagination of scientists. Their broad potential applications in supramolecular chemistry via noncovalent interactions, in particular, as molecular handcuffs, has been widely used to construct various water-soluble dynamic supramolecular polymer materials over the past decade.[163−167] Although, it was found that Q[8] could simultaneously include two chromophore dyes in its cavity to form a dimer assembly through π−π stacking, fluorescence quenching was generally observed, reducing its attractiveness for exploitation in luminescent materials. Recently, it has been discovered that π-conjugated pyridinium derivatives can serve as both electron-deficient and electron-rich groups that can dimerize inside the Q[8] cavity to form highly stable Q[8]-enhanced ternary complexes and polymers, which not only increases π−π stacking of the aromatic moieties but also enhances ICT of the inclusion guest dyes.[56,168−171] So, most of the reported Q[8]-based luminescent emissions in this section were derived from the synergistic effect of confinement of the Q[8] cavity and the corresponding supramolecular assembly fashions.

5.1. Fluorescence Emission from Q[8]-Based Simple Complexes

In the early development of Q[8]-dye systems, the fluorescence of chromophore dyes was generally quenched because of their dimerization in the Q[8] cavity. For example, Macartney and co-workers reported that the chromophore dye guests acridizinium bromide (**41**) and 9-aminoacridizinium bromide (**42**) were encapsulated by Q[8] to form 1:2 complexes (Q[8]/guest).[172] As shown in Figure 27, free **41**

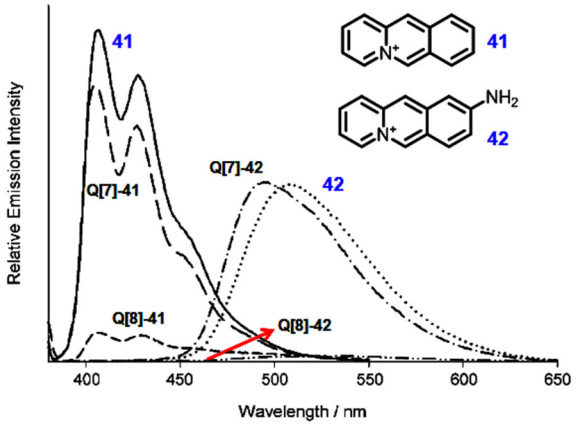

Figure 27. Chemical structures of **41** and **42** and the corresponding fluoresence spectra of **41** and **42** in the absence and presence of Q[7] and Q[8], respectively. Reproduced with permission from ref 172. Copyright 2007 Wiley-VCH.

and **42** exhibited blue and green fluorescence emissions in water, respectively. After addition of Q[8] to the guest solution, the corresponding emissions of **41** and **42** were almost completely quenched. The fluorescence could be effectively restored by addition of Q[7] to the complex solution because it competitively extracts the dye guest from the Q[8] cavity. Job plots indicated that a 1:2 complex (Q[8]/

https://doi.org/10.1021/acs.chemrev.1c01050
Chem. Rev. XXXX, XXX, XXX−XXX

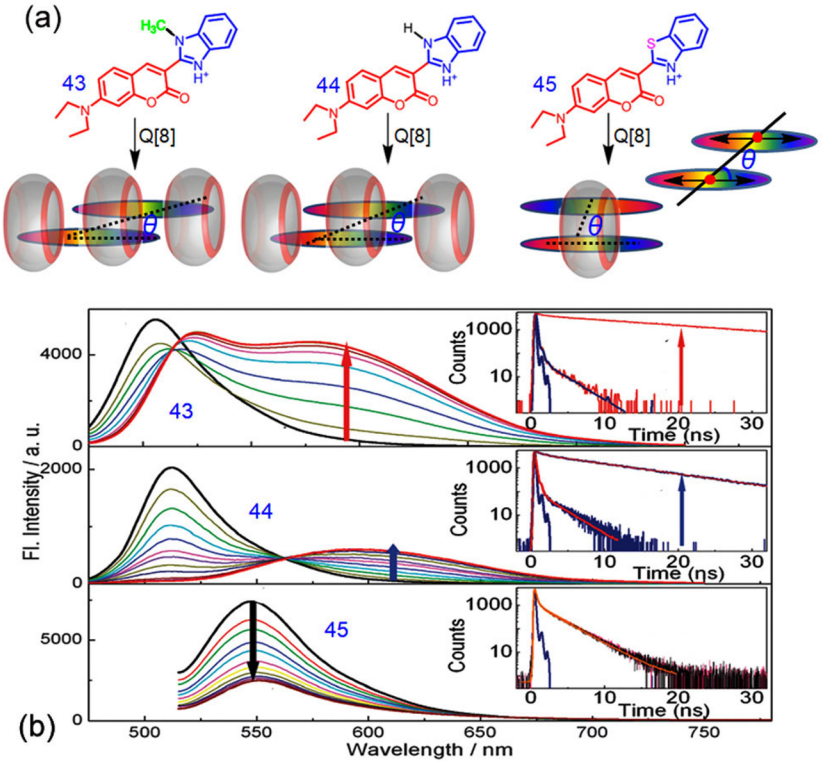

Figure 28. (a) Chemical structures of **43**−**45** (protonated forms) and the proposed geometries of the Q[8]-based host−guest complexes. (b) Fluorescence spectra and lifetime traces of **43**−**45** in the presence and absence of the Q[8] host. Reproduced with permission from ref 173. Copyright 2013 Royal Society of Chemistry.

guest) and a 1:1 complex (Q[7]/guest) were formed. The fluorescence quenching of guests can be attributed to $\pi-\pi$ stacking (*H*-dimer) of the guest molecules under the strong macrocyclic-confinement effect of the Q[8] cavity.

In order to further understand the influence of the Q[8]-dye assembly behavior on its fluorescence, Bhasikuttan et al. synthesized a series of coumarin derivatives (**43**−**45**) as the guest dyes, which differed only slightly with respect to the substitution/heteroatom on the benzimidazole unit.[173] Because of the finite structural variations at the benzimidazole ends of these dyes, dimeric/multiple inclusions by Q[8] can result in subtle differences in their spatial arrangement within the cavity, such as *H*- and *J*-type assembly. As can be seen from Figure 28a, guest dyes **43** and **44** displayed remarkable fluorescence spectral changes in the presence of the Q[8] host. Compound **43** underwent decreased emission intensity at 505 nm, accompanied by a new emission peak in the long wavelength region, upon addition of Q[8] to the solution. Similar fluorescence changes were observed with **44** under the same experimental conditions (Figure 28b). However, unlike **43** and **44**, **45** exhibited steady fluorescence quenching as the concentration of Q[8] was increased, without any additional band shift (Figure 28b). Moreover, in the presence of the Q[8] host, the fluorescence lifetime of **43** increased from 0.13 to 19.8 ns, and the fluorescence lifetime of **44** increased from 0.17 to 10 ns, whereas the fluorescence lifetime of **45** remained unaffected. Evidently, the fluorescence changes of **43**−**45** can be attributed to dimer formation in the Q[8] host, and the extent of overlap or slip among the dyes inside the cavity leads to *J*- or *H*-type complexes with varying slip angles, "θ" (Figure 28a), which was confirmed by ^{1}H NMR spectroscopy and semiempirical calculations. This study provides an ideal example that the macrocycle-based supramolecular emissions can be switched by rational molecular design under the same macrocyclic-confinement effect.

Fluorescence quenching is disadvantageous for high signal output in real time monitoring processes in situ. However, as the old Chinese saying goes, fortune and misfortune are two baskets in a well. For example, Zhang and co-workers found that fluorescence quenching of chromophore dye in the Q[8] confined cavity could be exploited as an activatable supramolecular photosensitizer for cancer imaging and photodynamic therapy.[174] As depicted in Figure 29, guest biotinylated toluidine blue (**46**) was designed as a photosensitizer, in which biotin acts as a cell-receptor anchoring unit and toluidine blue as an efficient singlet oxygen generator and fluorophore. Guest **46** as a free uncomplexed dye in water generates singlet oxygen. As a luminophore, free **46** also exhibits strong fluorescence emission around 650 nm. In the presence of Q[8], **46** assembles into a 1:2 complex (Q[8]-**46**), in a head-to-tail arrangement due to steric interaction between the bulky biotin groups, that can be released by competitive binding of other guest molecules such as *N*-terminal aromatic peptides. Dimerization of the toluidine blue moiety in the confined cavity of Q[8] leads to fluorescence quenching of **46** and its phototoxicity. The activity of **46** as a photosensitizer, therefore, was turned off/on by the assembly and disassembly of Q[8]-**46**. In addition, Q[8] also provides excellent protection of **46** from reduction by enzymes, which significantly enhances its stability in vivo. As shown in Figure 29, the biotin arm anchors the photoinactive 1:2 complex (Q[8]-**46**) onto the cell-surface receptor, which is then transported into the cell. Intracellular *N*-terminal aromatic peptides then release **46**, restoring photodynamic therapy

https://doi.org/10.1021/acs.chemrev.1c01050
Chem. Rev. XXXX, XXX, XXX−XXX

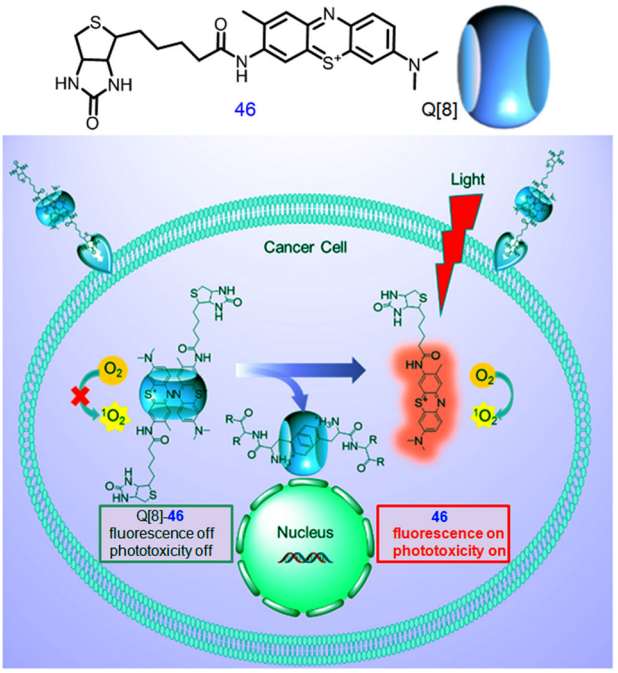

Figure 29. Chemical structures of **46** and the Q[8]-**46** complex as supramolecular active photosensitizers for cancer imaging and photodynamic therapy. Reproduced with permission from ref 174. Copyright 2016 American Chemical Society.

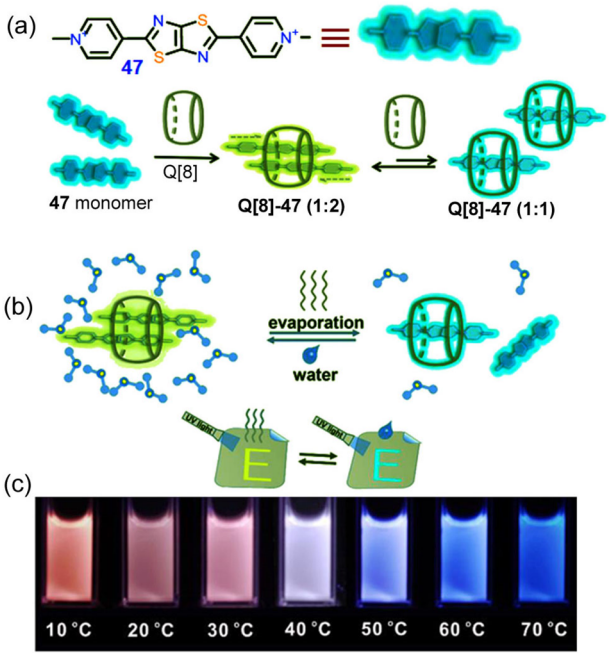

Figure 30. (a) Chemical structure of **47** and schematic representation of the dynamic host–guest assemblies of **47** with different equivalents of Q[8]. (b) Fluorescence change of the dynamic assemblies of Q[8]-**47** on paper under 365 nm irradiation. (c) Photographs of the hybrid solution at different temperatures. Reproduced with permission from ref 175. Copyright 2019 American Chemical Society.

activity and fluorescence emission. Accordingly, the intracellular self-activation ability of Q[8]-**46** greatly enhances its utility without the need for external inducers, which also gives it potential for disease-related applications.

Ma et al. demonstrated a humidity- and temperature-responsive luminescent material by inclusion of a blue-emissive thiazolothiazole methyl-viologen (**47**) guest inside the confined cavity of Q[8].[175] As shown in Figure 30a, two binding modes, including 1:2 and 1:1 complexes (Q[8]-**47**), can dynamically self-assemble in aqueous solution. The 1:2 complex of Q[8]-**47** exhibited concentration-dependent emissions. A bluish-white emission (460 nm) was observed at low concentrations (<0.05 mM), and a greenish-yellow emission (535 nm) was seen at higher concentrations (>0.1 mM). The changes in emission wavelength were attributed to a concentration-dependent binding equilibrium between free **47** (blue emission) and the *J*-dimers of **47** packed inside the Q[8] cavity (greenish-yellow emission). Furthermore, when 0.1 mM Q[8]-**47** complex (1:2) was dropped onto water-absorbent materials such as silica or paper surfaces, the blue emission dramatically declined and only the yellow fluorescence remained. Interestingly, upon evaporation, the greenish-yellow emission gradually changed to blue emission. The yellow emission could be recovered by dropping water onto it. Therefore, by simple variation of the humidity level, different luminescent colors were generated such that the system could be used as a fluorescent ink to print two-dimensional codes. The enhancement of the monomer emission intensity of **47** at 460 nm upon drying was attributed to dissociation of the 1:2 complex of Q[8]-**47** into free monomer **47** and the 1:1 complex of Q[8]-**47** (Figure 30b).

The 1:2 complex of Q[8]-**47** also dissociated at higher temperatures as evidenced by the remarkably increased intensity of the blue emission. To construct a thermotunable luminescent material, glutathione-ligand gold nanoclusters (GSH-AuNCs, 0.5 mg/mL) were mixed with the 1:2 complex of Q[8]-**47** (6 μM). The GSH-AuNCs have a similar excitation wavelength to the Q[8]-**47** complex, and its orange emission at 600 nm was utilized to fabricate a thermotunable white-light-emissive system via simple mixing. Thus, pure white-light emission (CIE 0.33, 0.33) with a quantum yield of 2.37% was obtained when the temperature was 40 °C in the hybrid solution. The white-light-emissive solution gradually turned pink when cooled to approximately 0 °C, while blue emission appeared at 70 °C (Figure 30c). This study indicated that the assembly fashion of fluorophores also plays an important role in controlling the macrocycle-based supramolecular emissions under the same confinement effect.

At the same time, Zhang, Xu, and co-workers developed a supramolecular radical dimer with high efficiency NIR-II photothermal conversion for photothermal therapy using the same 1:2 complex of Q[8]-**47**.[176] Single-crystal X-ray analysis provided unequivocal proof of the 1:2 complex structure of Q[8]-**47**, in which the two **47** guests were arranged in a typical *J*-type dimer conformation (Figure 31a). The Q[8] confined cavity-fixed π-extended assembly of **47** is believed to favor intermolecular charge transfer. The radical dimer of Q[8]-**47** could be generated through photoinduced electron transfer to cationic **47** by irradiation with 405 nm light in the presence of excess triethanolamine as the electron donor. As can be seen from Figure 31b, the radical dimer of Q[8]-**47** exhibited a strong absorption peak at 1004 nm (an ideal NIR-II biowindow). Next, it was found that the temperature of the aqueous solution of the Q[8]-**47** radical dimer (0.5 mM) was increased by 20.1, 30.7, 40.7, 46.0, and 51.4 °C when subjected to 1064 nm irradiation for 5 min at 0.50, 0.75, 1.00, 1.25, and 1.50 W cm^{-2}, respectively (Figure 31c). In addition, the radical

https://doi.org/10.1021/acs.chemrev.1c01050
Chem. Rev. XXXX, XXX, XXX−XXX

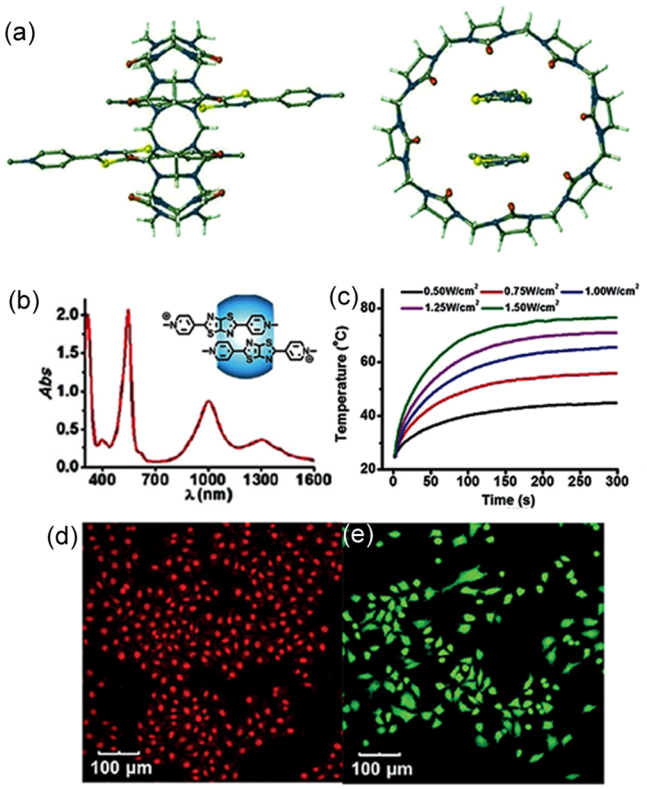

Figure 31. (a) X-ray crystal structure of Q[8]-**47**. (b) UV/vis-NIR absorption of the radical dimer of Q[8]-**47**. (c) Heating curves of the radical dimer of Q[8]-**47** with irradiation at different power densities. CLSM of the radical dimer of Q[8]-**47** induced photothermal ablation in the HepG2 cells with (d) and without (e) 1064 nm irradiation at 1.00 W for 1 min. Reproduced with permission from ref 176. Copyright 2019 Wiley-VCH.

dimer exhibited satisfactory photostability and thermostability under 1064 nm laser irradiation. The efficient and reliable photothermal conversion of the Q[8]-**47** radical dimer gives it potential for photothermal therapy of cancer. Very recently, the same group discovered that the macrocyclic-confinement-fixed supramolecular dimer of Q[8]-**47** dramatically promoted intersystem crossing to produce the triplet excited state. That is, the *J*-type conformation of Q[8]-**47** facilitated electron and energy transfer of the triplet excited state. Consequently, the 1:2 complex of Q[8]-**47** was further utilized as an efficiency photocatalyst for oxidative hydroxylation of arylboronic acids.[177]

5.2. Fluorescence Emission from Q[8]-Based Multiple Assemblies

In macrocycle-based host−guest interactions, it is well-known that the 1:1 binding stoichiometry only indicates that the complex contains equal amounts of both host and guest, such as 1:1, 2:2, or even a combination of *n*:*n* (*n* = 1, 2, 3, ...) in the case of a supramolecular polymer. In Q[*n*] chemistry, Scherman and co-workers found that ITC data, including enthalpy (Δ*H*) and entropy (Δ*S*) changes, can provide specific evidence to distinguish Q[8] triggered 1:1, 1:2, 1:1:1, and 2:2 complex modes.[178] In fact, fluorescence has become popular to monitor the dynamic processes of self-assembly,[179,180] conformational changes,[181] and molecular motion[182] in recent years, since fluorescence methods are highly sensitive and allow direct visualization in situ and in real time.[183−186]

In Q[*n*] chemistry, Scherman et al. reported that the 3:2 complex of Q[8] with the dye guest **48** and the 2:1 complex of Q[7] with **48** were easily distinguished by fluorescence spectra and the naked eye under UV light at 365 nm (Figure 32).[187]

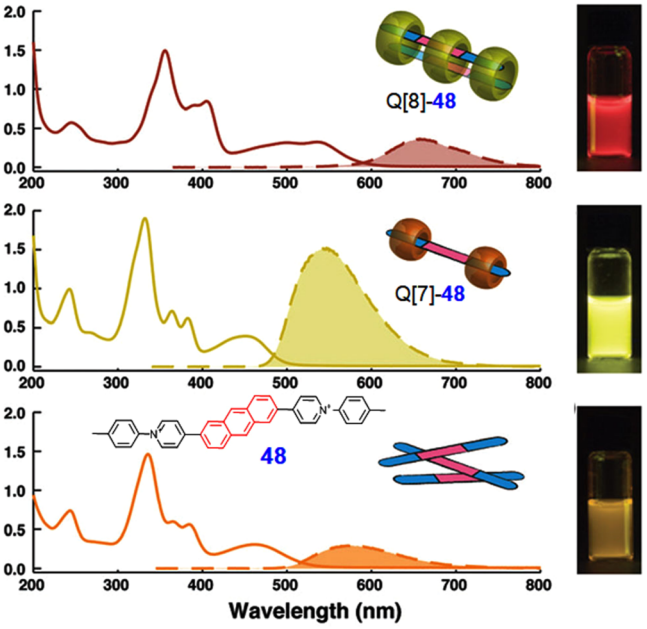

Figure 32. UV−vis absorption and fluorescence emission spectra of Q[8]-**48**, Q[7]-**48**, and **48** and related photographs of solutions excited by a 365 nm lamp. Reproduced with permission from ref 187. Copyright 2017 Royal Society of Chemistry.

Obviously, these color changes can be partly attributed to the different macrocyclic-confinement effects from the Q[7] and Q[8] hosts and partly due to the different stacking models of the dye guest in the host−guest assemblies. The same group then went on to conduct pioneering work on tunable fluorescence emission from Q[8] confined cavity-based 2:2 quaternary complexes in aqueous solution.[188,189] As shown in Figure 33a,[189] two arylpyridinium groups, well-known water-soluble cationic guests for Q[8] with high affinity, were selected as the rigid "clamping" modules linked through different fluorophores as the central cores (Figure 33b). The choice of rigid fluorophore linkages between the arylpyridinium moieties benefited formation of 2:2 complexes rather than extended supramolecular polymers. When 1.0 equiv of Q[8] was mixed with 1.0 equiv of the guest, 2:2 quaternary complexes were formed and stabilized by the two Q[8] clamps, which placed the two fluorophores in close proximity to each other as stacked dimers under the macrocyclic-confinement effect. Importantly, it should be noted that the aromatic fluorophores were not encapsulated in the Q[8] cavity, implying that even fluorophores larger than the cavity could be employed in this modular strategy. For example, the host−guest interaction study of guest **49b** indicated that the 2:1 stoichiometry was obtained in the Q[7]-**49b** complex, whereas it was found to be 1:1 in the Q[8]-**49b** system. Detailed characterization of the Q[8] complex suggested that it was actually a 2:2 assembly. Similar binding stoichiometries were also observed for other guests.

In the 2:2 supramolecular quaternary complexes, the preorganized fluorophore dimers were stabilized by two Q[8] hosts and, hence, the chromophores exhibited different

https://doi.org/10.1021/acs.chemrev.1c01050
Chem. Rev. XXXX, XXX, XXX−XXX

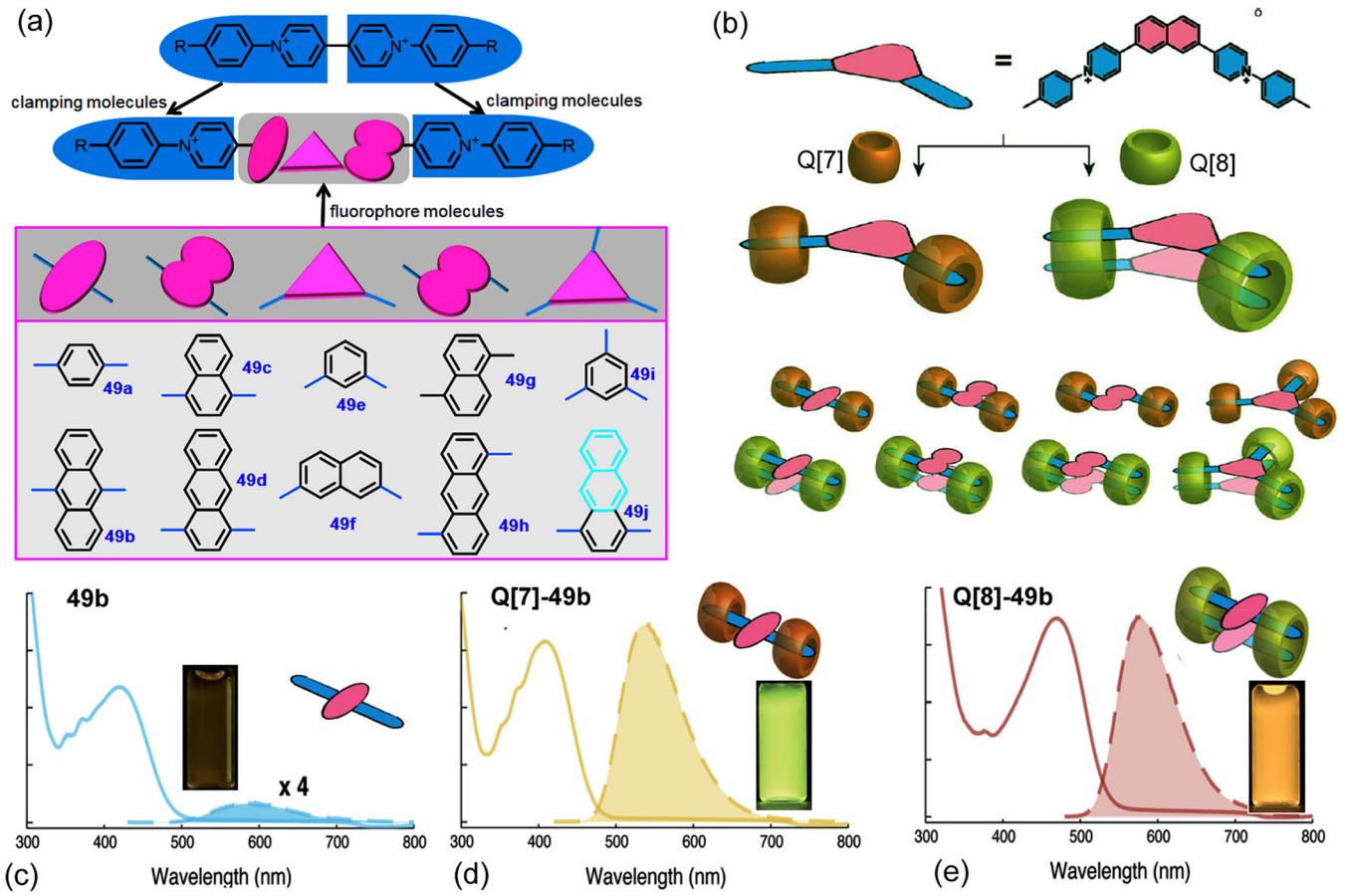

Figure 33. (a) Chemical structures of **49a–j** and the related modular designing strategy. Following this strategy (b) **49f** as an example of a nonparallel clamping module and other fluorophores with various arrangements of clamping modules are expected to form host–guest assemblies with Q[8] and Q[7]. Steady-state absorption (solid line) and emission (dashed line with filling color) spectra of (c) **49b**, (d) Q[7]-**49b**, and Q[8]-**49b** in water (inset: schematic representation of the corresponding guest and host–guest assemblies and the fluorescence photo images under 365 nm UV light). Reproduced with permission from ref 189. Copyright 2019 Royal Society of Chemistry.

photophysical properties.[189] Noticeable red-shifts in the absorption spectra and, upon photoexcitation, excimer-like emissions with longer lifetimes were observed. As a comparative study, the photophysical properties of the Q[7] complexes were also investigated because it was believed that the fluorophores were fixed as monomeric entities by the Q[7] host. As shown in Figure 33c–e, formation of a 2:2 supramolecular complex of Q[8] with **49b** resulted in a remarkable bathochromic shift of the maximum absorption relative to the solution of **49b** alone (from 419 to 469 nm), whereas a small hypsochromic shift (from 419 to 409 nm) was observed in the Q[7]-**49b** complex. The maximum emission peak of the Q[8]-**49b** quaternary complex was at 578 nm (Figure 33e), which was red-shifted compared to the Q[7]-**49b** complex (λ_{em} = 537 nm) (Figure 33d), although the solution of **49b** alone exhibited emission at 595 nm (Figure 33c). Consequently, variation of the fluorescence color of this derivative could be achieved by the cooperation of Q[7] or Q[8]. Furthermore, the quantum yield of **49b** was significantly enhanced upon complexation with Q[7] and Q[8] because of the remarkably restricted intracomplex motions. For example, the absolute QY of a solution of **49b** increased from 4% to 85% and 81%, upon complexation with Q[7] (1:2) and Q[8] (2:2), respectively. Meanwhile, similar variant photophysical behaviors were also observed for most other derivatives in the presence of the Q[7] and Q[8] hosts.

Using the same modular strategy, Scherman and co-workers successfully fabricated a 2:2 quantitative heterodimerization system for efficient energy transfer under the macrocyclic-confinement effect of the Q[8] host (Figure 34).[190] Chromophore guests were synthesized based on the bis(*N*-arylpyridinium) (BAP) moiety through one covalent reaction and then underwent dimerization through multiple Q[8] clamping. A heterodimer (AB) could be generated by simply mixing two homodimers (AA and BB) of guests **50a** and **50b** in aqueous media, but not quantitatively. This was attributed to similar binding free energies of 2:2 homodimers of **50a** and **50b** with the Q[8] host. Interestingly, when the methoxy group of **50b** was replaced by a bulkier end group (*N*,*N*-dimethylamino, NMe_2) to generate guest **50c**, it was found that the equilibria of 50/50 mixtures with **50a** and **50b** homodimers were significantly dominated by the heterodimer (92%). Following this observation, the authors proposed that increasing the size of one of the end groups (i.e., NMe_2) combined with a smaller complementary end group should further increase the binding constant. As a result, guest **50d** (NH_2 replaced by H) was designed. As expected, ^{1}H NMR spectroscopy revealed that the desired heterodimer was solely formed in an equimolar mixture of **50c** and **50d** homodimers. Fluorescence spectra indicated that nonradiative energy transfer occurred from the photoexcited naphthyl moiety (**50e**) to its neighboring anthracenyl group (**50f**) in the

https://doi.org/10.1021/acs.chemrev.1c01050
Chem. Rev. XXXX, XXX, XXX–XXX

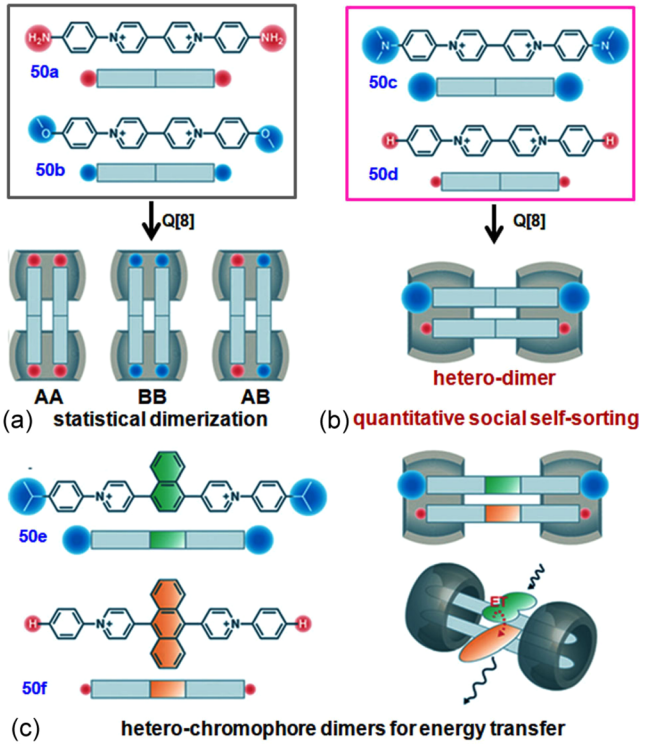

Figure 34. Schematic representation of (a) statistical dimerization with the coexistence of three species. (b) Quantitative supramolecular heterodimerization via self-sorting. (c) Pure heterochromophore dimers with efficient energy transfer generated from the **50e** to **50f**. Reproduced with permission from ref 190. Copyright 2020 Wiley-VCH.

discrete heterodimer with extremely high efficiency of energy transfer, which was estimated to be greater than 85%. Overall, this study provides a new insight into fabrication of noncovalent interaction triggered heterodimers without other equilibrium byproducts by introduction of shape-complementary moieties in a confined space of macrocycles. In particular, highly efficient preparation of various discrete chromophore dimers with novel optoelectronic properties is becoming possible.

Taking advantage of Q[8] cavity encapsulation triggered tunable fluorescent signals, Ni and co-workers reported a series of dynamic host−guest assemblies including 1:2, 2:2, 3:2, and 2:1 complexes (Q[8]/guest) that could be distinguished by naked-eye observation of the resulting quantitative fluorescence emissions.[191] As shown in Figure 35, alkyl chains of different lengths (carbon atoms from 1C to 9C) were introduced into π-conjugated bispyridinium parents (**51a**, **51b**, and **51c**) as the fluorophore guest molecules. When different concentrations of Q[8] were added to the guest solution, the fluorescence color was obviously changed from blue to pale yellow, bright green (and deep yellow), and pale green, corresponding to dynamic complex modes of Q[8] with the guests from 1:2 to 2:2 and to 2:1, except for guests **51a** (5C−6C) and **51b** (5C−6C), where significant red-shift emissions (orange color) were observed in the final formation of 3:2 complexes. However, guest **51c** (7C−9C), in which two methyl groups were introduced into the central fluorophore as a larger barrier, led to direct formation of 2:1 complex structures assisted by the terminal long alkyl chains (with a U-shaped conformation in the Q[8] cavity). The fluorescence lifetimes of these complexes were fully in line with the host−guest complex modes. That is, longer lifetimes generally corresponded to deep encapsulation of the chromophore in the Q[8] cavity, while shorter lifetimes indicated that the chromophore was less deeply buried or was farther from the Q[8] cavity. Accordingly, this study revealed that fluorescence decay times may be useful for characterizing binding modes in Q[8]-chromophore systems. This result provides an example that multiple host−guest assemblies with distinct luminescent signals in the same confinement environment of Q[n]s are becoming possible.

5.3. Fluorescence Emission from Q[8]-Based Supramolecular Polymers

Fluorescent supramolecular polymers, which combine the fluorescent properties of chromophores with dynamic noncovalent connections of supramolecular polymers, have attracted much attention as luminescent materials because of their superior optoelectronic properties, including stimuli-

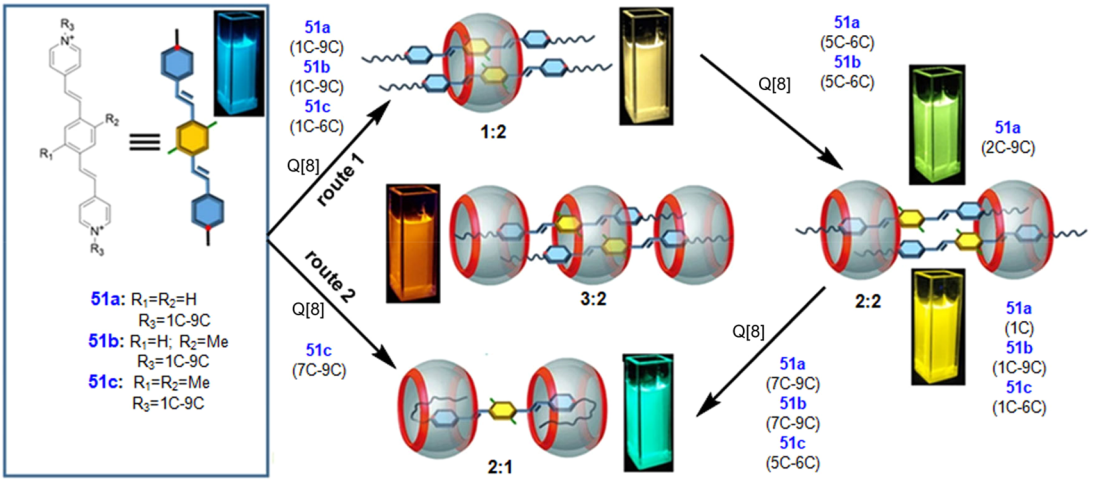

Figure 35. Chemical structures of **51a−c** and representation of Q[8]-based dynamic host−guest assemblies with multiple tunable fluorescence signals. Route 1: Q[8] concentration-dependent host−guest interactions of 1:2, 2:2, 3:2, and 2:1 (Q[8]/guest). Route 2: formation of a U-shaped conformation of Q[8] with **51c** (7C−9C). Reproduced with permission from ref 191. Copyright 2021 Royal Society of Chemistry.

https://doi.org/10.1021/acs.chemrev.1c01050
Chem. Rev. XXXX, XXX, XXX−XXX

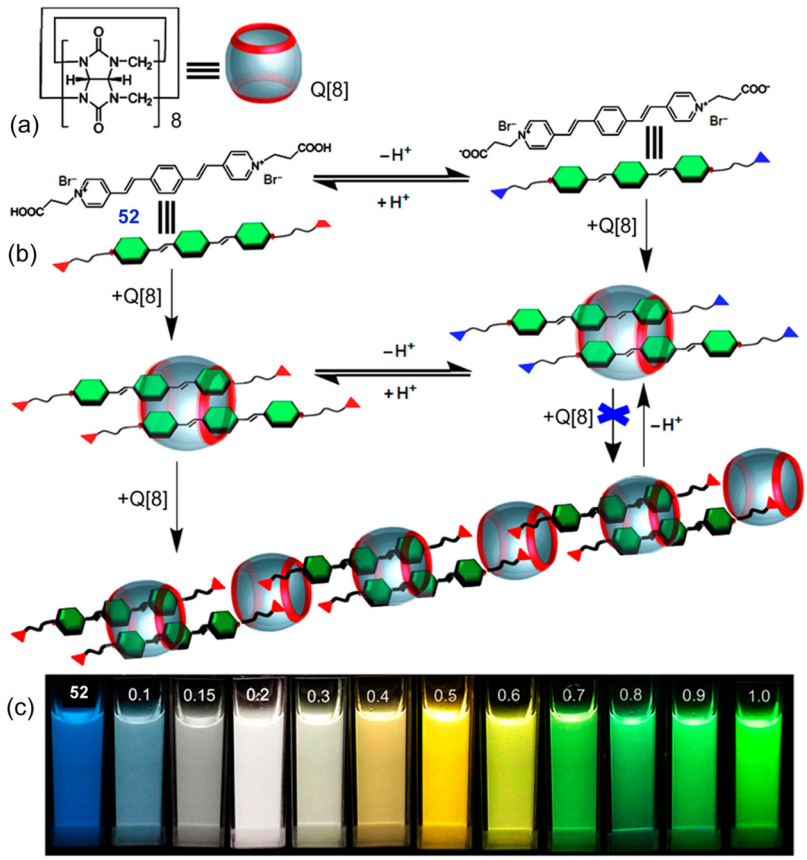

Figure 36. (a) Chemical structures of Q[8] and **52**. (b) Schematic representation of the Q[8]-based approach for fabricating smart luminescent materials, showing host−guest interactions of Q[8] with **52** that lead to different supramolecular assemblies in water. (c) Photographs of solutions of **52** (10.0 μM) upon addition of increasing concentrations of the Q[8] host (0−1.0 equiv) in aqueous media (pH 2.0) under UV light at 365 nm. Reproduced with permission from ref 56. Copyright 2016 American Chemical Society.

responsive and reversible features, compared with the monomeric units.[192−198] The ternary complex ability of Q[8] has been used to construct various fluorescent polymers with smart tunable emissions and high quantum efficiency. This is partly due to the extensive $\pi-\pi$ interactions (such as *J*-type assembly) of chromophores in a head-to-tail fashion in the Q[8] cavity and is partly due to the synergistic effect of the cavity-derived macrocyclic confinement and the rigid linear polymer structures that restricted the intramolecular motions.

For example, Ni et al. reported that a tunable fluorescent emission could be obtained in a host−guest interaction system of Q[8] with an oligo(*p*-phenylenevinylene) guest **52** in aqueous solution (Figure 36).[56] The propionic acid groups at the ends of **52** were selected to increase aqueous solubility and enable a reversible switch between neutral and anionic states by pH titration. Free **52** emits blue light at 475 nm in aqueous solution when excited at 398 nm. After addition of Q[8] (0.5 equiv) to the solution (pH 2.0), a stronger visible yellow emission with higher QY and long lifetime at 580 nm was observed. These spectral changes can be attributed to formation of *J*-dimers of **52** inside the Q[8] cavity. The extensive $\pi-\pi$ interactions or intermolecular orbital overlap between the homodimers (head-to-tail) under the macrocyclic-confinement effect of the Q[8] cavity led to the remarkable red-shift of the emission and absorption. When the concentration of Q[8] was increased to 1.0 equiv, an apparent blue-shift was observed in the absorption and emission spectra corresponding to transition of the complexation mode from the 1:2 dimer complex to the 1:1 supramolecular polymer. Essentially, the two N-substituted propionic acid groups were simultaneously encapsulated in the excess Q[8] cavity, playing a key role in the formation of the rigid supramolecular polymer structure. In particular, the carbonyl groups of the Q[8] portal would decrease the electron-withdrawing ability of the pyridinium group of **52** and ICT could be suppressed. Therefore, an enhanced blue-shifted emission was observed in the polymer solution. Notably, because both of the fluorescent emissions from the free guest and the complex species can be excited by the same wavelength, multiple tunable fluorescent colors, including blue, cyan, white, yellow and green, were emitted depending on the amount of added Q[8] host. In addition, electrostatic repulsions between the carboxylate groups and the carbonyl portals of the Q[8] host led to reversible conversion of the head-to-tail polymer assembly of Q[8]-**52** to the *J*-dimer complex at higher pH values, accompanied by a variation of emission from green to yellow. Accordingly, a smart stimulus-responsive tuning of fluorescent colors was achieved in a simple operation by using a single organic chromophore guest and a single macrocycle in solution.

The above work indicated that white-light emission could be fabricated by the two complementary blue (free **52**) and yellow fluorescence emissions (*J*-dimer complex of Q[8]-**52**), which could be efficiently generated independently in solution using the same excitation wavelength rather than energy transfer. However, it was noted that the yellow emission of the

https://doi.org/10.1021/acs.chemrev.1c01050
Chem. Rev. XXXX, XXX, XXX−XXX

J-dimer of Q[8]-**52** still appeared in the solid state, while free **52** exhibited aggregation in the solid state and emitted pale yellow emission at 554 nm. To inhibit its aggregation in the solid state, Q[7] was used to encapsulate **52**.[57] In the solid state, the 1:1 complex of Q[7]-**52** emitted at 487 nm, indicating that aggregation of **52** was strongly disrupted by the rigid Q[7] barrel confined structure. Most interestingly, it was found that the Q[7]-**52** complex and the *J*-dimer complex of Q[8]-**52** shared the same UV−vis absorption peaks, indicating that the two fluorescence emissions (blue and yellow) could be independently excited by the same wavelength (Figure 37).

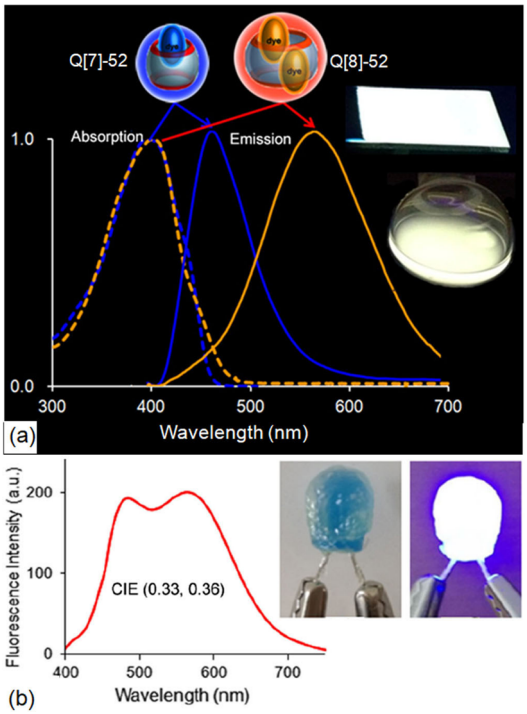

Figure 37. (a) Normalized absorption and fluorescence spectra from Q[7]-**52** and Q[8]-**52** in solution. (b) Fluorescence spectra of the solid mixture of Q[7]-**52** and Q[8]-**52** with CIE (0.33, 0.36) and white light from an ultraviolet LED chip. Reproduced with permission from ref 57. Copyright 2018 American Chemical Society.

This feature enables efficient production of pure white light by mixing the solid Q[7]-**52** complex and the *J*-dimer of Q[8]-**52** in the correct proportion in a single-dye system. To demonstrate the practical application of this approach, a white-light-emitting diode was fabricated by coating a poly(methyl methacrylate)-fixed solid mixture of Q[7]-**52** and Q[8]-**52** on the surface of a commercially available ultraviolet LED chip. Bright white light was observed at a potential of 3.8 V. Compared to the white-light emission produced by energy transfer between different fluorophore dyes, this study provided an excellent example of the advantages of Q[*n*]-based host−guest complexation and the corresponding macrocyclic confinement in preparing multicolor luminescent materials that do not rely on the principle of FRET through "single excitation with multiple independent emissions".

As another example of a highly fluorescent linear supramolecular polymer, a cyanostilbene derivative bearing pyridinium moieties (**53**) has been used as the monomer guest to complex with the Q[8] host (Figure 38).[59] Monomer

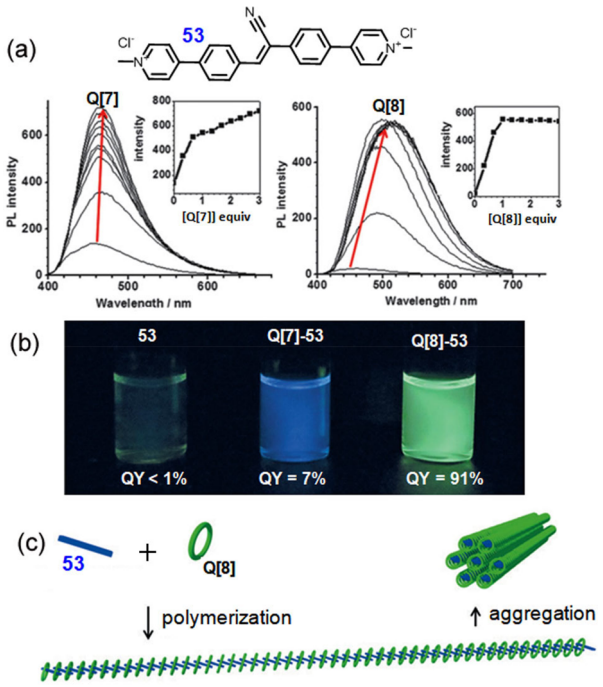

Figure 38. (a) Chemical structure of **53** and fluorescence spectra of **53** in the presence of increasing concentrations of Q[7] and Q[8] in water. (b) Fluorescence photo images and the QYs of **53**, Q[7]-**53**, and Q[8]-**53**. (c) Schematic representation of Q[8]-**53** polymer formation. Reproduced with permission from ref 59. Copyright 2016 Wiley-VCH.

53 displayed weak fluorescent emission in water due to AIE. Upon formation of a 1:1 complex with Q[7], a slight red-shift was observed in the florescence emission (from 460 to 464 nm) of **53** and the QY increased from 1% to 7%. When Q[8] was added to the solution of **53**, dramatically enhanced green emission at 516 nm with a high QY of 91% was observed, attributed to formation of a 1D supramolecular polymer. The supramolecular polymer formation was investigated in detail by a combination of ITC, dynamic light scattering, matrix-assisted laser desorption/ionization time-of-flight mass spectrometry, and TEM. The red-shifted fluorescence emission was ascribed to *J*-type alignment of **53** inside the Q[8] cavity. In particular, the high QY is mainly due to the synergistic enhancement of the radiative decay channel and the restricted intramolecular rotation of the chromophore (AIE effect) by the confinement effect of the Q[8] cavity and the resulting rigid polymer structures.

In 2017, the same group reported an elegant example of a light-harvesting supramolecular block copolymer system using three other cyanostilbene derivatives **54**, **55**, and **56** (Figure 39a) under the confined space of the Q[8] host.[199] Similar to **53**, complexation of these derivatives with the Q[8] host afforded 1D homopolymers that displayed apparent fluorescence enhancement with three different colors (blue (480 nm), yellow (522 nm), and red (630 nm)) due to the AIE effect (Figure 39b). Subsequently, color tunable nanobundles Q[8]-**54**/Q[8]-**56** were obtained in aqueous solution as a consequence of their large spectral overlap (an important prerequisite for energy transfer). In this system, Q[8]-**54** acted as the donor because its emission at 480 nm overlapped appreciably with the absorption of Q[8]-**56** polymer at 464 nm. Upon gradual addition of Q[8]-**56** to the solution of

https://doi.org/10.1021/acs.chemrev.1c01050
Chem. Rev. XXXX, XXX, XXX−XXX

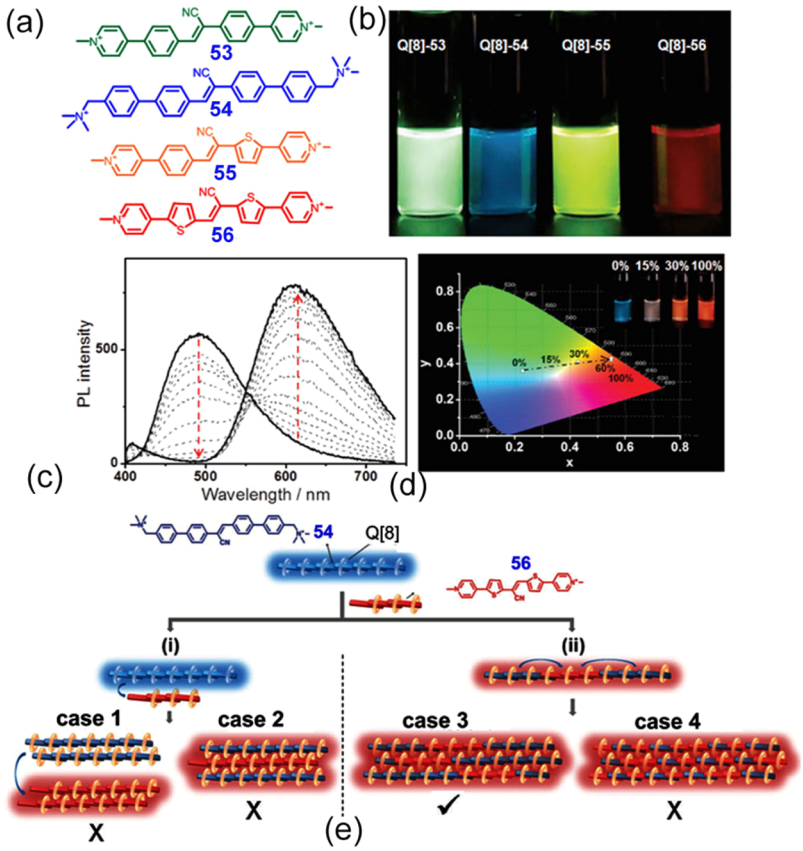

Figure 39. (a) Chemical structures of **53**−**56**. (b) Fluorescence photo images of Q[8]-**53**, Q[8]-**54**, Q[8]-**55**, and Q[8]-**56** in water under 365 nm UV light. (c) Fluorescence spectra of Q[8]-**54** in water upon addition of Q[8]-**56** from 0 to 1 equiv. (d) CIE chromaticity diagram showing the fluorescence changes of the Q[8]-**54** 1:1 complex with different doping equivalents of the Q[8]-**56** 1:1 complex (0%, 15%, 30%, 60%, and 100%) in water, with the inserted photo of the light-harvesting system under 365 nm UV light. (e) Schematic representation of the four light-harvesting systems based on the supramolecular polymer assembly of Q[8] with **54** and **56**. Reproduced with permission from ref 199. Copyright 2017 Wiley-VCH.

Q[8]-**54**, the fluorescent color of the mixture was progressively tuned from blue to red, which was confirmed by photoluminescence intensities and CIE chromaticities (Figure 39c and d). In principle, four different copolymer assemblies could be present in the solution of Q[8]-**54**/Q[8]-**56** (Figure 39e). However, in the FRET system, the donor−acceptor distance is an important factor in the efficiency of energy transfer. So, Case 1 was easily eliminated because the altered concentration of the mixture did not induce any obvious changes in the photoluminescence spectrum. In addition, because of the slight change in the UV−vis spectrum, Case 3 was considered to be more reasonable than Case 2 and Case 4, since it is believed that no changes of the absorption peaks would be caused by Case 2 or Case 4. The higher binding constant of monomer **56** toward Q[8] (**56** had >10^4-fold higher affinity than **54**) also supported the structure in Case 3. The efficient energy transfer of the dynamic supramolecular block copolymer system in this work indicated that Q[8] cavity confined supramolecular assemblies have outstanding properties for light-harvesting and photoluminescent applications.

In another study in 2018, Liu and co-workers reported a binary supramolecular assembly that exhibited near-infrared emission by combination of Q[8] triggered 1D linear supramolecular polymers and amphiphilic calixarenes (SC4AD) (Figure 40).[200] Anthracylpyridinium derivative (**57**) emitted very weak fluorescence emission at 625 nm in water due to $\pi-\pi$ stacking of the anthracene rings and an intramolecular charge transfer effect between the anthracene and pyridinium moieties. Addition of Q[8] to the aqueous solution of **57** produced a red-shifted, much brighter emission at 655 nm due to the formation of a rigid *J*-type linear polymer in the Q[8] cavity under the corresponding macrocyclic-confinement effect, which was classified as the first-stage emission. The initially formed supramolecular polymers were transformed into nanorod-like 3D structures by self-aggregation in water. When amphiphilic SC4AD was added to the solution of nanorods, a morphological transition to nanoparticles was accompanied by further fluorescence enhancement at 655 nm. As a control experiment, encapsulation of **57** in the SC4AD cavity gave emission at 605 nm, which indicated that the fluorescence enhancement was due to formation of Q[8]-**57**-SC4AD ternary aggregates (Figure 40b and c). The rigid nanoparticle assemblies of Q[8]-**57**-SC4AD not only further limited the single-bond rotation of **57** but also provided a hydrophobic environment from the self-assembly-induced confinement effect[52] to enhance the emission of **57**. This assembly mode was proposed as the second-stage enhancement of fluorescence (Figure 40d). The excellent brightness of the NIR emissive nanoparticles was exploited as a cell imaging agent (Figure 40e−g).

Liu, Stoddart, and co-workers reported a photoresponsive supramolecular fluorescent system using a combination of cationic supramolecular nanofibers derived from a styrylpyridinium conjugated diarylethene derivative (**58**) with Q[8] and

https://doi.org/10.1021/acs.chemrev.1c01050
Chem. Rev. XXXX, XXX, XXX−XXX

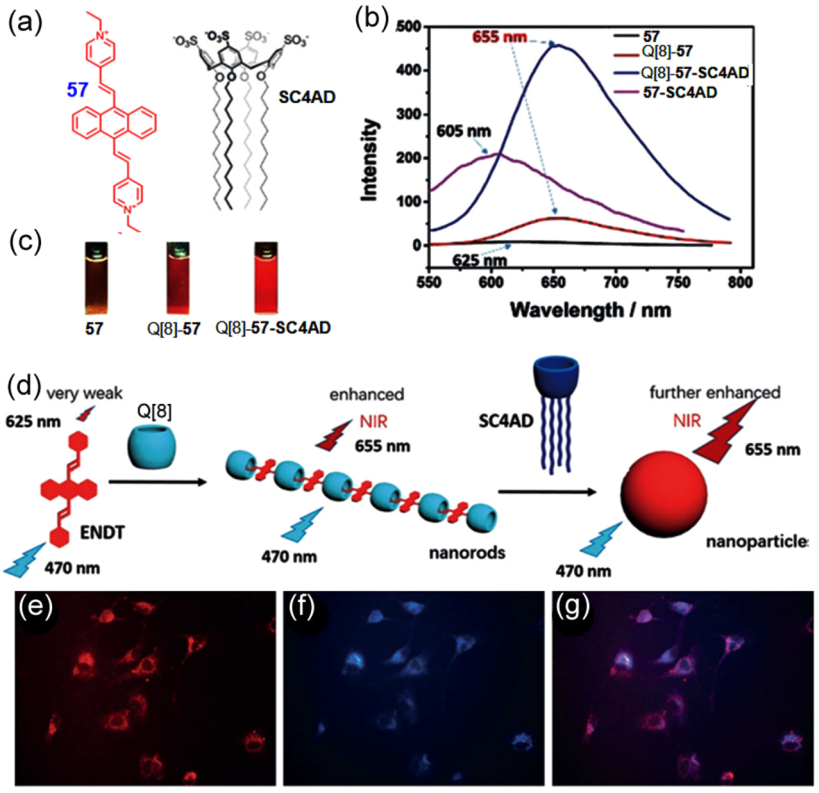

Figure 40. (a) Chemical structures of **57** and SC4AD. (b) Fluorescence spectra of **57**, Q[8]-**57**, Q[8]-**57**-SC4AD, and **57**-SC4AD. (c) Photo images of **57**, Q[8]-**57**, and Q[8]-**57**-SC4AD. (d) Schematic representation of NIR fluorescent supramolecular assemblies and related supramolecular aggregates and CLSM images of A549 cells costained with (e) Q[8]-**57**-SC4AD and (f) LysoTracker Blue. (g) Merged image of Parts e and f. Reproduced with permission from ref 200. Copyright 2018 Wiley-VCH.

anionic carbon dots (CDs) (Figure 41).[201] In aqueous solution, **58** could be reversibly converted between an open-ring form (**58-OF**) and a closed-ring form (**58-CF**) by UV-light (254 nm) and visible-light (>600 nm) irradiation (Figure 41a). When Q[8] was added to the solution of **58-OF**, TEM and AFM images revealed that micrometer-sized 1D nanofibers were formed. The red-shifted absorption (from 395 to 420 nm) and fluorescence emission (from 560 to 582 nm with a 16-fold increase of intensity) indicated that a *J*-type linear polymer of the styrylpyridinium moieties was present in the Q[8] cavity with strong macrocyclic confinement.

The reversible photoreaction was also observed with Q[8]-**58-OF**. For instance, the fluorescence intensity of Q[8]-**58-OF** at 582 nm was gradually quenched upon irradiation with UV light (254 nm, 2.0 min). The yellow emission was recovered by irradiating this weakly emissive solution with visible light (>600 nm, 40 s) (Figure 41b). These results suggested that the composition of **58** could be interconverted between **58-OF** and **58-CF** in the host−guest complex upon light irradiation, with outstanding photoconversion cycles. In an attempt to fabricate a multicolor emissive system, CDs with anionic carboxylates on their surface that emitted blue light (λ_{em} = 458 nm) were combined with the host−guest polymer solution. Large spherical nanoparticles with ∼700 nm diameter were formed by binding of the anionic CDs to the positively charged nanofibrils via electrostatic interactions (Figure 41e). Consequently, different fluorescent colors could be obtained by varying the ratio of CDs and Q[8]-**58-OF** or by photoirradiation. For example, multiple fluorescent emissions from blue to yellow were obtained by addition of increasing concentrations of Q[8]-**58-OF** to the solution of CDs (Figure 41c). When the same aqueous solution of CDs-Q[8]-**58-OF** was irradiated with UV light (254 nm), the emission peak at 582 nm decreased dramatically, with only a slight reduction in the emission at 458 nm (Figure 41d). As a result, reversible fluorescent color changes from yellow to blue, including pure white-light emission, were triggered by UV-light irradiation (Figure 41f). The emission reverted to yellow from blue upon visible-light (>600 nm) irradiation. It is expected that such confined structure triggered photoresponsive luminescent emissions have potential applications in the design of anticounterfeiting materials and photocontrolled molecular switches.

Very recently, Liu and co-workers further reported that Q[8]-based fluorescent polymers could be utilized as two-photon agents with the assistance of *β*-cyclodextrin-modified hyaluronic acid (HA-CD) (Figure 42a).[202] Guest **59** displayed very weak fluorescence at 650 nm in aqueous solution. After assembly with Q[8], two-axial netlike supramolecular polymers Q[8]-**59** (which further aggregated to nanosquares in water) were formed with enhanced and red-shifted fluorescence at 680 nm. When the cancer cell-targeting agent HA-CD was added to the solution of Q[8]-**59**, the nanosquare structure was converted to nanoparticles via secondary assembly, accompanied by further enhancement of the NIR emission at 680 nm (Figure 42b). In addition, because **59** has a classical D−*π*−*A* structure, the strong push−pull dipolar effect and large conjugation lengths favor two-photon absorption. As expected, the fluorescence spectrum of Q[8]-**59**-HA-CD displayed similar emission peaks when excited at 840 nm

https://doi.org/10.1021/acs.chemrev.1c01050
Chem. Rev. XXXX, XXX, XXX−XXX

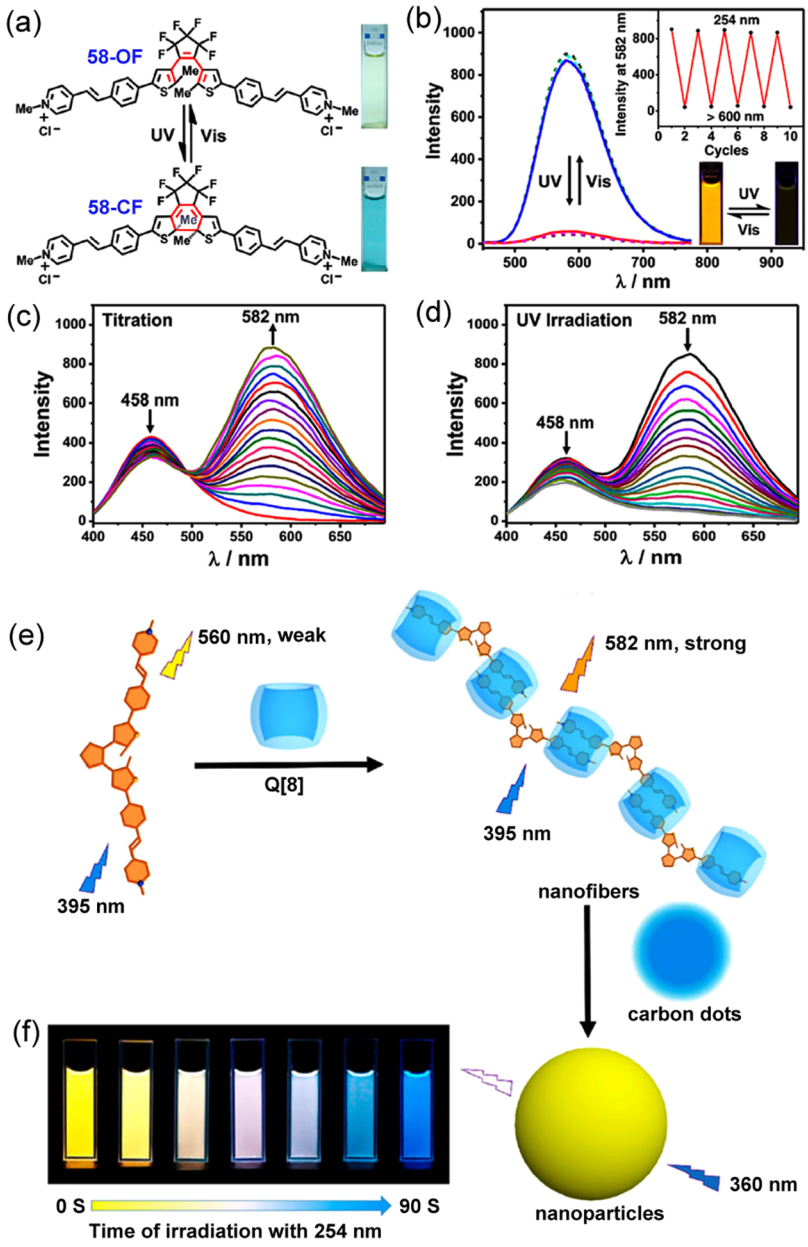

Figure 41. (a) Chemical structures and photo images of **58** upon alternating irradiation with UV and visible light. (b) Emission spectra and intensity (insert) changes of Q[8]-**58-OF** at 582 nm upon alternating irradiation with UV (254 nm, 2.0 min) and visible light (>600 nm, 40 s) in water. (c) Fluorescence spectra of CDs with increasing concentrations of Q[8]-**58-OF** in a neutral water. (d) Fluorescence spectra of CDs-Q[8]-**58-OF** upon irradiation with UV light (254 nm, 1.5 min) in a neutral water. (e) Schematic representation of the in situ photoswitched multicolor luminescence supramolecular assembly. (f) Fluorescence photo images of CDs-Q[8]-**58-OF** upon irradiation with 254 nm light. Reproduced with permission from ref 201. Copyright 2019 American Chemical Society.

and upon one-photon excitation at 450 nm. This system has been successfully exploited for mitochondrial-targeted cell imaging of A549 cancer cells (Figure 42c). It should be noted that the macrocyclic-confinement effect of the Q[8] host is the key factor in amplification of the two-photon signal in this system by promoting the ICT effect between the D−A moieties of **59**.

5.4. Fluorescence Emission from Q[8]-Based Supramolecular Organic Frameworks (SOFs)

Supramolecular organic frameworks (SOFs)[203,204] are a new type of porous framework that are assembled by noncovalent interactions, including hydrogen bonds, $\pi-\pi$ stacking, and van der Waals interactions. Since the driving force for their synthesis stems from diverse supramolecular interactions, SOFs are generally easy to assemble and show good reversibility. Notably, the ternary binding ability of Q[8] has unique advantages for the construction of fluorescent SOFs by employing appropriately π-conjugated chromophore guests. So far, Q[8]-based fluorescent SOFs have mostly been derived from TPE derivatives.[205−211] These form 2D nanostructures with high AIE fluorescence since complex binding induces restricted intramolecular rotation and *J*-type stacking of the TPE chromophore guests inside the Q[8] confined cavity. Compared to the 1D polymers, the 2D SOF assemblies provide a more rigid scaffold to extend the confinement effect of Q[8] host.

https://doi.org/10.1021/acs.chemrev.1c01050
Chem. Rev. XXXX, XXX, XXX−XXX

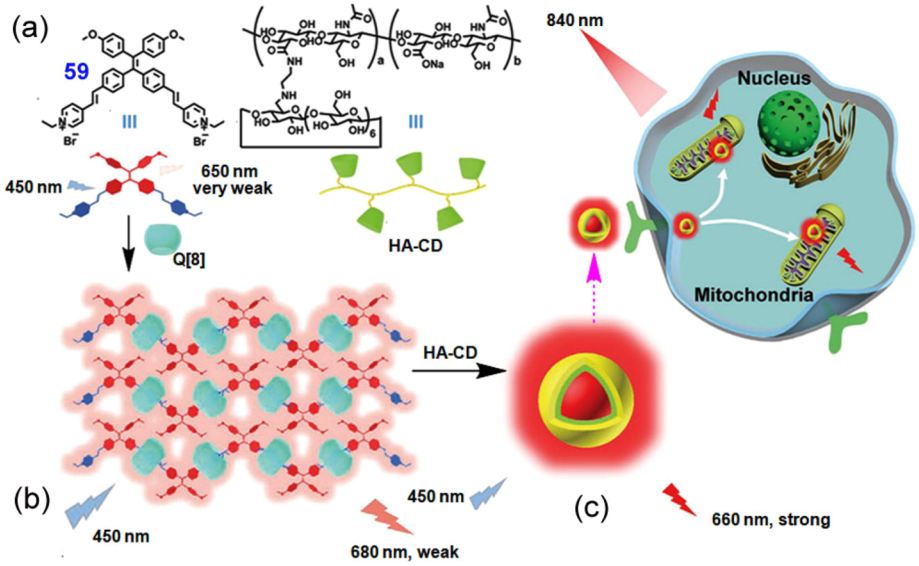

Figure 42. (a) Chemical structures of **59** and HA-CD. (b) Formation of a supramolecular nanoparticle with NIR emission. (c) Supramolecular nanoparticle with NIR emission used for two-photon mitochondria targeted imaging of the A549 cell. Reproduced with permission from ref 202. Copyright 2021 Wiley-VCH.

For example, Zhao and co-workers reported supramolecular 2D nanostructures with bright fluorescence by combining Q[8] with guest **60** (Figure 43).[205] As expected, non-

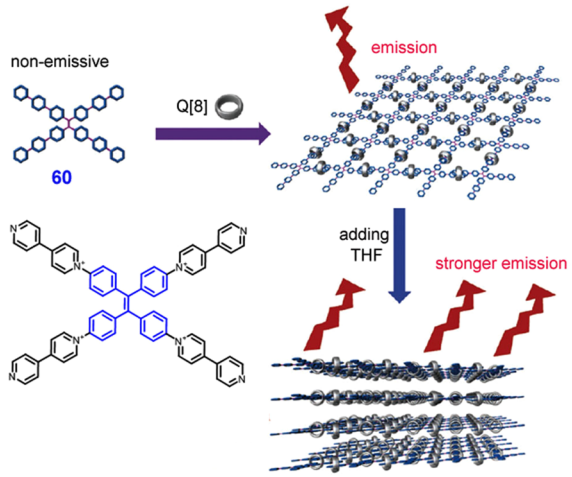

Figure 43. Chemical structure of **60** and schematic representation of the formation of a 2D SOF from the Q[8]-**60** complex and enhancement of fluorescence by THF in water. Reproduced with permission from ref 205. Copyright 2015 Royal Society of Chemistry.

fluorescent emission was observed for the TPE-derived cationic guest **60** because of its greater solubility in water. Remarkably enhanced fluorescence emission was observed when Q[8] was complexed with the four arms of **60** to form a monolayered 2D SOF in water. Moreover, the emission of the monolayered SOF underwent further enhancement when a poor solvent, such as THF, was added to the aqueous solution due to the presence of stacked layers together with the primary 2D layered structures.

Cao and co-workers demonstrated another type of Q[8]-based fluorescent and shape controllable SOF (Figure 44a).[206] TPE derivatives **61** and **62** were synthesized, containing pyridinium and vinyl-pyridinium moieties, respectively, as the four arms. Addition of Q[8] to the solution of **61** produced a 1:2 complex of Q[8]-**61**, and the fluorescence emission of **61** was red-shifted from 579 to 632 nm with a slight enhancement of the QY (from 6.7% to 7.4%) (Figure 44b). Similar stoichiometry and photophysical behaviors were observed for the Q[8]-**62** complex in aqueous solution (35.8%) in the presence of 2.0 equiv of Q[8], but the red-shifted emission (722 nm) had lower QY efficiency (0.6%) compared to the original orange emission (640 nm) of **62** (Figure 44c). Interestingly, planar and curved layers of SOFs from the host–guest interactions of Q[8] with **61** and **62** were formed first, which eventually aggregated to form regular supramolecular cuboids of Q[8]-**61** (Figure 44d) and flattened spheroids of Q[8]-**62** (Figure 44e), respectively. Dynamic reversibility of the guest inside the Q[8] cavity allowed the SOFs to be dissociated in the presence of a competitive guest, such as 3,5-dimethyl-1-adamantylamine·HCl (Me_2ADA), which has a higher binding constant with Q[8] compared to **61** and **62**, thereby leading to the recovery of the original fluorescence of **61** and **62** in water. The fluorescence emission of Q[8]-**62** was used for imaging of HeLa cells (Figure 44f and g). This result indicated that the extend macrocyclic-confinement effect of the Q[8] host is not always conducive to high quality luminescence in the supramolecular polymers, and the mechanism of the fluorescence quenching is not clear so far.

The same group later discovered that an achiral Q[8]-based fluorescent SOF exhibited adaptive chirality in the presence of L-/D-phenylalanine (Phe) in water due to the dynamic rotational conformation of the TPE groups in the confined Q[8] cavity.[207] From a structural viewpoint, TPE molecules can exist as anticlockwise-type (*M*) and propeller-like clockwise-type (*P*) due to the rotational conformation of the four phenyl rings. Therefore, the TPE moiety was designed as the dynamic chirality-responsive component and fluorophore of guest **63**, with four coumarin arms as linking units at the terminus for dimerization inside the Q[8] cavity (Figure 45a). As expected, a 2D SOF of Q[8]-**63** was stably formed with strong fluorescence enhancement in aqueous media due to the extended confinement effect from the Q[8] cavity to the

https://doi.org/10.1021/acs.chemrev.1c01050
Chem. Rev. XXXX, XXX, XXX−XXX

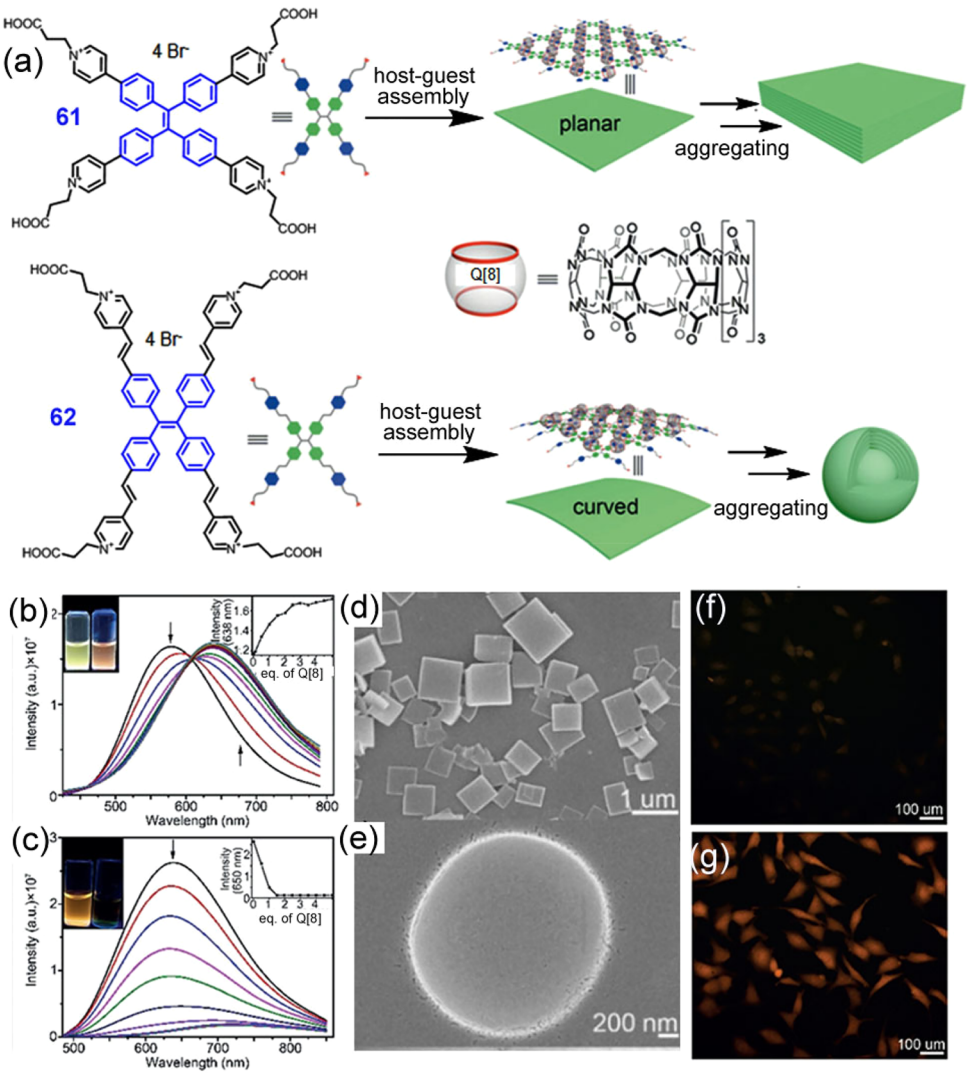

Figure 44. (a) Chemical structures of **61** and **62** and schematic representations of related formation of supramolecular network-type layers and frameworks. Florescence spectra of **61** (b) and **62** (c) with increasing concentrations of Q[8] in water (pH 6.3). SEM images of (d) Q[8]-**61** and (e) Q[8]-**62**. CLSM of HeLa cells costained with (f) Q[8]-**62** and (g) the addition of Me_2ADA. Reproduced with permission from ref 206. Copyright 2018 Wiley-VCH.

polymer structure. A Cotton effect experiment suggested that the TPE units in the SOFs adopted a racemic rotational conformation, indicating that homodirectional rotational *P* or *M* conformations were not induced by SOF assembly. However, the high selectivity of the SOFs toward Phe led to discovery of the adaptive chirality property of the SOFs via ternary host−guest assemblies between the Q[8] cavity and the Phe/pyridinium-coumarin arm of **63**. As shown in Figure 45b, addition of L-Phe to the solution of Q[8]-**63** induced a remarkable positive Cotton effect at 323−470 nm, while a similar negative Cotton effect was induced at 323−470 nm when D-Phe was added to the SOFs solution. The mirror-image circular dichroism spectra confirmed the adaptive chirality of Q[8]-**63** with *P* or *M* rotational conformations of the TPE groups (*M*-TPE and *P*-TPE exhibit similar positive and negative circular dichroism signals, respectively) being induced by the enantiomers. In other words, the suitable larger confined space of the Q[8] cavity, which enables the dynamic reversibility of Q[8]-**63** binding with chiral guests, is the key factor to form the secondary supramolecular assembly, in which the chirality of chiral guests can be transferred to the SOFs by tuning the homodirectional (*P* or *M*) rotation of the TPE units. The authors also found that the adaptive chirality of the SOFs could be induced by small amounts of ATP or ADP via electrostatic interactions (Figure 45c). This result provides new insights for fabrication of chiral host−guest assemblies under the suitable confinement effect.

Continuing study of the confinement assembly of Q[8] with TPE derivatives, Tang and co-workers developed a series of Q[8]-TPE-based supramolecular fluorescent emission systems for cell line identification, cell contamination evaluation, and cancer cell discrimination.[208] As shown in Figure 46a, three guests (**64**−**66**) were simply synthesized by appending different numbers of vinyl-pyridinium groups to the TPE core and used to construct various host−guest assemblies with Q[8], including linear supramolecular polymers, hyperbranched structures, and SOFs. Fluorescence spectra showed that all of the Q[8]-based TPE complexes exhibited similarly stronger fluorescence intensities than the corresponding free guests. However, bioimaging studies suggested that different fluorescent intensities were observed depending on the amount of these supramolecular assemblies accumulated in cells. For

https://doi.org/10.1021/acs.chemrev.1c01050
Chem. Rev. XXXX, XXX, XXX−XXX

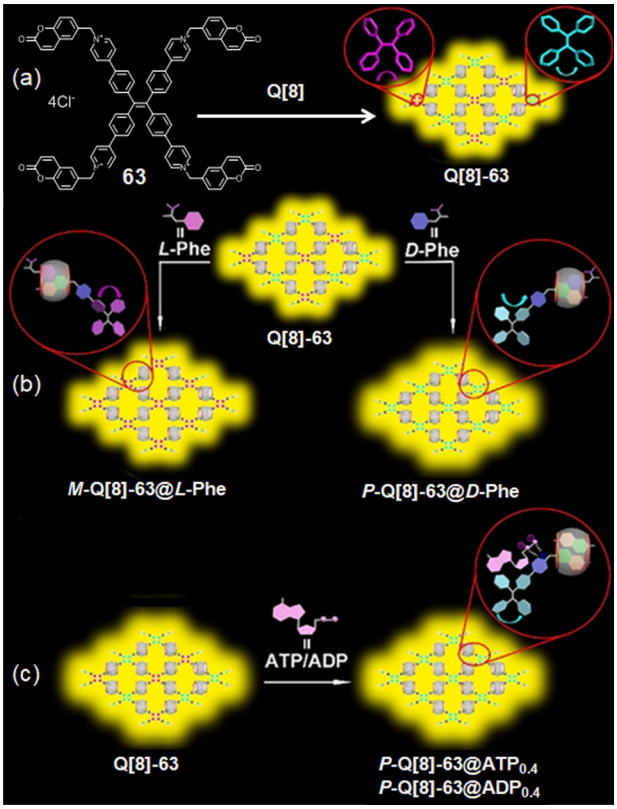

Figure 45. (a) Chemical structure of **63** and a schematic representation of the formation of SOFs of Q[8]-**63** via homodimerization between Q[8] and the two coumarin arms in **63**. (b) Adaptive chirality of SOFs of Q[8]-**63** induced by L-/D-Phe via heterodimerization with partial Q[8] and one coumarin arm of **63** on the SOFs. (c) Adaptive chirality of SOFs of Q[8]-**63** induced by ATP/ADP via electrostatic interactions (dashed lines) within the positively charged pores of the SOFs. Reproduced with permission from ref 207. Copyright 2021 Wiley-VCH.

example, the Q[8]-**64** complex stained both the cell membrane and the inside of the cells, while Q[8]-**65** and Q[8]-**66** assemblies were only observed inside the cells (Figure 46c). Overall, cells treated with Q[8]-**64** had the strongest fluorescence, followed by cells treated with Q[8]-**65** and then those treated with Q[8]-**66**. The authors proposed that this phenomenon was due to the differing sizes and shapes of the host–guest assemblies (Figure 46b). For example, the Q[8]-**64** assembly was the smallest and readily stained the cells. The behaviors of the Q[8]-**65** and Q[8]-**66** assemblies, which were a similar size, were influenced by their shapes. The spherical assemblies of Q[8]-**65** were taken up much more easily by cells than the square assemblies of Q[8]-**66**. Most interestingly, the authors found that the same types of host–guest assembly exhibited different fluorescence responses if incubated with different cell lines. For example, T24 cells (cancer) incubated with Q[8]-**64** for 20 min exhibited double growth ratio compared with SV-HUC-1 cells (normal). In other words, differences in the microscopic affinities of different cells for different supramolecular fluorescent assemblies in this work could be quickly converted into macroscopic fluorescent signals. The data were transformed into a general fingerprint using linear discriminant analysis, which enabled clustering and classification of all the cells, including normal cell lines, different cancer cell lines, and different metastasized cancer cell lines. In addition, these host–guest systems could also be used to evaluate cross-contamination of cell lines and for semiquantitative discrimination of cancer cells.

5.5. RTP Emission from Q[8]-Based Host–guest Assemblies

Unlike pure organic RTP emission from the 1:1 tight binding of phosphors in the rigid hydrophobic cavity of Q[6]/Q[7] with a strong macrocyclic-confinement effect to enhance intersystem crossing, pure organic RTP emission from Q[8]-based complexes is mainly due to the fixed dimer conformation of phosphors with a heavy atom effect in the Q[8] confined cavity. In other words, the high quality of the pure organic RTP emission of the Q[8] complex is partly due to the hydrophobic effect induced by the macrocyclic confinement and partly due to the confined space fixed distance of the phosphor in the Q[8] cavity. For instance, Ma and co-workers reported an example in aqueous solution using a Q[8]-based dimer assembly of **67**, in which two phosphor 4-(4-bromophenyl)pyridinium branches were linked to a triazine core (Figure 47a).[61] In the presence of Q[8] host, guest **67** was encapsulated to form a 2:2 quaternary complex. Single-crystal structure analysis provided unequivocal proof of the dimer assembly of **67**. As shown in Figure 47b, the phosphor 4-(4-bromophenyl)pyridinium groups were confined within the Q[8] cavity with cofacial parallel and staggered arrangements, producing a structure-restricted dimer with a new charge-transfer triplet state that gave yellow RTP emission at 565 nm in water under visible-light excitation (Figure 47c). The lifetime of the yellow emission was 0.19 ms. Notably, the greatly enhanced intensity of this band under N_2 atmosphere clearly suggested its phosphorescent nature. In addition, free guest **67** displayed blue fluorescence at 445 nm. Therefore, tunable emission color from blue to yellow, including white light, was achieved depending on the presence of different amounts of Q[8] in aqueous media through combination of dual fluorescence–phosphorescence emission (Figure 47d).

Similar work was reported by Liu et al. in 2021,[212] in which a 4-(4-bromophenyl)pyridinium-active pure organic RTP emission system based on Q[8] was fabricated by taking advantage of the Q[8] confined rigid hydrophobic cavity. The phosphor 4-(4-bromophenyl)pyridinium containing diethanolamine (**68**) assembled into a dimer structure in head-to-tail fashion due to the strong confinement of the Q[8] host (Figure 48). In particular, the hydrogen bonding between the Q[8] portals and **68** further strengthened the dimer assembly. Consequently, this inclusion form of the assembly promoted halogen bonding by shortening the distance between the carbonyl groups and bromine, leading to efficient phosphorescence from the host–guest complex in aqueous media.

On the basis of the above results, the authors subsequently reported the construction of another type of purely organic light-harvesting phosphorescence energy transfer system for mitochondria-targeted imaging.[213] In this system, 4-(4-bromophenyl)-pyridine-modified β-cyclodextrin (CD-PY) was the donor, rhodamine B (RhB) was the acceptor, Q[8] acted as a mediator, and adamantane-appended hyaluronic acid (HA-ADA) was the cancer-cell-targeting agent. The CD-PY donor remained silent with no RTP emission in the free state in water. RTP emission at 510 nm was activated when Q[8] was added to the solution to form a 1:2 supramolecular complex (Q[8]-CD-PY). Subsequently, the RhB acceptor,

https://doi.org/10.1021/acs.chemrev.1c01050
Chem. Rev. XXXX, XXX, XXX–XXX

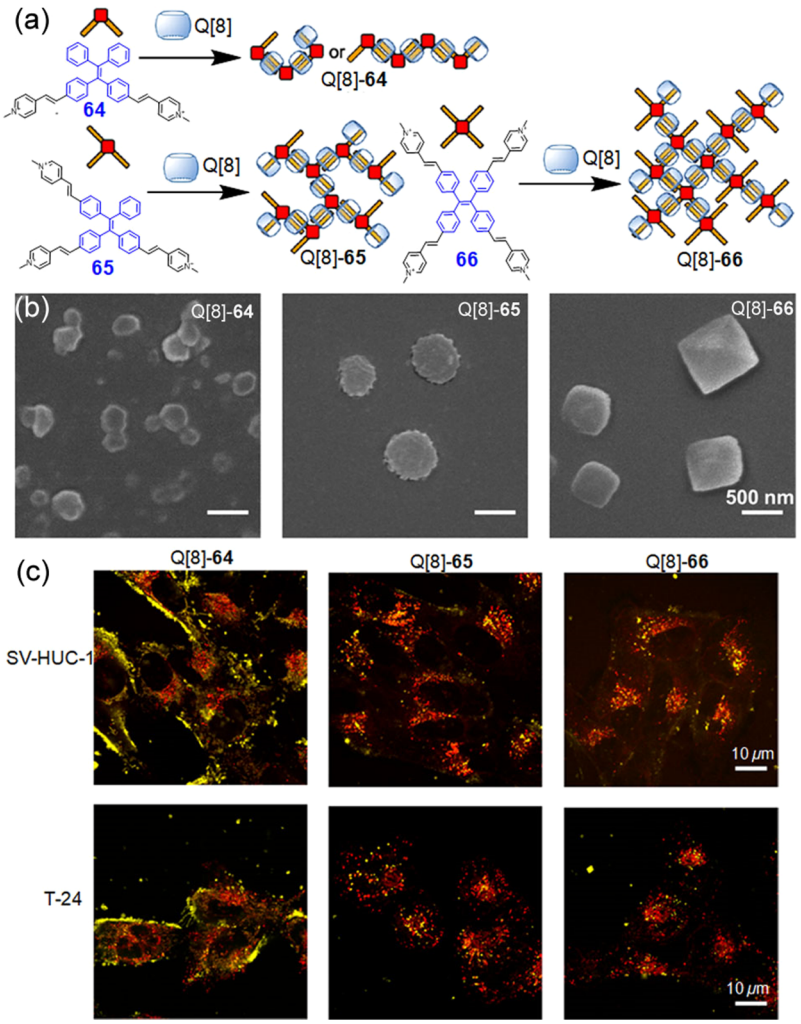

Figure 46. (a) Chemical structures of **64**−**66** and schematic representation of the formation of the supramolecular AIE complexes of Q[8]-**64**, Q[8]-**65**, and Q[8]-**66**. (b) SEM images of Q[8]-**64**, Q[8]-**65**, and Q[8]-**66**. (c) CLSM images of SV-HUC-1 cells (normal) and T24 cells (cancer) costained with Q[8]-**64**, Q[8]-**65**, and Q[8]-**66** at 37 °C. Reproduced with permission from ref 208. Copyright 2020. American Chemical Society.

which was included in the cavity of β-cyclodextrin and exhibited a broad absorption bond at 480−570 nm, was added to the solution of Q[8]-CD-PY. As a result, highly efficient energy transfer and an ultrahigh antenna effect (36.42) occurred between Q[8]-CD-PY and RhB, since there is ideal overlap of the absorption spectrum of RhB and the phosphorescence emission of Q[8]-CD-PY. Interestingly, enhanced delayed emission at 590 nm was observed when Q[8]-CD-PY@RhB was assembled with HA-ADA into nanoparticles (Figure 49a). Such supramolecular assembly induced delayed emission has been successfully exploited for mitochondria-targeted imaging of A549 cancer cells (Figure 49b). Herein, the Q[8] as mediator and the resulting confinement effect play the crucial role in the phosphorescence energy transfer system by switching the phosphorescence emission at 510 nm.

Similarly, Liu and co-workers further successfully fabricated an efficient ultralong purely organic RTP emission system from Q[8]-based supramolecular pins in the confined cavity (Figure 50).[214] Unlike the representative examples described above, in which the two 4-(4-bromophenyl)pyridine-modified guests were simultaneously encapsulated by Q[8] in a head-to-tail complex fashion, the supramolecular pins have one guest included in the Q[8] cavity with a head-to-head complex model under the macrocyclic-confinement effect. As shown in Figure 50a, fluorophore guest **69** was synthesized from phenylpyridinium salt with donor−acceptor moieties linked by an alkyl chain. Guest **69** formed a 1:1 complex with the Q[8] host, in which the bromo-substituted group was folded back and stacked with the thioether-substituted phenylpyridinium moiety in the Q[8] confined cavity, and an effective ICT was triggered (Figure 50b). The effective ICT further increased the rate of intersystem crossing by reducing the energy gap between singlet and triplet states of the fluorophore, which thereby led to an efficient red-shifted RTP emission. Additionally, the strict encapsulation of the guest in the Q[8] confined cavity and the resulting formation of intramolecular halogen bonds also favored RTP emission by increasing the rate of radiative decay of **69** from T_1 to S_0. As a result, RTP emission at 628 nm appeared after addition of Q[8] with a lifetime of 133 μs. The remarkably enhanced intensity of this band upon vacuum degassing of the solution further confirmed the phosphorescent nature of the supramolecular pins. In order to reduce the ACQ-induced nonradiative transition of phosphors, polyacrylamide, poly(vinyl alcohol), and γ-cyclodextrin (ratio of phosphors was

https://doi.org/10.1021/acs.chemrev.1c01050
Chem. Rev. XXXX, XXX, XXX−XXX

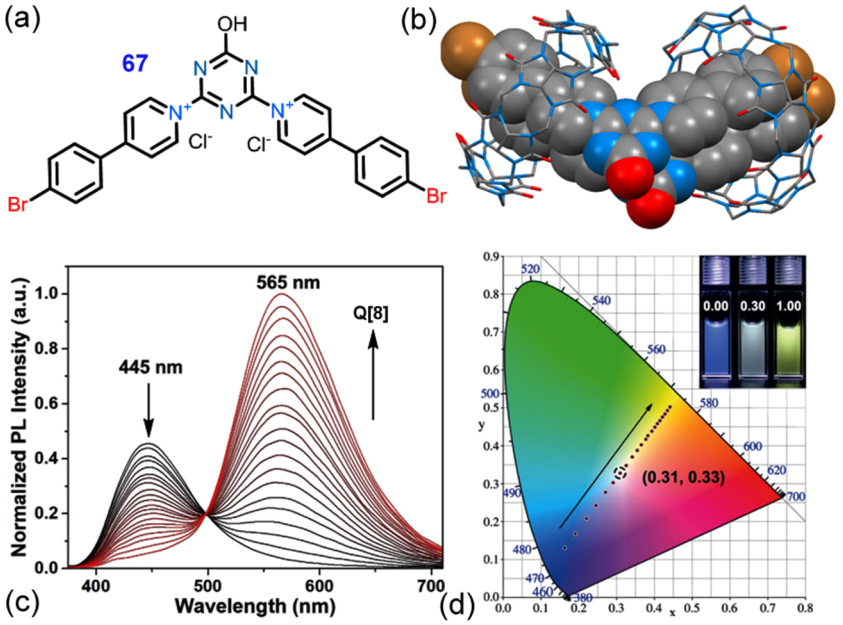

Figure 47. (a) Chemical structure of **67**. (b) X-ray crystal structure of Q[8]-**67**. (c) Normalized emission spectra of **67** with increasing concentrations of Q[8] from 0 to 1.0 equiv in water at 298 K. (d) CIE of **67** with different amounts of Q[8]. Inset: photographs of **67** with 0, 0.3, and 1.0 equiv of Q[8] in water. Reproduced with permission from ref 61. Copyright 2020 Wiley-VCH.

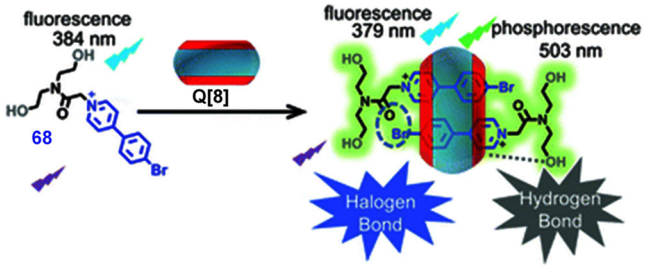

Figure 48. Chemical structure of **68** and schematic illustration of the phosphorescent supramolecular assembly of Q[8]-**68**. Reproduced with permission from ref 212. Copyright 2021 Royal Society of Chemistry.

5%) were added to the solution of Q[8]-**69**. The solution was then dripped onto treated filter paper. It was found that the phosphorescent material in the filter paper exhibited the highest phosphorescence QY (99.38%) with a visible afterglow lasting up to 110.2 ms. Benefiting from the red-shift of the absorption peak of the host−guest interaction-induced ICT, the red phosphorescence of the supramolecular pins was used for cell imaging, exhibiting good colocalization with Mito-Tracker Green (mitochondria marker) (Figure 50d).

6. SUPRAMOLECULAR ORGANIC LUMINESCENT EMISSIONS FROM THE Q[10] HOST

Although the larger homologues *t*Q[13−15],[35,36] containing more glycoluril units than Q[10], have been synthesized by Tao and co-workers in recent years, their cavities are no larger

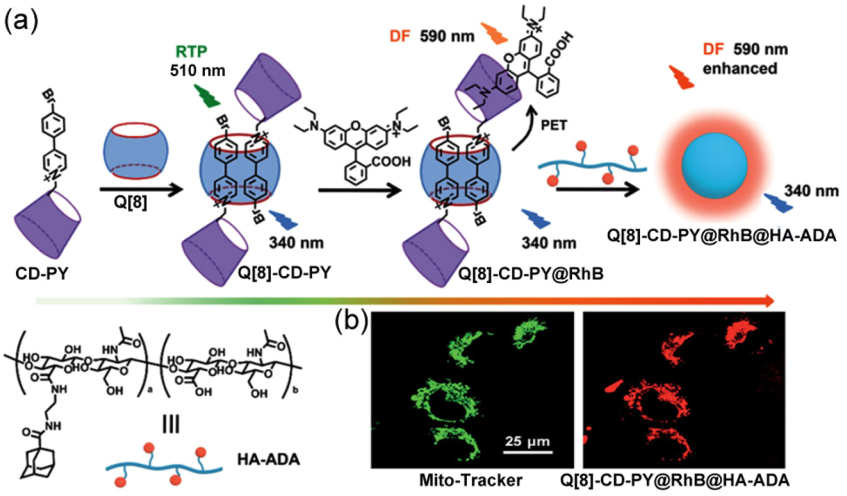

Figure 49. (a) Schematic representation of construction of the supramolecular assembly for a purely organic light-harvesting phosphorescence energy transfer system and related molecules. (b) CLSM images of A549 cells costained with Mito-Tracker Green and Q[8]-CD-PY@RhB@HA-ADA. Reproduced with permission from ref 213. Copyright 2020 Royal Society of Chemistry.

https://doi.org/10.1021/acs.chemrev.1c01050
Chem. Rev. XXXX, XXX, XXX−XXX

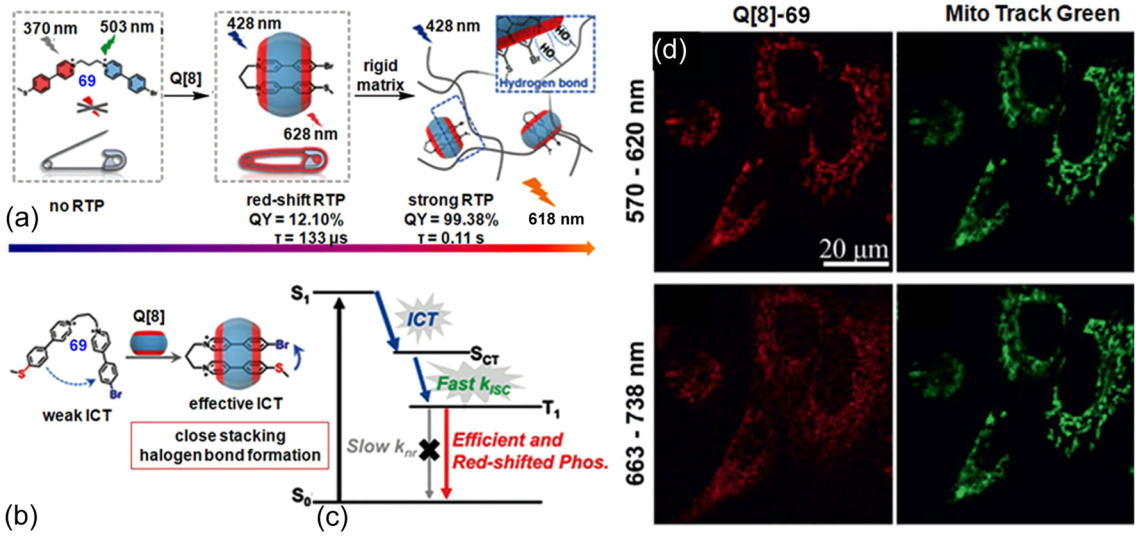

Figure 50. (a) Schematic illustration of the formation of supramolecular pin Q[8]-**69**. (b) Proposed mechanism of the enhancement of ICT resulting from molecular folding. (c) Possible mechanism of efficient and red-shifted phosphorescence. (d) CLSM images of A549 cells incubated with Q[8]-**69**. Reproduced with permission from ref 214. Copyright 2021 Wiley-VCH.

than that of Q[8] because of their "twisted" conformations. Consequently, Q[10] has the largest cavity of the Q[*n*] family.[34] It is expected that there are many opportunities for the development of unique supramolecular systems based on the Q[10] host. In the light-emission field, reported studies indicate that the capacious cavity of Q[10] makes it possible to include bulkier dyes with stronger macrocyclic-confinement effects,[215−218] and the resulting enhanced luminescent emission systems have potential application as chemosensors and in cell imaging.[219−224]

Wallace and co-workers reported host−guest complexes of Q[10] with a series of iridium(III) polypyridyl complexes (Figure 51).[225,226] It was suggested that there was an obvious blue-shift and enhanced luminescence of these cyclometalated complexes with a 1:1 molar ratio. The larger cavity of Q[10] enables accommodation of the whole cyclometalated complex (**IrCHO**) fully within the rigid confined cavity with the strong confinement effect, which thus shortens the metal−ligand bonds and increases the ligand-field strength. As a result, this host−guest complex behavior is expected to lower $d-\pi$ levels and, hence, raise the metal-to-ligand charge-transfer energy to produce an enhanced blue-shifted emission. Utilizing the larger cavity of Q[10], a [2]rotaxane with a Q[10] wheel and a TPE-ended axle was described by Cao and co-workers.[227] The axle guest was synthesized by appending two TPE groups as the end stopper groups on a positively charged 4,4′-bipyridine parent. This was included in the cavity of Q[10] through ion−dipole interactions in dimethyl sulfoxide after heating at 95 °C. Encapsulation of the axle efficiently restricted rotation of the TPE moieties, turning on fluorescent emission. The addition of a poor solvent to the [2]rotaxane solution further induced an AIE phenomenon. Later, Liu and co-workers revealed that the TPE moiety can be included in the Q[10] cavity, and remarkable fluorescence enhancement was observed due to the restricted intramolecular rotation of TPE under the confinement effect of the Q[10] host.[218]

In 2017, Ni et al. reported a unique Q[10]-$[Cd_4Cl_{16}]^{8-}$-based pillared diamond porous supramolecular framework Q[10]-SOFs-**1** by mixing Q[10] and $CdCl_2$ in aqueous HCl (8.0 mol/L) at room temperature.[228] The X-ray crystal

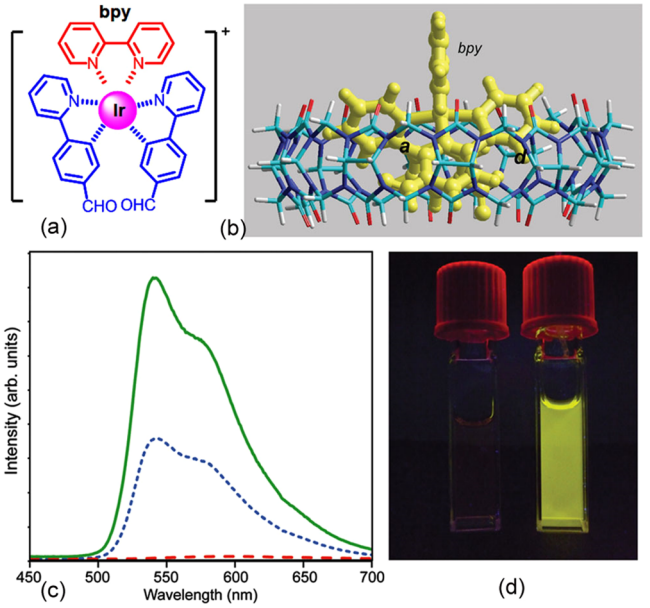

Figure 51. (a) Chemical structure of the iridium(III) complex $[Ir(ppy\text{-}CHO)_2(bpy)]^+$ (ppy-CHO = 2-pyridinebenzaldehyde, bpy = 2,2′-bipyridine) (**IrCHO**). (b) Molecular representation of **IrCHO** encapsulated within Q[10]. (c) Emission spectra in aqueous buffer solution (pH 4.7) at 22 °C: free **IrCHO** (dashed, red); with added Q[10] in 1:1 molar ratio (dotted, blue); and with excess Q[10] (solid, green). (d) Fluorescence images of free **IrCHO** (left) and Q[10]-encapsulated **IrCHO**. Reproduced with permission from ref 225. Copyright 2013 Royal Society of Chemistry.

structure revealed that the 3D-open-nanotube-based pillared diamond framework was assembled through outer-surface interactions of Q[10] and poly(cadmium chloride) cluster anions ($[Cd_4Cl_{16}]^{8-}$) (Figure 52). SOFs-**1** was dipped into acetonitrile/water (9:1, v/v) solutions containing rhodamine B (**70a**), pyrenemethanamine hydrochloride (**70b**), and bath-ocuproine hydrochloride (**70c**). These guest dyes were efficiently adsorbed by Q[10]-SOFs-**1** to form solid RGB fluorescent materials with excellent luminescent properties, including high QY, as a consequence of the confinement effect

https://doi.org/10.1021/acs.chemrev.1c01050
Chem. Rev. XXXX, XXX, XXX−XXX

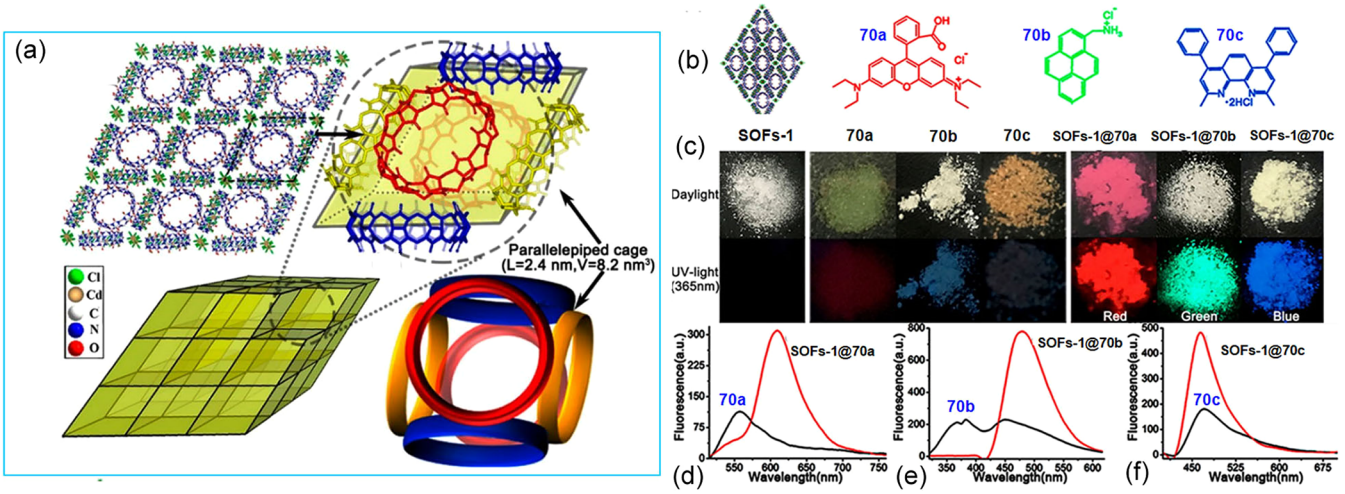

Figure 52. (a) Crystal stacking structure and schematic representation of the 3D open-nanotube-based pillared diamond framework of Q[10]-SOFs-**1** through the outer-surface interactions of Q[10] with $[Cd_4Cl_{16}]^{8-}$. (b) Structures of the microcrystal of Q[10]-SOFs-**1@70a-c**. (c) Comparison of the colors of Q[10]-SOFs-**1**, **70a**, **70b**, **70c**, Q[10]-SOFs-**1@70a**, Q[10]-SOFs-**1@70b**, and Q[10]-SOFs-**1@70c** under daylight and UV light (365 nm). (d) Fluorescence spectra of solid **70a** and Q[10]-SOFs-**1@70a**. (e) Fluorescence spectra of solid **70b** and Q[10]-SOFs-**1@70b**. (f) Fluorescence spectra of solid **70c** and Q[10]-SOFs-**1@70c**. Reproduced with permission from ref 228. Copyright 2017 American Chemical Society.

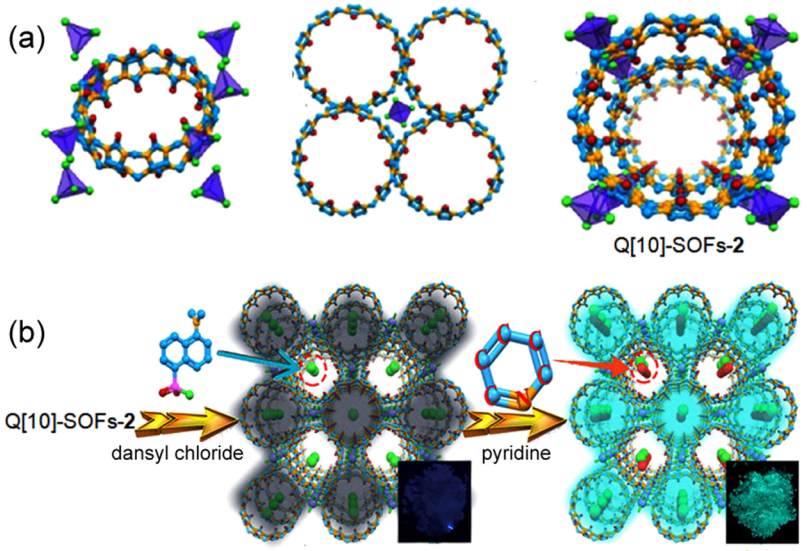

Figure 53. (a) Crystal structures of Q[10]-SOFs-**2**. (b) Schematic representation of the sensing mechanism of Q[10]-SOFs-**2** for pyridine. Reproduced with permission from ref 229. Copyright 2021 American Chemical Society.

from the open portal size and large cavity of Q[10]. The ACQ effect of these dyes in the solid state was inhibited by the numerous regular nanopores of Q[10]-SOFs-**1**, isolating the fluorophores by loading them into the rigid confined cavities and channels under the nanoconfinement effect. Consequently, three solid-state fluorescent materials with efficient red, green, and blue emission were successfully fabricated from Q[10]-SOFs-**1@70a**, Q[10]-SOFs-**1@70b**, and Q[10]-SOFs-**1@70c**, respectively. A white-light-emission system with CIE coordinates (0.32, 0.28) was obtained by simple mixing of Q[10]-SOFs-**1@70a**, Q[10]-SOFs-**1@70b**, and Q[10]-SOFs-**1@70c** at a certain ratio by balancing the energy transfer between the Q[10]-SOFs-**1**-loaded dyes. This study provides an example of Q[10]-based supramolecular inorganic−organic frameworks in the confined space-based solid luminescent materials.

Using the same strategy, Xiao et al. described another type of Q[10]-$[CdCl_4]^{2-}$-based 1D-nanotube-like supramolecular framework, Q[10]-SOFs-**2**, by mixing Q[10] and $CdCl_2$ in aqueous HCl (6.0 mol/L) at room temperature.[229] The crystal structure exhibited perfectly aligned 1D Q[10]-based nanotubes along the *c*-axis. Each $[CdCl_4]^{2-}$ anion connected with four Q[10] molecules through C−H···Cl^- bonds, and each Q[10] molecule connected with eight $[CdCl_4]^{2-}$ anions in the same way (Figure 53a). Each nanotube was assembled via the outer surfaces of neighboring Q[10] molecules. After loading of pyrene into Q[10]-SOFs-**2**, the material exhibited a fluorescence quenching response to pyridine. Loading of dansyl chloride in Q[10]-SOFs-**2** produced a rapid response to pyridine with significant enhancement of fluorescence (Figure 53b). The fluorescence quenching of pyrene in Q[10]-SOFs-**2** after adsorption of pyridine can be attributed to electron

https://doi.org/10.1021/acs.chemrev.1c01050
Chem. Rev. XXXX, XXX, XXX−XXX

transfer from the pyrene unit to electron-deficient pyridine in the Q[10] cavity-based nanotubes. In the case of the Q[10]-SOFs-**2**@dansyl chloride system, the enhanced fluorescence emission can be ascribed to a stronger ICT effect from the reaction of pyridine with sulfonyl chloride to form sulfonylpyridinium chloride in the Q[10]-SOFs-**2** confined channel space. This study highlights the potential application of Q[10]-SOFs-derived nanoconfinement in luminescent materials.

7. SUPRAMOLECULAR ORGANIC LUMINESCENT EMISSIONS FROM Q[*N*] PARTICLES

Because of the unique property of the rigid confined spaces including the polar portals rimmed with carbonyl groups, Q[*n*] hosts have attracted continuous attention for the construction of various Q[*n*] triggered assemblies of nanoparticles via host–guest interactions,[230−247] but there are few examples of supramolecular luminescent emission systems derived from the assembly of Q[*n*] particles. In 2020, Ma and co-workers used Q[7] and Q[8] to prepare bright Au nanoclusters in water via host–guest-interaction triggered supramolecular assemblies (Figure 54a).[248] FGGC-AuNCs were synthesized

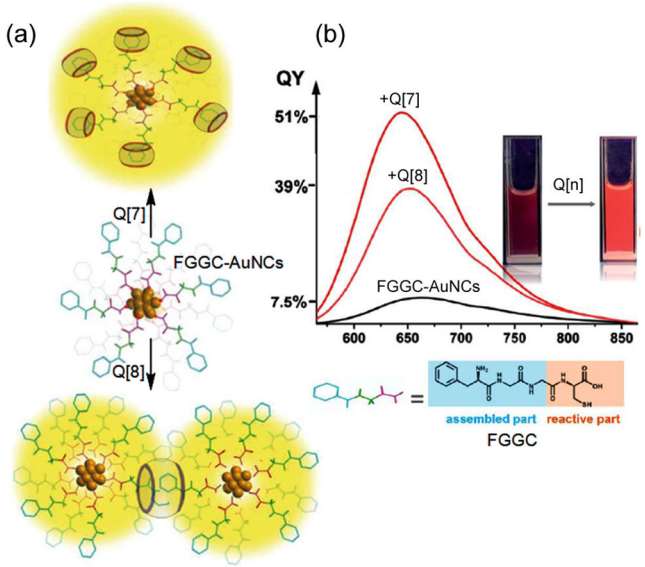

Figure 54. (a) Schematic representation of the host–guest assembly of Q[7] and Q[8] with FGGC-AuNCs. (b) Corresponding emission spectra and luminescence photographs. Reproduced with permission from ref 248. Copyright 2020 Royal Society of Chemistry.

by introducing FGGC (*N*-terminal Phe–Gly–Gly–Cys peptide) to the surface of gold nanoclusters (AuNCs). The FGG moiety of the FGGC peptide served as a binding site for Q[7] and Q[8], and the cysteine residue was used to form the compressed Au(I)-thiolate surface of AuNCs. FGGC-AuNCs exhibited red emission in water with low QY (7.5%). Remarkably enhanced luminescence was observed after addition of Q[7] or Q[8] to the solution (Figure 54b). Fluorescence is enhanced because the Au nanoparticles have a more rigid structure after host–guest self-assembly driven by the cavity-derived confinement effect, ion–dipole interaction, and H-bonds. However, the Q[7]/FGGC-AuNCs' supramolecular assembly exhibited brighter red emission at 645 nm with a high QY of 51% compared to a QY of 39% for Q[8]/FGGC-AuNCs. This can be attributed to the different host–guest binding modes of Q[7] and Q[8] with the FGGC-AuNCs. The relatively small cavity of Q[7] means that it can only form a cap on the surface of one AuNC by anchoring one FGG moiety, while Q[8] is expected to form a 1:2 complex because of its larger cavity. A unique dimer assembly of AuNCs was, therefore, formed in the presence of the Q[8] host.

Very recently, Ni et al. found that a Q[*n*] portal-based host–guest assembly can be used to promote the formation of carbon dots (CDs) with a tunable particle size and high fluorescence emission via hydrothermal reaction from a single organic precursor in water (Figure 55a).[249] The organic molecule tobias acid (TBA) (**71**) formed CDs via a conventional hydrothermal route, but a very weak excitation wavelength-dependent blue luminescence was observed. In the presence of Q[7] or Q[8] host, the yield of the CDs was significantly improved (from <10% to >60%), and they exhibited uniformly spherical morphology with a high degree of crystallinity. Fluorescence spectra revealed that both Q[*n*] CDs exhibited excitation wavelength-independent fluorescence. As shown in Figure 55b, Q[7] CDs exhibited strong blue fluorescence (λ_{max} = 465 nm, QY: 56.75%) with a lifetime up to 96 ns, while yellow emission with a maximum at 545 nm was observed for Q[8] CDs. The fluorescence lifetime and QY of Q[8] CDs were determined to be 5.43 ns and 35.5%. Notably, the ^{1}H NMR spectra revealed that the original rigid macrocyclic skeletons of Q[7] and Q[8] were stably retained during the fabrication of the CDs, which was essentially the reason for the excellent optical properties of the host-attached CDs. Like Ma's study, the different fluorescence of the Q[7] and Q[8] systems is ascribed to their different cavity sizes triggering different host–CD interactions. Importantly, ^{1}H NMR spectra indicated that the host–guest complexes of Q[7/8] with guest **71** were through portal-based ion–dipole interactions rather than the cavities. This binding behavior greatly promoted and catalyzed the polymerization of **71** to form CDs (Figure 55c). Additionally, fluorescence from the dynamic host–particle interaction of Q[8] CDs can be further exploited as a sensitive biosensor for the adamantylamine molecules (Figure 55d) and cell imaging (Figure 55e and f). This study suggests that the Q[*n*]-portal-interaction-derived confinement effect may offer opportunities to develop a new tool for fabricating smart and tunable CDs with new properties.

8. SUPRAMOLECULAR ORGANIC LUMINESCENT EMISSIONS FROM Q[8]-BASED RING-IN-RING(S) COMPLEXES

In this example, taking advantage of the optical and electronic properties of the linear π systems of oligo(*p*-phenylenevinylene) (OPV) dyes strongly depends upon structural features,[56,57,191] and unique **OPV**$^{4+}$-based binary and ternary ring-in-ring(s) complexes with tunable fluorescent emission have been reported by Stoddart and co-workers, which gives a better understanding the effect of Q[*n*] macrocyclic confinement in regulating the superstructure and electronic properties of the chromophore guest.[55] As show in Figure 56a, the X-ray crystal structure revealed that cyclophane **OPVEBox**$^{4+}$ adopted a boxlike geometry with average dimensions 18.7 × 7.6 Å in the solid state. Cyclophane **OPVEBox**$^{4+}$ as guest ring exhibited sky blue fluorescence emission (482 nm) in aqueous solution. During the formation of the binary Q[8]-**OPVEBox**$^{4+}$ (1:1) and ternary Q[8]-**OPVEBox**$^{4+}$ (2:1) ring-in-ring(s) complexes, tunable fluorescent emissions from sky blue to cyan, green, and

https://doi.org/10.1021/acs.chemrev.1c01050
Chem. Rev. XXXX, XXX, XXX−XXX

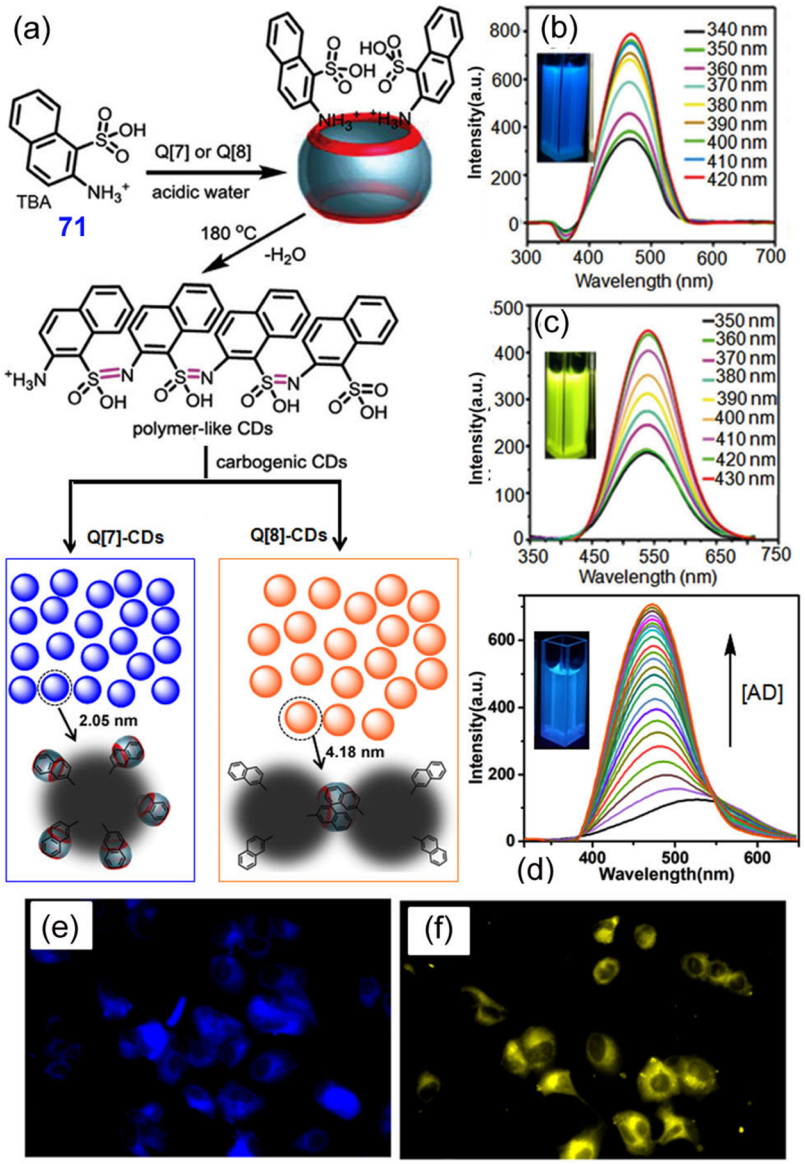

Figure 55. (a) Schematic representation of the Q[7/8]-assisted formation of tunable CDs from single organic precursors TBA (**71**) in acidic water. Fluorescence spectra of (b) Q[7] CDs and (c) Q[8] CDs at different excitation wavelengths. (d) Fluorescence spectra obtained for Q[8] CDs upon increasing the concentration of adamantylamine in water. Fluorescence images of MCF-7 cells labeled with (e) Q[7] CDs and (f) Q[8] CDs. Reproduced with permission from ref 249. Copyright 2021 Royal Society of Chemistry.

yellow are observed, due to the narrowing in the energy gaps of the cyclophane ring within the rigid hydrophobic cavities of the Q[8] cavity (Figure 56e). Namely, the nanoconfined space of the Q[8] host promotes the tighter $\pi-\pi$ stacking of the OPV chromophores in the cyclophane guest. Density functional theory (DFT) calculations were performed by the authors to confirm this issue. In the case of the binary Q[8]-**OPVEBox**$^{4+}$ (1:1) complex (Figure 56b), the **OPV**$^{2+}$ chromophores were compelled to bend into the cavity of the cyclophane with the centroid-to-centroid distance being reduced to 3.9 Å, and the strain energy was calculated to be 28.6 kcal/mol. In the case of the ternary Q[8]-**OPVEBox**$^{4+}$ (2:1) complex (Figure 56c), the whole **OPVEBox**$^{4+}$ ring was squeezed, which is attributed to the compression from the two Q[8] hosts, and the strain energy was found to be 42.9 kcal/mol. Meanwhile, the *p*-xylylene linkers were forced to bend, with the distance between their two peripheral nitrogen atoms of 5.3 Å. Importantly, the Q[8] host also underwent an ellipsoidal deformation in order to form the ring-in-ring(s) complexes. Electrostatic potential analysis results (Figure 56d) suggested that after complexing with one and two Q[8] hosts, the electronic cloud density in the original electron-deficient **OPVEBox**$^{4+}$ cyclophane increases gradually as a result of intermolecular charge transfer. Undoubtedly, this study provides clear evidence for the role of the confinement effect in Q[*n*]-based supramolecular luminescent emissions.

9. CONCLUSION AND OUTLOOK

Q[*n*]s as classical macrocyclic hosts distinguish themselves from other artificial organic macrocycles for fabricating smart supramolecular organic luminescent emissions in recent years, due to the tunable macrocyclic-confinement effect from the confined rigid molecular spaces with different sizes.[250−262] Generally, the characterization of Q[*n*]-based supramolecular organic emissions with the size-dependent confinement effect can be classified by the following: (1) The rigid confined cavity

https://doi.org/10.1021/acs.chemrev.1c01050
Chem. Rev. XXXX, XXX, XXX−XXX

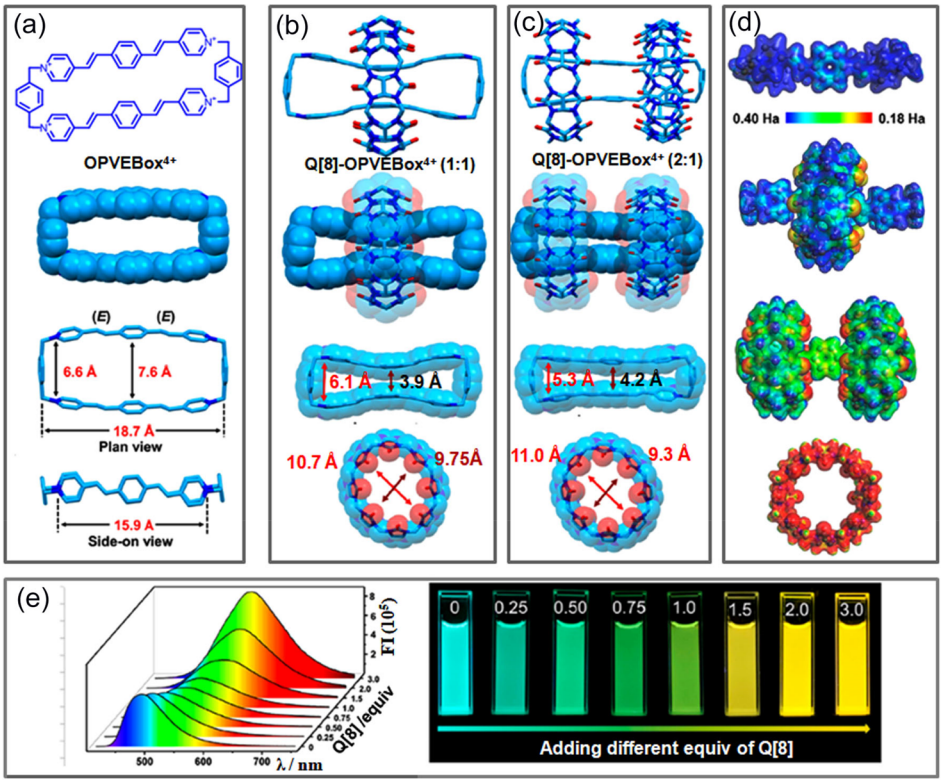

Figure 56. (a) Chemical and crystal structure of **OPVEBox**$^{4+}$. (b) Ring-in-ring(s) representations of the optimized superstructure of the binary Q[8]-**OPVEBox**$^{4+}$ (1:1) complex determined by DFT calculations. (c) Ring-in-ring(s) representations of the optimized superstructure of the ternary 2Q[8]-**OPVEBox**$^{4+}$ (2:1) complex determined by DFT calculations. (d) Electrostatic potential maps of the free **OPVEBox**$^{4+}$ complex, binary Q[8]-**OPVEBox**$^{4+}$ (1:1) complex, ternary Q[8]-**OPVEBox**$^{4+}$ (2:1) complex, and free Q[8], respectively. (e) Emission spectra and fluorescent photographs of **OPVEBox**$^{4+}$ with different equivalents of Q[8] in aqueous solution. Reproduced with permission from ref 55. Copyright 2021 American Chemical Society.

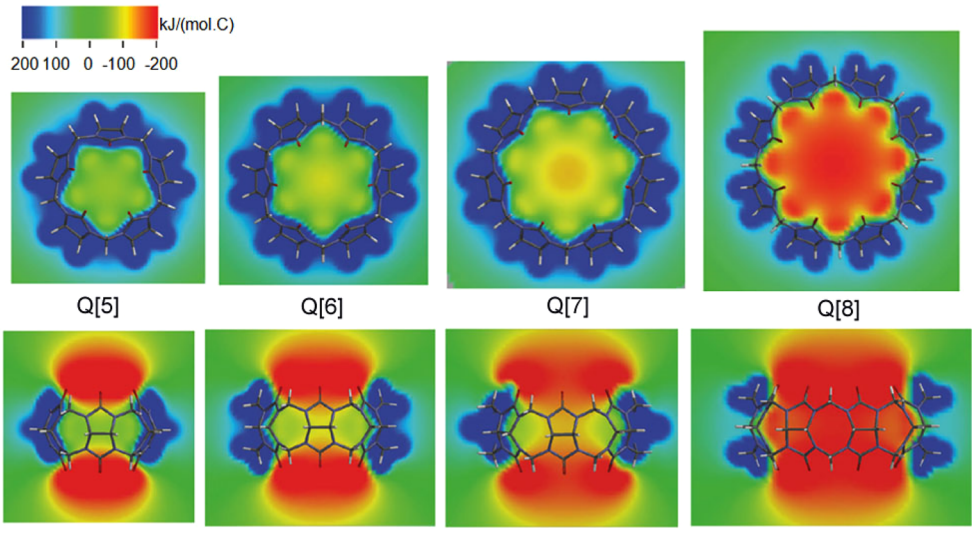

Figure 57. Calculated electrostatic potential at the B3LYP/6-31G* level of theory for Q[5], Q[6], Q[7], and Q[8]. Reproduced with permission from ref 263. Copyright 2012 American Chemical Society.

and the carbonyl oxygen atoms at the rim of the polar Q[*n*] portal can efficiently change the electron density distribution or charge transfer of the dye guest molecules. In particular, they can switch the luminescence properties of the dye molecule simply and efficiently through multiple noncovalent interactions without the need for complicated organic synthesis. (2) Q[*n*] confined cavities with different sizes can induce different luminescent emissions from the same included dye guest and in some cases undergo larger Stokes shifts. It is possible to prepare multicolor luminescent materials that do not rely on the principle of Fourier resonance energy transfer (FRET) through "single excitation with multiple independent emissions". (3) The confined hydrophobic cavity of Q[*n*]s can effectively improve the emission lifetime, quantum yield. and

https://doi.org/10.1021/acs.chemrev.1c01050
Chem. Rev. XXXX, XXX, XXX−XXX

thermal stability of the encapsulated luminescent dyes. (4) The confined barrel structure of the Q[*n*]s effectively ensures that the dye guest has high luminescence efficiency at low concentration and aggregation state, which may be a powerful supplement to the phenomena of ACQ and AIE in the light-emission field. (5) The dynamic reversibility of the supramolecular noncovalent bonds of the Q[*n*] host−guest self-assembly offers the potential to construct smart stimulus-responsive luminescent materials.

However, the macrocyclic confinement is generally regarded as the hydrophobic effect in Q[*n*] chemistry, and little attention has been received. In fact, the electrostatic potential calculations on Q[*n*]s suggested that the portals of Q[*n*]s are similarly highly electronegative, but there is a remarkable increase in negative electrostatic potential within the cavities from Q[5] to Q[8] (Figure 57).[263] Obviously, this phenomenon can be ascribed to the different size-dependent confinement effects of Q[*n*]s. So, the effect of the different negative electrostatic potentials in the confined Q[*n*] cavity should be given attention in the corresponding host−guest complexes in the next studies. Meanwhile, it is worth noting that the extended confinement effect is imposed by the synergistic restriction of molecules between the Q[*n*]s and the resulting polymer, and SOF structures also display excellent advantage in construction of high quality emitting materials. For example, the extended confinement effect of the Q[8] host has been utilized to fabricate tunable RTP and circularly polarized luminescence materials in aqueous solution by Liu[264] and Ma,[265] respectively. Furthermore, in comparison with most of the RTP materials in the solid state (with disadvantages such as inefficient photoluminescence efficiency and poor water solubility, which restrict their potential applications in biological systems), the confinement of Q[*n*]-derived pure organic RTPs exhibited high efficiency emission in aqueous solution and may provide widely potential applications of Q[*n*]-based supramolecular chemistry in luminescent materials.

The key challenge of Q[*n*]-based luminescent emissions under the corresponding macrocyclic confinement in the future is to develop more efficient luminescent systems such as NIR excitation and emission with better biological compatibility and stability, RTPs with tunable emission, longer lifetime, and higher QY in aqueous environment and the solid state, delayed fluorescence with ultralong lifetime, FRET between the fluorophores and phosphors with a more efficient pathway, and so on.[200,202,213,214,266−276] Especially, it should be noted that nearly all the Q[*n*]-derived RTP systems to date were derived from the 4-(4-bromophenyl)pyridinium guest as the phosphor. So, the discovery of more unique Q[*n*]-based supramolecular luminescent systems and their practical applications can be eagerly expected. Furthermore, Q[10], which has the largest cavity in the Q[*n*] family so far, warrants more attention to exploit its confinement properties. Of note, a facile and highly efficient approach to isolate Q[10] from Q[*n*] mixtures was reported by Liu and co-workers in 2018.[277] Of course, the twisted structure of *t*Q[13−15] may provide additional insight into the macrocyclic-confinement effect of Q[*n*]s in the luminescent host−guest chemistry. In particular, the two cavities from the figure-of-eight conformation of *t*Q[13−15] showed structural flexibility and present a high density of portal carbonyl groups, leading to new applications of Q[*n*]s in supramolecular chemistry[278−283] including supramolecular luminescent assemblies.[284−286] For example, Huang and co-workers reported that *t*Q[14] can significantly increase the fluorescence emission of the encapsulated dyes and exhibit flexible stimuli-responsive supramolecular assemblies.[284,285]

Overall, this review can enrich the concept of macrocyclic confinement of Q[*n*]s in luminescent materials including polydimensional luminescent materials (such as MOFs and SOFs), dynamic luminescent polymers, photocatalysts, OLEDs, imaging agents in biological and environmental systems, photodynamic therapy, anticounterfeiting, and information encryption, and so on.

AUTHOR INFORMATION

Corresponding Authors

Xin-Long Ni − *Key Laboratory of Chemical Biology and Traditional Chinese Medicine (Ministry of Educational of China), Key Laboratory of the Assembly and Application of Organic Functional Molecules of Hunan Province, Hunan Normal University, Changsha, Hunan 410081, China; Key Laboratory of Macrocyclic and Supramolecular Chemistry of Guizhou Province, Guizhou University, Guiyang 550025, China;* orcid.org/0000-0002-5557-1631; Email: longni333@163.com

Yu Liu − *College of Chemistry, State Key Laboratory of Elemento-Organic Chemistry, Nankai University, Tianjin 300071, China;* orcid.org/0000-0001-8723-1896; Email: yuliu@nankai.edu.cn

Authors

Haigen Nie − *Key Laboratory of Chemical Biology and Traditional Chinese Medicine (Ministry of Educational of China), Key Laboratory of the Assembly and Application of Organic Functional Molecules of Hunan Province, Hunan Normal University, Changsha, Hunan 410081, China*

Zhen Wei − *College of Chemistry, State Key Laboratory of Elemento-Organic Chemistry, Nankai University, Tianjin 300071, China*

Complete contact information is available at: https://pubs.acs.org/10.1021/acs.chemrev.1c01050

Notes

The authors declare no competing financial interest.

Biographies

Haigen Nie received his B.Sc. degree in chemistry from Huanghuai University (China) in 2018. He then joined Prof. Jianxin Song's group at Hunan Normal University as an M.Sc. candidate and continued as a Ph.D. student in Prof. Xin-Long Ni's group. His research focuses on cucurbit[8]uril-derived supramolecular materials.

Zhen Wei received his M.S. degree in chemistry at Guizhou University, China, in 2007. He then joined Tianjin Agricultural University (China) as a lecturer. In 2016, he received his doctoral degree in materials science from Tianjin University, China. In 2021, he was a visiting scholar in Prof. Yu Liu's group. His research focuses on macrocycle-based fluorescent materials.

Xin-Long Ni received his M.S. degree in chemistry at Guizhou University, China, in 2008 and received his Ph.D. from Saga University, Japan, in 2011. Then, he joined the faculty at Guizhou University as an Associate Professor, and he became a Full Professor of chemistry at Guizhou University in 2015. Now, he is a Professor at Hunan Normal University. His current research interests lie in

https://doi.org/10.1021/acs.chemrev.1c01050
Chem. Rev. XXXX, XXX, XXX−XXX

cucurbit[*n*]urils-based coordination chemistry and fluorescent materials.

Yu Liu graduated from the University of Science and Technology of China in 1977 and received his Ph.D. degree from Himeji Institute of Technology, Japan, in 1991. Then, he moved to Nankai University as a Full Professor in 1993. His research focuses on molecular recognition and assembly of macrocyclic receptors.

ACKNOWLEDGMENTS

This work was supported by the National Natural Science Foundation of China (Nos. 21871063, 22131008, and 21772099) and the Science and Technology Foundation of Hunan Province (Nos. 2020JJ2021 and 2021RC4059).

ABBREVIATIONS

ACQ aggregation-caused quenching
AIE aggregation-induced emission
RTP room temperature phosphorescence
QY quantum yield
ITC isothermal titration calorimetry
TPE tetraphenylethylene
FID fluorescent indicator displacement
FRET Förster resonance energy transfer
AD adamantylamine
NIR near-infrared
PET photoinduced electron transfer
ROS reactive oxygen species
ICT intramolecular charge transfer
CLSM confocal laser scanning microscopy
CDs carbon dots
SOFs supramolecular organic frameworks
FGGC N-terminal Phe-Gly-Gly-Cys peptide
AuNCs gold nanoclusters

REFERENCES

(1) Lastusaari, M. M.; Laamanen, T.; Malkamäki, M.; Eskola, K. O.; Kotlov, A.; Carlson, S.; Welter, E.; Brito, H. F.; Bettinelli, M.; Jungner, H.; et al. The Bologna Stone: History's First Persistent Luminescent Material. *Eur. J. Mineral* **2012**, *24*, 885−890.
(2) Stelzer, E. H. K. Light-Sheet Fluorescence Microscopy for Quantitative Biology. *Nat. Methods* **2015**, *12*, 23−26.
(3) Loizzo, M. R.; Tundis, R.; Conforti, F.; Statti, G. A.; Menichini, F. Inhibition of Angiotensin Converting Enzyme Activity by Five Senecio Species. *Pharm. Biol.* **2009**, *47*, 516−520.
(4) Tang, C. W.; VanSlyke, S. A. Organic Electroluminescent Diodes. *Appl. Phys. Lett.* **1987**, *51*, 913−915.
(5) Chen, L.; Nakamura, M.; Schindler, T. D.; Parker, D.; Bryant, Z. Engineering Controllable Bidirectional Molecular Motors Based on Myosin. *Nat. Nanotechnol.* **2012**, *7*, 252−256.
(6) Feldmann, C.; Jüstel, T.; Ronda, C. R.; Schmidt, P. J. Inorganic Luminescent Materials: 100 Years of Research and Application. *Adv. Fun. Mater.* **2003**, *13*, 511−516.
(7) Su, L.; Fan, X.; Yin, T.; Wang, H.; Li, Y.; Liu, F.; Li, J.; Zhang, H.; Xie, H. Inorganic 2D Luminescent Materials: Structure, Luminescence Modulation, and Applications. *Adv. Opt. Mater.* **2020**, *8*, 1900978.
(8) Gamelin, D. R.; Güdel, H. U. Design of Luminescent Inorganic Materials: New Photophysical Processes Studied by Optical Spectroscopy. *Acc. Chem. Res.* **2000**, *33*, 235−242.
(9) Liu, J.; Kaczmarek, A. M.; Van Deun, R. Advances in Tailoring Luminescent Rare-Earth Mixed Inorganic Materials. *Chem. Soc. Rev.* **2018**, *47*, 7225−7238.
(10) Benin, B. M.; McCall, K. M.; Wörle, M.; Morad, V.; Aebli, M.; Yakunin, S.; Shynkarenko, Y.; Kovalenko, M. V. The $Rb_7Bi_{3-3x}Sb_{3x}C_{l16}$ Family: A Fully Inorganic Solid Solution with Room-Temperature Luminescent Members. *Angew. Chem., Int. Ed.* **2020**, *59*, 14490−14497.
(11) Höppe, H. A. Recent Developments in the Field of Inorganic Phosphors. *Angew. Chem., Int. Ed.* **2009**, *48*, 3572−3582.
(12) Zhao, Z.; Wang, Z.; Tavakoli, J.; Shan, G.; Zhang, J.; Peng, C.; Xiong, Y.; Zhang, X.; Cheung, T. S.; Tang, Y.; et al. Revisiting an Ancient Inorganic Aggregation-Induced Emission System: An Enlightenment to Clusteroluminescence. *Aggregate* **2021**, *2*, No. e36.
(13) Yang, Z.; Sharma, A.; Qi, J.; Peng, X.; Lee, D. Y.; Hu, R.; Lin, D.; Qu, J.; Kim, J. S. Super-Resolution Fluorescent Materials: an Insight Into Design and Bioimaging Applications. *Chem. Soc. Rev.* **2016**, *45*, 4651−4667.
(14) Han, J.; Guo, S.; Lu, H.; Liu, S.; Zhao, Q.; Huang, W. Recent Progress on Circularly Polarized Luminescent Materials for Organic Optoelectronic Devices. *Adv. Opt. Mater.* **2018**, *6*, 1800538.
(15) Yang, J.; Fang, M.; Li, Z. Organic Luminescent Materials: The Concentration on Aggregates from Aggregation-Induced Emission. *Aggregate* **2020**, *1*, 6−18.
(16) Zhu, M.; Yang, C. Blue Fluorescent Emitters: Design Tactics and Applications in Organic Light-Emitting Diodes. *Chem. Soc. Rev.* **2013**, *42*, 4963−4976.
(17) Baldo, M. A.; Thompson, M. E.; Forrest, S. R. High-Efficiency Fluorescent Organic Light-Emitting Devices Using a Phosphorescent Sensitizer. *Nature* **2000**, *403*, 750−753.
(18) Poriel, C.; Rault-Berthelot, J. Blue Single-Layer Organic Light-Emitting Diodes Using Fluorescent Materials: A Molecular Design View Point. *Adv. Fun. Mater.* **2020**, *30*, 1910040.
(19) Sun, J. W.; Lee, J.-H.; Moon, C.-K.; Kim, K.-H.; Shin, H.; Kim, J.-J. A Fluorescent Organic Light-Emitting Diode with 30% External Quantum Efficiency. *Adv. Mater.* **2014**, *26*, 5684−5688.
(20) Frath, D.; Massue, J.; Ulrich, G.; Ziessel, R. Luminescent Materials: Locking π-Conjugated and Heterocyclic Ligands with Boron(III). *Angew. Chem., Int. Ed.* **2014**, *53*, 2290−2310.
(21) Ju, C.-W.; Bai, H.; Li, B.; Liu, R. Machine Learning Enables Highly Accurate Predictions of Photophysical Properties of Organic Fluorescent Materials: Emission Wavelengths and Quantum Yields. *J. Chem. Inf. Model.* **2021**, *61*, 1053−1065.
(22) Anthony, S. P. Organic Solid-State Fluorescence: Strategies for Generating Switchable and Tunable Fluorescent Materials. *ChemPlusChem.* **2012**, *77*, 518−531.
(23) Li, B.; Ali, A. I. M.; Ge, H. Recent Advances in Using Transition-Metal-Catalyzed C−H Functionalization to Build Fluorescent Materials. *Chem.* **2020**, *6*, 2591−2657.
(24) Suzuki, K.; Kubo, S.; Shizu, K.; Fukushima, T.; Wakamiya, A.; Murata, Y.; Adachi, C.; Kaji, H. Triarylboron-Based Fluorescent Organic Light-Emitting Diodes with External Quantum Efficiencies Exceeding 20%. *Angew. Chem., Int. Ed.* **2015**, *54*, 15231−15235.
(25) Shao, A.; Xie, Y.; Zhu, S.; Guo, Z.; Zhu, S.; Guo, J.; Shi, P.; James, T. D.; Tian, H.; Zhu, W.-H. Far-Red and Near-IR AIE-active Fluorescent Organic Nanoprobes with Enhanced Tumor-Targeting Efficacy: Shape-Specific Effects. *Angew. Chem., Int. Ed.* **2015**, *54*, 7275−7280.
(26) Cai, X.; Su, S.-J. Marching Toward Highly Efficient, Pure-Blue, and Stable Thermally Activated Delayed Fluorescent Organic Light-Emitting Diodes. *Adv. Fun. Mater.* **2018**, *28*, 1802558.
(27) Birks, J. B. *Photophysics of Aromatic Molecules*; Wiley: London, 1970.
(28) Hong, Y.; Lam, J. W. Y.; Tang, B. Z. Aggregation-Induced Emission. *Chem. Soc. Rev.* **2011**, *40*, 5361−5388.
(29) Luo, J.; Xie, Z.; Lam, J. W. Y.; Cheng, L.; Chen, H.; Qiu, C.; Kwok, H. S.; Zhan, X.; Liu, Y.; Zhu, D.; et al. Aggregation-Induced Emission of 1-Methyl-1, 2, 3, 4, 5-Pentaphenylsilole. *Chem. Commun.* **2001**, 1740−1741.
(30) Mei, J.; Leung, N. L. C.; Kwok, R. T. K.; Lam, J. W. Y.; Tang, B. Z. Aggregation-Induced Emission: Together We Shine, United We Soar! *Chem. Rev.* **2015**, *115*, 11718−11940.
(31) Hu, R.; Leung, N. L. C.; Tang, B. Z. AIE Macromolecules: Syntheses, Structures and Functionalities. *Chem. Soc. Rev.* **2014**, *43*, 4494−4562.

https://doi.org/10.1021/acs.chemrev.1c01050
Chem. Rev. XXXX, XXX, XXX−XXX

(32) Kim, J.; Jung, I.-S.; Kim, S.-Y.; Lee, E.; Kang, J.-K.; Sakamoto, S.; Yamaguchi, K.; Kim, K. New Cucurbituril Homologues: Syntheses, Isolation, Characterization, and X-ray Crystal Structures of Cucurbit[*n*]uril (*n* = 5, 7, and 8). *J. Am. Chem. Soc.* **2000**, *122*, 540−541.
(33) Day, A.; Arnold, A. P.; Blanch, R. J.; Snushall, B. Controlling Factors in the Synthesis of Cucurbituril and Its Homologues. *J. Org. Chem.* **2001**, *66*, 8094−8100.
(34) Day, A. I.; Blanch, R. J.; Arnold, A. P.; Lorenzo, S.; Lewis, G. R.; Dance, I. A Cucurbituril-Based Gyroscane: A New Supramolecular Form. *Angew. Chem., Int. Ed.* **2002**, *41*, 275−277.
(35) Cheng, X.-J.; Liang, L.-L.; Chen, K.; Ji, N.-N.; Xiao, X.; Zhang, J.-X.; Zhang, Y.-Q.; Xue, S.-F.; Zhu, Q.-J.; Ni, X.-L.; et al. Twisted Cucurbit[14]uril. *Angew. Chem., Int. Ed.* **2013**, *52*, 7252−7255.
(36) Li, Q.; Qiu, S.-C.; Zhang, J.; Chen, K.; Huang, Y.; Xiao, X.; Zhang, Y.; Li, F.; Zhang, Y.-Q.; Xue, S.-F.; et al. Twisted Cucurbit[*n*]urils. *Org. Lett.* **2016**, *18*, 4020−4023.
(37) Liu, Z.; Krishna, S.; Nalluri, M.; Stoddart, J. F. Surveying Macrocyclic Chemistry: From Flexible Crown Ethers to Rigid Cyclophanes. *Chem. Soc. Rev.* **2017**, *46*, 2459−2478.
(38) Murray, J.; Kim, K.; Ogoshi, T.; Yao, W.; Gibb, B. C. The Aqueous Supramolecular Chemistry of Cucurbit[*n*]urils, Pillar[*n*]-arenes and Deep-Cavity Cavitands. *Chem. Soc. Rev.* **2017**, *46*, 2479−2496.
(39) Lagona, J.; Mukhopadhyay, P.; Chakrabarti, S.; Isaacs, L. The Cucurbit[*n*]uril Family. *Angew. Chem., Int. Ed.* **2005**, *44*, 4844−4870.
(40) Lee, J. W.; Samal, S.; Selvapalam, N.; Kim, H.-J.; Kim, K. Cucurbituril Homologues and Derivatives: New Opportunities in Supramolecular Chemistry. *Acc. Chem. Res.* **2003**, *36*, 621−630.
(41) Masson, E.; Ling, X.; Joseph, R.; Kyeremeh-Mensah, L.; Lu, X. Cucurbituril Chemistry: A Tale of Supramolecular Success. *RSC Adv.* **2012**, *2*, 1213−1247.
(42) Isaacs, L. Stimuli Responsive Systems Constructed Using Cucurbit[*n*]uril-Type Molecular Containers. *Acc. Chem. Res.* **2014**, *47*, 2052−2062.
(43) Liu, J.; Lan, Y.; Yu, Z.; Tan, C. S.Y.; Parker, R. M.; Abell, C.; Scherman, O. A. Cucurbit[*n*]uril-Based Microcapsules Self-Assembled within Microfluidic Droplets: A Versatile Approach for Supramolecular Architectures and Materials. *Acc. Chem. Res.* **2017**, *50*, 208−217.
(44) Kaifer, A. E. Toward Reversible Control of Cucurbit[n]uril Complexes. *Acc. Chem. Res.* **2014**, *47*, 2160−2167.
(45) Barrow, S. J.; Kasera, S.; Rowland, M. J.; del Barrio, J.; Scherman, O. A. Cucurbituril-Based Molecular Recognition. *Chem. Rev.* **2015**, *115*, 12320−12406.
(46) Assaf, K. I.; Nau, W. M. Cucurbiturils: From Synthesis to High-Affinity Binding and Catalysis. *Chem. Soc. Rev.* **2015**, *44*, 394−418.
(47) Lü, J.; Lin, J.-X.; Cao, M.-N.; Cao, R. Cucurbituril: A Promising Organic Building Block for the Design of Coordination Compounds and Beyond. *Coord. Chem. Rev.* **2013**, *257*, 1334−1356.
(48) Yang, D.; Liu, M.; Xiao, X.; Tao, Z.; Redshaw, C. Polymeric Self-Assembled Cucurbit[*n*]urils: Synthesis, Structures and Applications. *Coord. Chem. Rev.* **2021**, *434*, 213733.
(49) Lin, R.-L.; Liu, J.-X.; Chen, K.; Redshaw, C. Supramolecular Chemistry of Substituted Cucurbit[*n*]urils. *Inorg. Chem. Front.* **2020**, *7*, 3217−3246.
(50) Zhang, X.-D.; Chen, K.; Sun, W.-Y. Potential Applications of Cucurbit[*n*]urils and Their Derivatives in the Capture of Hazardous Chemicals. *Chem.—Eur. J.* **2021**, *27*, 5107−5119.
(51) Liu, W.; Stoddart, J. F. Emergent Behavior in Nanoconfined Molecular Containers. *Chem.* **2021**, *7*, 919−947.
(52) Grommet, A. B.; Feller, M.; Klajn, R. Chemical Reactivity Under Nanoconfinement. *Nat. Nanotechnol.* **2020**, *15*, 256−271.
(53) Dsouza, R. N.; Pischel, U.; Nau, W. M. Fluorescent Dyes and Their Supramolecular Host/Guest Complexes with Macrocycles in Aqueous Solution. *Chem. Rev.* **2011**, *111*, 7941−7980.
(54) Verstraete, L.; De Feyter, S. 2D Self-assembled Molecular Networks and On-Surface Reactivity Under Nanoscale Lateral Confinement. *Chem. Soc. Rev.* **2021**, *50*, 5884−5897.
(55) Wu, H.; Wang, Y.; Jones, L. O.; Liu, W.; Song, B.; Cui, Y.; Cai, K.; Zhang, L.; Shen, D.; Chen, X.-Y.; et al. Ring-in-Ring(s) Complexes Exhibiting Tunable Multicolor Photoluminescence. *J. Am. Chem. Soc.* **2020**, *142*, 16849−16860.
(56) Ni, X.-L.; Chen, S.; Yang, Y.; Tao, Z. Facile Cucurbit[8]uril-Based Supramolecular Approach To Fabricate Tunable Luminescent Materials in Aqueous Solution. *J. Am. Chem. Soc.* **2016**, *138*, 6177−6183.
(57) Xia, Y.; Chen, S.; Ni, X.-L. White Light Emission from Cucurbituril-Based Host−Guest Interaction in the Solid State: New Function of the Macrocyclic Host. *ACS Appl. Mater. Interfaces* **2018**, *10*, 13048−13052.
(58) Ma, X.; Wang, J.; Tian, H. Assembling-Induced Emission: An Efficient Approach for Amorphous Metal-Free Organic Emitting Materials with Room-Temperature Phosphorescence. *Acc. Chem. Res.* **2019**, *52*, 738−748.
(59) Kim, H.-J.; Whang, D. R.; Gierschner, J.; Park, S. Y. Highly Enhanced Fluorescence of Supramolecular Polymers Based on a Cyanostilbene Derivative and Cucurbit[8]uril in Aqueous Solution. *Angew. Chem., Int. Ed.* **2016**, *55*, 15915−15919.
(60) Zhang, Z.-Y.; Chen, Y.; Liu, Y. Efficient Room-Temperature Phosphorescence of a Solid-State Supramolecule Enhanced by Cucurbit[6]uril. *Angew. Chem., Int. Ed.* **2019**, *58*, 6028−6032.
(61) Wang, J.; Huang, Z.; Ma, X.; Tian, H. Visible-Light-Excited Room-Temperature Phosphorescence in Water by Cucurbit[8]uril-Mediated Supramolecular Assembly. *Angew. Chem., Int. Ed.* **2020**, *59*, 9928−9933.
(62) Bhasikuttan, A. C.; Pal, H.; Mohanty, J. Cucurbit[*n*]uril Based Supramolecular Assemblies: Tunable Physico-Chemical Properties and Their Prospects. *Chem. Commun.* **2011**, *47*, 9959−9971.
(63) Bhaumik, S. K.; Biswas, R.; Banerjee, S. Cucurbituril Based Luminescent Materials in Aqueous Media and Solid State. *Chem.—Asian J.* **2021**, *16*, 2195−2210.
(64) Ni, X.-L.; Xiao, X.; Cong, H.; Liang, L.-L.; Cheng, K.; Cheng, X.-J.; Ji, N.-N.; Zhu, Q.-J.; Xue, S.-F.; Tao, Z. Cucurbit[n]uril-Based Coordination Chemistry: From Simple Coordination Complexes to Novel Poly-Dimensional Coordination Polymers. *Chem. Soc. Rev.* **2013**, *42*, 9480−9508.
(65) Ni, X.-L.; Xue, S.-F.; Tao, Z.; Zhu, Q.-J.; Lindoy, L. F.; Wei, G. Advances in the Lanthanide Metallosupramolecular Chemistry of the Cucurbit[*n*]urils. *Coord. Chem. Rev.* **2015**, *287*, 89−113.
(66) Wu, Y.; Hua, H.; Wang, Q. A CB[5] Analogue Based Supramolecular Polymer with AIE Behaviors. *New J. Chem.* **2018**, *42*, 8320−8324.
(67) Gao, Z.-W.; Feng, X.; Mu, L.; Ni, X.-L.; Liang, L.-L.; Xue, S.-F.; Tao, Z.; Zeng, X.; Chapman, B. E.; Kuchel, P. W.; et al. Cucurbit[5]uril−Metal Complex-Induced Room-Temperature Phosphorescence of α-Naphthol and β-Naphthol. *Dalton Trans.* **2013**, *42*, 2608−2615.
(68) Ni, X.-L.; Xiao, X.; Cong, H.; Zhu, Q.-J.; Xue, S.-F.; Tao, Z. Self-Assemblies Based on the "Outer-Surface Interactions" of Cucurbit[n]urils: New Opportunities for Supramolecular Architectures and Materials. *Acc. Chem. Res.* **2014**, *47*, 1386−1395.
(69) Song, D.; Li, B.; Li, X.; Sun, X.; Li, J.; Li, C.; Xu, T.; Zhu, Y.; Li, F.; Wang, N. Orthogonal Supramolecular Assembly Triggered by Inclusion and Exclusion Interactions with Cucurbit[7]uril for Photocatalytic H_2 Evolution. *ChemSusChem* **2020**, *13*, 394−399.
(70) Behrend, R.; Meyer, E.; Rusche, F. I. Ueber Condensationsproducte Aus Glycoluril Und Formaldehyde. *Justus Liebigs Ann. Chem.* **1905**, *339*, 1−35.
(71) Freeman, W. A.; Mock, W. L.; Shih, N.-Y. Cucurbituril. *J. Am. Chem. Soc.* **1981**, *103*, 7367−7368.
(72) Mock, W. L. Cucurbituril. *Top. Curr. Chem.* **1995**, *175*, 1.
(73) Hoffmann, R.; Knoche, W.; Fenn, C.; Buschmann, H.-J. Host−Guest Complexes of Cucurbituril with the 4-Methylbenzylammonium Ion, Alkali-Metal Cations and NH_4^+. *J. Chem. Soc., Faraday Trans.* **1994**, *90*, 1507.
(74) Jeon, Y.-M.; Kim, J.; Whang, D.; Kim, K. Molecular Container Assembly Capable of Controlling Binding and Release of Its Guest

https://doi.org/10.1021/acs.chemrev.1c01050
Chem. Rev. XXXX, XXX, XXX−XXX

Molecules: Reversible Encapsulation of Organic Molecules in Sodium Ion Complexed Cucurbituril. *J. Am. Chem. Soc.* **1996**, *118*, 9790−9791.
(75) Mock, W. L.; Irra, T. A.; Wepsiec, J. P.; Manimaran, T. L. Cycloaddition Induced by Cucurbituril. A Case of Pauling Principle Catalysis. *J. Org. Chem.* **1983**, *48*, 3619−3620.
(76) Moses, J. E.; Moorhouse, A. D. The Growing Applications of Click Chemistry. *Chem. Soc. Rev.* **2007**, *36*, 1249−1262.
(77) Hou, X.; Ke, C.; Stoddart, J. F. Cooperative Capture Synthesis: Yet Another Playground for Copper-Free Click Chemistry. *Chem. Soc. Rev.* **2016**, *45*, 3766−3780.
(78) Wagner, B. D.; Fitzpatrick, S. J.; Gill, M. A.; MacRae, A. I.; Stojanovic, N. A Fluorescent Host-Guest Complex of Cucurbituril in Solution: a Molecular Jack O'Lantern. *Can. J. Chem.* **2001**, *79*, 1101−1104.
(79) Wagner, B. D.; MacRae, A. I. The Lattice Inclusion Compound of 1,8-ANS and Cucurbituril: A Unique Fluorescent Solid. *J. Phys. Chem. B* **1999**, *103*, 10114−10119.
(80) Jun, S. I.; Lee, J. W.; Sakamoto, S.; Yamaguchi, K.; Kim, K. Rotaxane-Based Molecular Switch with Fluorescence Signaling. *Tetrahedron Lett.* **2000**, *41*, 471−475.
(81) Zhao, Y.; Wang, Q.; Liu, M.; Tian, T. Barium-Driven [2]Pseudorotaxane with Fluorescence Addresses. *Sci. China-Chem.* **2010**, *40*, 364−371.
(82) Praetorius, A.; Bailey, D. M.; Schwarzlose, T.; Nau, W. M. Design of a Fluorescent Dye for Indicator Displacement from Cucurbiturils: A Macrocycle-Responsive Fluorescent Switch Operating through a pK_a Shift. *Org. Lett.* **2008**, *10*, 4089−4092.
(83) Klöck, C.; Dsouza, R. N.; Nau, W. M. Cucurbituril-Mediated Supramolecular Acid Catalysis. *Org. Lett.* **2009**, *11*, 2595−2598.
(84) Ghale, G.; Nau, W. M. Dynamically Analyte-Responsive Macrocyclic Host−Fluorophore Systems. *Acc. Chem. Res.* **2014**, *47*, 2150−2159.
(85) Pluth, M. D.; Bergman, R. G.; Raymond, K. N. Acid Catalysis in Basic Solution: a Supramolecular Host Promotes Orthoformate Hydrolysis. *Science* **2007**, *316*, 85−88.
(86) Bai, Q.; Zhang, S.; Chen, H.; Sun, T.; Redshaw, C.; Zhang, J.-X.; Ni, X.-L.; Wei, G.; Tao, Z. Alkyl Substituted Cucurbit[6]uril Assisted Competitive Fluorescence Recognition of Lysine and Methionine in Aqueous Solution. *ChemistrySelect* **2017**, *2*, 2569−2573.
(87) Hou, X.; Ke, C.; Bruns, C. J.; McGonigal, P. R.; Pettman, R. B.; Stoddart, J. F. Tunable Solid-state Fluorescent Materials for Supramolecular Encryption. *Nat. Commun.* **2015**, *6*, 6884.
(88) Yuan, W. Z.; Shen, X. Y.; Zhao, H.; Lam, J. W. Y.; Tang, L.; Lu, P.; Wang, C.; Liu, Y.; Wang, Z.; Zheng, Q.; et al. Crystallization-Induced Phosphorescence of Pure Organic Luminogens at Room Temperature. *J. Phys. Chem. C* **2010**, *114*, 6090−6099.
(89) Yang, J.; Zhen, X.; Wang, B.; Gao, X.; Ren, Z.; Wang, J.; Xie, Y.; Li, J.; Peng, Q.; Pu, K.; et al. The Influence of the Molecular Packing on the Room Temperature Phosphorescence of Purely Organic Luminogens. *Nat. Commun.* **2018**, *9*, 840.
(90) Liu, H.; Bian, Z.; Cheng, Q.; Lan, L.; Wang, Y.; Zhang, H. Controllably Realizing Elastic/Plastic Bending Based on a Room-Temperature Phosphorescent Waveguiding Organic Crystal. *Chem. Sci.* **2019**, *10*, 227−232.
(91) Yuan, Z.; Wang, J.; Chen, L.; Zou, L.; Gong, X.; Ma, X. Methanol Dynamically Activated Room-Temperature Phosphorescence from a Twisted 4-Bromobiphenyl System. *CCS Chem.* **2020**, *2*, 158−167.
(92) Wang, Y.; Yang, J.; Fang, M.; Yu, Y.; Zou, B.; Wang, L.; Tian, Y.; Cheng, J.; Tang, B. Z.; Li, Z. Förster Resonance Energy Transfer: An Efficient Way to Develop Stimulus-Responsive Room-Temperature Phosphorescence Materials and Their Applications. *Matter* **2020**, *3*, 449−463.
(93) Singh, M.; Liu, K.; Qu, S.; Ma, H.; Shi, H.; An, Z.; Huang, W. Recent Advances of Cocrystals with Room Temperature Phosphorescence. *Adv. Opt. Mater.* **2021**, *9*, 2002197.
(94) Zhang, L.; Li, M.; Gao, Q.-Y.; Chen, C.-F. An Ultralong Room-Temperature Phosphorescent Material Based on the Combination of Small Singlet−Triplet Splitting Energy and H-Aggregation. *Chem. Commun.* **2020**, *56*, 4296−4299.
(95) Li, S.; Fu, L.; Xiao, X.; Geng, H.; Liao, Q.; Liao, Y.; Fu, H. Regulation of Thermally Activated Delayed Fluorescence to Room-Temperature Phosphorescent Emission Channels by Controlling the Excited-States Dynamics via *J*- and *H*-Aggregation. *Angew. Chem., Int. Ed.* **2021**, *60*, 18059−18064.
(96) Yuan, J.; Wang, S.; Ji, Y.; Chen, R.; Zhu, Q.; Wang, Y.; Zheng, C.; Tao, Y.; Fan, Q.; Huang, W. Invoking Ultralong Room Temperature Phosphorescence of Purely Organic Compounds Through H-Aggregation Engineering. *Mater. Horiz.* **2019**, *6*, 1259−1264.
(97) Yang, Z.; Xu, C.; Li, W.; Mao, Z.; Ge, X.; Huang, Q.; Deng, H.; Zhao, J.; Gu, F. L.; Zhang, Y.; et al. Boosting the Quantum Efficiency of Ultralong Organic Phosphorescence Up to 52% via Intramolecular Halogen Bonding. *Angew. Chem., Int. Ed.* **2020**, *59*, 17451−17455.
(98) Bolton, O.; Lee, K.; Kim, H. J.; Lin, K. Y.; Kim, J. Activating Efficient Phosphorescence from Purely Organic Materials by Crystal Design. *Nat. Chem.* **2011**, *3*, 205−210.
(99) Zhou, J.; Stojanović, L.; Berezin, A. A.; Battisti, T.; Gill, A.; Kariuki, B. M.; Bonifazi, D.; Crespo-Otero, R.; Wasielewski, M. R.; Wu, Y.-L. Organic Room-Temperature Phosphorescence from Halogen-Bonded Organic Frameworks: Hidden Electronic Effects in Rigidified Chromophores. *Chem. Sci.* **2021**, *12*, 767−773.
(100) Gao, H.; Ma, X. Recent Progress on Pure Organic Room Temperature Phosphorescent Polymers. *Aggregate* **2021**, *2*, e38.
(101) Liu, X.; Yang, L.; Li, X.; Zhao, L.; Wang, S.; Lu, Z.-H.; Ding, J.; Wang, L. An Electroactive Pure Organic Room-Temperature Phosphorescence Polymer Based on a Donor-Oxygen-Acceptor Geometry. *Angew. Chem., Int. Ed.* **2021**, *60*, 2455−2463.
(102) Wu, H.; Chi, W.; Chen, Z.; Liu, G.; Gu, L.; Bindra, A. K.; Yang, G.; Liu, X.; Zhao, Y. Design of Metal-Free Polymer Carbon Dots: A New Class of Room-Temperature Phosphorescent Materials. *Adv. Funct. Mater.* **2019**, *29*, 1807243−1807252.
(103) Tao, S.; Lu, S.; Geng, Y.; Zhu, S.; Redfern, S. A. T.; Song, Y.; Feng, T.; Xu, W.; Yang, B. Design of Metal-Free Polymer Carbon Dots: A New Class of Room-Temperature Phosphorescent Materials. *Angew. Chem., Int. Ed.* **2018**, *57*, 2393−2398.
(104) Chen, H.; Ma, X.; Wu, S.; Tian, H. A Rapidly Self-Healing Supramolecular Polymer Hydrogel with Photostimulated Room-Temperature Phosphorescence Responsiveness. *Angew. Chem., Int. Ed.* **2014**, *53*, 14149−14152.
(105) Gan, N.; Shi, H.; An, Z.; Huang, W. Recent Advances in Polymer-Based Metal-Free Room-Temperature Phosphorescent Materials. *Adv. Funct. Mater.* **2018**, *28*, 1802657.
(106) Fang, M.-M.; Yang, J.; Li, Z. Recent Advances in Purely Organic Room Temperature Phosphorescence Polymer. *Chin. J. Polym. Sci.* **2019**, *37*, 383−393.
(107) Ma, X.-K.; Liu, Y. Purely Organic Room-Temperature Phosphorescence. *Acc. Chem. Res.* **2021**, *54*, 3403−3414.
(108) Zhang, Z.-Y.; Liu, Y. Ultralong Room-Temperature Phosphorescence of a Solid-state Supramolecule Between Phenylmethylpyridinium and Cucurbit[6]uril. *Chem. Sci.* **2019**, *10*, 7773−7778.
(109) Shetty, D.; Khedkar, J. K.; Park, K. M.; Kim, K. Can We Beat the Biotin−Avidin Pair?: Cucurbit[7]uril-Based Ultrahigh Affinity Host−Guest Complexes and Their Applications. *Chem. Soc. Rev.* **2015**, *44*, 8747−8761.
(110) Mohanty, J.; Pal, H.; Ray, A. K.; Kumar, S.; Nau, W. M. Supramolecular Dye Laser with Cucurbit[7]uril in Water. *ChenPhyChem.* **2007**, *8*, 54−56.
(111) Mohanty, J.; Jagtap, K.; Ray, A. K.; Nau, W. M.; Pal, H. Molecular Encapsulation of Fluorescent Dyes Affords Efficient Narrow-band Dye Laser Operation in Water. *ChenPhyChem.* **2010**, *11*, 3333−3338.
(112) Barooah, N.; Mohanty, J.; Pal, H.; Bhasikuttan, A. C. Stimulus-Responsive Supramolecular pK_a Tuning of Cucurbit[7]uril

https://doi.org/10.1021/acs.chemrev.1c01050
Chem. Rev. XXXX, XXX, XXX−XXX

Encapsulated Coumarin 6 Dye. *J. Phys. Chem. B* **2012**, *116*, 3683−3689.
(113) Saleh, N.; Koner, A. L.; Nau, W. M. Activation and Stabilization of Drugs by Supramolecular pK_a Shifts: Drug-Delivery Applications Tailored for Cucurbiturils. *Angew. Chem., Int. Ed.* **2008**, *47*, 5398−5401.
(114) Martyn, T. A.; Moore, J. L.; Halterman, R. L.; Yip, W. T. Cucurbit[7]uril Induces Superior Probe Performance for Single-Molecule Detection. *J. Am. Chem. Soc.* **2007**, *129*, 10338−10339.
(115) Wang, R.; Yuan, L.; Macartney, D. H. Stabilization of the (E)-1-Ferrocenyl-2-(1-methyl-4-pyridinium)ethylene Cation by Inclusion in Cucurbit[7]uril. *Organometallics* **2006**, *25*, 1820−1823.
(116) Gonzalez-Carrero, S.; Francés-Soriano, L.; González-Béjar, M.; Agouram, S.; Galian, R. E.; Pérez-Prieto, J. The Luminescence of $CH_3NH_3PbBr_3$ Perovskite Nanoparticles Crests the Summit and Their Photostability under Wet Conditions is Enhanced. *Small* **2016**, *12*, 5245−5250.
(117) Zhang, H.; Liu, L.; Gao, C.; Sun, R.; Wang, Q. Enhancing Photostability of Cyanine dye by Cucurbituril Encapsulation. *Dyes Pigm.* **2012**, *94*, 266−270.
(118) Wang, S.-R.; Song, Y.-Y.; Wei, L.; Liu, C.-X.; Fu, B.-S.; Wang, J.-Q.; Yang, X.-R.; Liu, Y.-N.; Liu, S.-M.; Tian, T.; et al. Cucurbit-[7]uril-Driven Host−Guest Chemistry for Reversible Intervention of 5-Formylcytosine-Targeted Biochemical Reactions. *J. Am. Chem. Soc.* **2017**, *139*, 16903−16912.
(119) Zhou, X.; Su, X.; Pathak, P.; Vik, R.; Vinciguerra, B.; Isaacs, L.; Jayawickramarajah, J. Host−Guest Tethered DNA Transducer: ATP Fueled Release of a Protein Inhibitor from Cucurbit[7]uril. *J. Am. Chem. Soc.* **2017**, *139*, 13916−13921.
(120) Jeon, Y. J.; Kim, S.-Y.; Ko, Y. H.; Sakamoto, S.; Yamaguchi, K.; Kim, K. Novel Molecular Drug Carrier: Encapsulation of Oxaliplatin in Cucurbit[7]uril and Its Effects on Stability and Reactivity of the Drug. *Org. Biomol. Chem.* **2005**, *3*, 2122−2125.
(121) Robinson, E. L.; Zavalij, P. Y.; Isaacs, L. Synthesis of a Disulfonated Derivative of Cucurbit[7]uril and Investigations of Its Ability to Solubilise Insoluble Drugs. *Supra. Chem.* **2015**, *27*, 288−297.
(122) Halterman, R. L.; Moore, J. L.; Mannel, L. M. Disrupting Aggregation of Tethered Rhodamine B Dyads through Inclusion in Cucurbit[7]uril. *J. Org. Chem.* **2008**, *73*, 3266−3269.
(123) Gadde, S.; Batchelor, E. K.; Weiss, J. P.; Ling, Y.; Kaifer, A. E. Control of *H*-and *J*-Aggregate Formation via Host-Guest Complexation Using Cucurbituril Hosts. *J. Am. Chem. Soc.* **2008**, *130*, 17114−17119.
(124) Bhaumik, S. K.; Banerjee, S. Tunable Multi-color Luminescence from a Self-Assembled Cyanostilbene and Cucurbit[7]uril in Aqueous Media. *Chem. Commun.* **2020**, *56*, 655−658.
(125) Liu, K.; Liu, Y.; Yao, Y.; Yuan, H.; Wang, S.; Wang, Z.; Zhang, X. Supramolecular Photosensitizers with Enhanced Antibacterial Efficiency. *Angew. Chem., Int. Ed.* **2013**, *52*, 8285−8289.
(126) Liu, K.; Yao, Y.; Kang, Y.; Liu, Y.; Han, Y.; Wang, Y.; Li, Z.; Zhang, X. A Supramolecular Approach to Fabricate Highly Emissive Smart Materials. *Sci. Rep.* **2013**, *3*, 2372.
(127) Song, Q.; Li, F.; Wang, Z.; Zhang, X. A Supramolecular Strategy for Tuning the Energy Level of Naphthalenediimide: Promoted Formation of Radical Anions with Extraordinary Stability. *Chem. Sci.* **2015**, *6*, 3342−3346.
(128) Jiao, Y.; Liu, K.; Wang, G.; Wang, Y.; Zhang, X. Supramolecular Free Radicals: Near-Infrared Organic Materials with Enhanced Photothermal Conversion. *Chem. Sci.* **2015**, *6*, 3975−3980.
(129) Jiao, Y.; Li, W.-L.; Xu, J.-F.; Wang, G.; Li, J.; Wang, Z.; Zhang, X. A Supramolecularly Activated Radical Cation for Accelerated Catalytic Oxidation. *Angew. Chem., Int. Ed.* **2016**, *55*, 8933−8937.
(130) Yang, Y.; He, P.; Wang, Y.; Bai, H.; Wang, S.; Xu, J.-F.; Zhang, X. Supramolecular Radical Anions Triggered by Bacteria in Situ for Selective Photothermal Therapy. *Angew. Chem., Int. Ed.* **2017**, *56*, 16239−16242.
(131) Yuan, B.; Wu, H.; Wang, H.; Tang, B.; Xu, J.-F.; Zhang, X. Self-Degradable Supramolecular Photosensitizer with High Photodynamic Therapeutic Efficiency and Improved Safety. *Angew. Chem., Int. Ed.* **2021**, *60*, 706−710.
(132) Freitag, M.; Gundlach, L.; Piotrowiak, P.; Galoppini, E. Fluorescence Enhancement of Di-p-tolyl Viologen by Complexation in Cucurbit[7]uril. *J. Am. Chem. Soc.* **2012**, *134*, 3358−3366.
(133) Buyukcakir, O.; Yasar, F. T.; Bozdemir, O. A.; Icli, B.; Akkaya, E. U. Autonomous Shuttling Driven by an Oscillating Reaction: Proof of Principle in a Cucurbit[7]uril-Bodipy Pseudorotaxane. *Org. Lett.* **2013**, *15*, 1012−1015.
(134) Singh, A.; Yip, W.-T.; Halterman, R. L. Fluorescence-on Response via CB7 Binding to Viologen−Dye Pseudorotaxanes. *Org. Lett.* **2012**, *14*, 4046−4049.
(135) Ryan, S. T. J.; Del Barrio, J.; Ghosh, I.; Biedermann, F.; Lazar, A. I.; Lan, Y.; Coulston, R. J.; Nau, W. M.; Scherman, O. A. Efficient Host−Guest Energy Transfer in Polycationic Cyclophane−Perylene Diimide Complexes in Water. *J. Am. Chem. Soc.* **2014**, *136*, 9053−9060.
(136) Bai, H.; Yuan, H.; Nie, C.; Wang, B.; Lv, F.; Liu, L.; Wang, S. A Supramolecular Antibiotic Switch for Antibacterial Regulation. *Angew. Chem., Int. Ed.* **2015**, *54*, 13208−13213.
(137) Wu, D.; Sedgwick, A. C.; Gunnlaugsson, T.; Akkaya, E. U.; Yoon, J.; James, T. D. Fluorescent Chemosensors: the Past, Present and Future. *Chem. Soc. Rev.* **2017**, *46*, 7105−7123.
(138) Sinn, S.; Biedermann, F. Chemical Sensors Based on Cucurbit[*n*]uril Macrocycles. *Isr. J. Chem.* **2018**, *58*, 357−412.
(139) Liu, Y.-C.; Nau, W. M.; Hennig, A. A Supramolecular Five-Component Relay Switch that Exposes the Mechanistic Competition of Dissociative Versus Associative Binding to Cucurbiturils by Ratiometric Fluorescence Monitoring. *Chem. Commun.* **2019**, *55*, 14123−14126.
(140) Biedermann, F.; Hathazi, D.; Nau, W. M. Associative Chemosensing by Fluorescent Macrocycle−Dye Complexes−a Versatile Enzyme Assay Platform Beyond Indicator Displacement. *Chem. Commun.* **2015**, *51*, 4977−4980.
(141) Hennig, A.; Bakirci, H.; Nau, W. M. Label-Free Continuous Enzyme Assays with Macrocycle-Fluorescent Dye Complexes. *Nat. Methods* **2007**, *4*, 629−632.
(142) Ghale, G.; Lanctôt, A. G.; Kreissl, H. T.; Jacob, M. H.; Weingart, H.; Winterhalter, M.; Nau, W. M. Chemosensing Ensembles for Monitoring Biomembrane Transport in Real Time. *Angew. Chem., Int. Ed.* **2014**, *53*, 2762−2765.
(143) Ghale, G.; Ramalingam, V.; Urbach, A. R.; Nau, W. M. Determining Protease Substrate Selectivity and Inhibition by Label-Free Supramolecular Tandem Enzyme Assays. *J. Am. Chem. Soc.* **2011**, *133*, 7528−7535.
(144) Ghale, G.; Kuhnert, N.; Nau, W. M. Monitoring Stepwise Proteolytic Degradation of Peptides by Supramolecular Domino Tandem Assays and Mass Spectrometry for Trypsin and Leucine Aminopeptidase. *Nat. Prod. Commun.* **2012**, *7*, 343−348.
(145) Li, Z.; Sun, S.; Yang, Z.; Zhang, S.; Zhang, H.; Hu, M.; Cao, J.; Wang, J.; Liu, F.; Song, F.; et al. The Use of a Near-Infrared RNA Fluorescent Probe with a Large Stokes Shift for Imaging Living Cells Assisted by the Macrocyclic Molecule CB7. *Biomaterials* **2013**, *34*, 6473−6481.
(146) Xiao, B.; Wang, Q.; Zhang, S.; Li, X.-Y.; Long, S.-Q.; Xiao, Y.; Xiao, S.; Ni, X.-L. Cucurbit[7]uril-Anchored Polymer Vesicles Enhance Photosensitization in the Nucleus. *J. Mater. Chem. B* **2019**, *7*, 5966−5971.
(147) Bockus, A. T.; Smith, L. C.; Grice, A. G.; Ali, O. A.; Young, C. C.; Mobley, W.; Leek, A.; Roberts, J. L.; Vinciguerra, B.; Isaacs, L.; et al. Cucurbit[7]uril−Tetramethylrhodamine Conjugate for Direct Sensing and Cellular Imaging. *J. Am. Chem. Soc.* **2016**, *138*, 16549−16552.
(148) Gong, B.; Choi, B.-K.; Kim, J.-Y.; Shetty, D.; Ko, Y. H.; Selvapalam, N.; Lee, N. K.; Kim, K. High Affinity Host−Guest FRET Pair for Single-Vesicle Content-Mixing Assay: Observation of Flickering Fusion Events. *J. Am. Chem. Soc.* **2015**, *137*, 8908−8911.

https://doi.org/10.1021/acs.chemrev.1c01050
Chem. Rev. XXXX, XXX, XXX−XXX

(149) Gong, Y.; Chen, H.; Ma, X.; Tian, H. A Cucurbit [7] uril Based Molecular Shuttle Encoded by Visible Room-Temperature Phosphorescence. *ChemPhysChem* **2016**, *17*, 1934−1938.
(150) Xu, L.; Zou, L.; Chen, H.; Ma, X. Room-Temperature Phosphorescence of Cucurbit[7]uril Recognized Naphthalimide Derivative. *Dyes Pigm.* **2017**, *142*, 300−305.
(151) Li, T.; Ma, X. Host-Guest Supramolecular Amphiphile Enhanced Photodecomposition with Responsive Room-Temperature Phosphorescence Signals. *Dyes Pigm.* **2018**, *148*, 306−312.
(152) Zhang, Z.-Y.; Xu, W.-W.; Xu, W.-S.; Niu, J.; Sun, X.-H.; Liu, Y. A Synergistic Enhancement Strategy for Realizing Ultralong and Efficient Room-Temperature Phosphorescence. *Angew. Chem., Int. Ed.* **2020**, *59*, 18748−18754.
(153) Jon, S. Y.; Ko, Y. H.; Park, S. H.; Kim, H.-J.; Kim, K. A Facile, Stereoselective [2 + 2] Photoreaction Mediated by Cucurbit[8]uril. *Chem. Commun.* **2001**, 1938−1939.
(154) Pattabiraman, M.; Natarajan, A.; Kaliappan, R.; Mague, J. T.; Ramamurthy, V. Template Directed Photodimerization of Trans-1,2-bis (n-pyridyl) Ethylenes and Stilbazoles in Water. *Chem. Commun.* **2005**, 4542−4544.
(155) Pattabiraman, M.; Natarajan, A.; Kaanumalle, L. S.; Ramamurthy, V. Templating Photodimerization of trans-Cinnamic Acids with Cucurbit[8]uril and γ-Cyclodextrin. *Org. Lett.* **2005**, *7*, 529−532.
(156) Kang, Y.; Tang, X.; Yu, H.; Cai, Z.; Huang, Z.; Wang, D.; Xu, J.-F.; Zhang, X. Supramolecular Catalyst Functions in Catalytic Amount: Cucurbit[8]uril Accelerates the Photodimerization of Brooker's Merocyanine. *Chem. Sci.* **2017**, *8*, 8357−8361.
(157) Tang, X.; Huang, Z.; Chen, H.; Kang, Y.; Xu, J.-F.; Zhang, X. Supramolecularly Catalyzed Polymerization: From Consecutive Dimerization to Polymerization. *Angew. Chem., Int. Ed.* **2018**, *57*, 8545−8549.
(158) Tabet, A.; Forster, R. A.; Parkins, C. C.; Wu, G.; Scherman, O. A. Modulating Stiffness With Photo-Switchable Supramolecular Hydrogels. *Polym. Chem.* **2019**, *10*, 467−472.
(159) Jeon, W. S.; Kim, H.-J.; Lee, C.; Kim, K. Control of the Stoichiometry in Host−Guest Complexation by Redox Chemistry of Guests: Inclusion of Methylviologen in Cucurbit[8]uril. *Chem. Commun.* **2002**, 1828−1829.
(160) Ziganshina, A. Y.; Ko, Y. H.; Jeon, W. S.; Kim, K. Stable π-Dimer of a Tetrathiafulvalene Cation Radical Encapsulated in the Cavity of Cucurbit[8]uril. *Chem. Commun.* **2004**, 806−807.
(161) Kim, H.-J.; Heo, J.; Jeon, W. S.; Lee, E.; Kim, J.; Sakamoto, S.; Yamaguchi, K.; Kim, K. Selective Inclusion of a Hetero-Guest Pair in a Molecular Host: Formation of Stable Charge-Transfer Complexes in Cucurbit[8]uril. *Angew. Chem., Int. Ed.* **2001**, *40*, 1526−1529.
(162) Ko, Y. H.; Kim, E.; Hwang, I.; Kim, K. Supramolecular Assemblies Built with Host-Stabilized Charge-Transfer Interactions. *Chem. Commun.* **2007**, 1305−1315.
(163) Rauwald, U.; Scherman, O. A. Supramolecular Block Copolymers with Cucurbit[8]uril in Water. *Angew. Chem., Int. Ed.* **2008**, *47*, 3950−3953.
(164) Appel, E. A.; Biedermann, F.; Rauwald, U.; Jones, S. T.; Zayed, J. M.; Scherman, O. A. Supramolecular Cross-Linked Networks via Host−Guest Complexation with Cucurbit[8]uril. *J. Am. Chem. Soc.* **2010**, *132*, 14251−14260.
(165) Liu, Y.; Yu, Y.; Gao, J.; Wang, Z.; Zhang, X. Water-Soluble Supramolecular Polymerization Driven by Multiple Host-Stabilized Charge-Transfer Interactions. *Angew. Chem., Int. Ed.* **2010**, *49*, 6576−6579.
(166) Zou, H.; Liu, J.; Li, Y.; Li, X.; Wang, X. Cucurbit[8]uril-Based Polymers and Polymer Materials. *Small* **2018**, *14*, 1802234.
(167) Pazos, E.; Novo, P.; Peinador, C.; Kaifer, A. E.; García, M. D. Cucurbit[8]uril (CB[8])-Based Supramolecular Switches. *Angew. Chem., Int. Ed.* **2019**, *58*, 403−416.
(168) Li, S.-H.; Xu, X.; Zhou, Y.; Zhao, Q.; Liu, Y. Reversibly Tunable White-Light Emissions of Styrylpyridiniums with Cucurbiturils in Aqueous Solution. *Org. Lett.* **2017**, *19*, 6650−6653.
(169) Yin, H.; Dumur, F.; Niu, Y.; Ayhan, M. M.; Grauby, O.; Liu, W.; Wang, C.; Siri, D.; Rosas, R.; Tonetto, A.; et al. Chameleonic Dye Adapts to Various Environments Shining on Macrocycles or Peptide and Polysaccharide Aggregates. *ACS Appl. Mater. Interfaces* **2017**, *9*, 33220−33228.
(170) Si, Y.; Zhang, Q.; Jin, W.; Yang, S.; Wang, Z.; Qu, D. Aqueous Highly Emissive Host-Guest Systems by Host Enhanced Intramolecular Charge Transfer. *Dyes Pigm.* **2020**, *173*, 107919.
(171) Schoder, S.; Schröder, H. V.; Cera, L.; Puttreddy, R.; Güttler, A.; Resch-Genger, U.; Rissanen, K.; Schalley, C. A. Strong Emission Enhancement in pH-Responsive 2:2 Cucurbit[8]uril Complexes. *Chem.—Eur. J.* **2019**, *25*, 3257−3261.
(172) Wang, R.; Yuan, L.; Ihmels, H.; Macartney, D. H. Cucurbit[8]uril/Cucurbit[7]uril Controlled Off/On Fluorescence of the Acridizinium and 9-Aminoacridizinium Cations in Aqueous Solution. *Chem.—Eur. J.* **2007**, *13*, 6468−6473.
(173) Barooah, N.; Mohanty, J.; Bhasikuttan, A. C. Cucurbit[8]uril-Templated *H* and *J* Dimers of Bichromophoric Coumarin Dyes: Origin of Contrasting Emission. *Chem. Commun.* **2015**, *51*, 13225−13228.
(174) Wang, X.-Q.; Lei, Q.; Zhu, J.-Y.; Wang, W.-J.; Cheng, Q.; Gao, F.; Sun, Y.-X.; Zhang, X.-Z. Cucurbit[8]uril Regulated Activatable Supramolecular Photosensitizer for Targeted Cancer Imaging and Photodynamic Therapy. *ACS Appl. Mater. Interfaces* **2016**, *8*, 22892−22899.
(175) Jiang, T.; Wang, X.; Wang, J.; Hu, G.; Ma, X. Humidity-and Temperature-Tunable Multicolor Luminescence of Cucurbit[8]uril-Based Supramolecular Assembly. *ACS Appl. Mater. Interfaces* **2019**, *11*, 14399−14407.
(176) Tang, B.; Li, W.-L.; Chang, Y.; Yuan, B.; Wu, Y.; Zhang, M.-T.; Xu, J.-F.; Li, J.; Zhang, X. A Supramolecular Radical Dimer: High-Efficiency NIR-II Photothermal Conversion and Therapy. *Angew. Chem., Int. Ed.* **2019**, *58*, 15526−15531.
(177) Tang, B.; Xu, W.; Xu, J.-F.; Zhang, X. Transforming a Fluorochrome to an Efficient Photocatalyst for Oxidative Hydroxylation: A Supramolecular Dimerization Strategy Based on Host-Enhanced Charge Transfer. *Angew. Chem., Int. Ed.* **2021**, *60*, 9384−9388.
(178) Wu, G.; Olesińska, M.; Wu, Y.; Matak-Vinkovic, D.; Scherman, O. A. Mining 2:2 Complexes from 1:1 Stoichiometry: Formation of Cucurbit[8]uril−Diarylviologen Quaternary Complexes Favored by Electron-Donating Substituents. *J. Am. Chem. Soc.* **2017**, *139*, 3202−3208.
(179) Wagner, W.; Wehner, M.; Stepanenko, V.; Würthner, F. Supramolecular Block Copolymers by Seeded Living Polymerization of Perylene Bisimides. *J. Am. Chem. Soc.* **2019**, *141*, 12044−12054.
(180) Liu, X.-T.; Wang, K.; Chang, Z.; Zhang, Y.-H.; Xu, J.; Zhao, Y.; Bu, X.-H. Engineering Donor−Acceptor Heterostructure Metal−Organic Framework Crystals for Photonic Logic Computation. *Angew. Chem., Int. Ed.* **2019**, *58*, 13890−13896.
(181) Ye, X.; Liu, Y.; Lv, Y.; Liu, G.; Zheng, X.; Han, Q.; Jackson, K. A.; Tao, X. In situ Microscopic Observation of the Crystallization Process of Molecular Microparticles by Fluorescence Switching. *Angew. Chem., Int. Ed.* **2015**, *54*, 7976−7980.
(182) Vukotic, V. N.; Zhu, K.; Baggi, G.; Loeb, S. J. Optical Distinction between "Slow" and "Fast" Translational Motion in Degenerate Molecular Shuttles. *Angew. Chem., Int. Ed.* **2017**, *56*, 6136−6141.
(183) Guan, W.; Zhou, W.; Lu, C.; Tang, B. Z. Synthesis and Design of Aggregation-Induced Emission Surfactants: Direct Observation of Micelle Transitions and Microemulsion Droplets. *Angew. Chem., Int. Ed.* **2015**, *54*, 15160−15164.
(184) Fu, M.; Wang, A.; Zhang, X.; Dai, L.; Li, J. Direct Observation of the Distribution of Gelatin in Calcium Carbonate Crystals by Super-Resolution Fluorescence Microscopy. *Angew. Chem., Int. Ed.* **2016**, *55*, 908−911.
(185) Huang, C. B.; Xu, L.; Zhu, J. L.; Wang, Y. X.; Sun, B.; Li, X.; Yang, H. B. Real-time Monitoring the Dynamics of Coordination-

https://doi.org/10.1021/acs.chemrev.1c01050
Chem. Rev. XXXX, XXX, XXX−XXX

driven Self-assembly by Fluorescence-Resonance Energy Transfer. *J. Am. Chem. Soc.* **2017**, *139*, 9459−9462.
(186) Huang, Z.; Jiang, T.; Wang, J.; Ma, X.; Tian, H. Real-time Visual Monitoring of Kinetically Controlled Self-Assembly. *Angew. Chem., Int. Ed.* **2021**, *60*, 2855−2860.
(187) Wu, G.; Szabó, I.; Rosta, E.; Scherman, O. A. Cucurbit[8]uril-Mediated Pseudo[2,3]rotaxanes. *Chem. Commun.* **2019**, *55*, 13227−13230.
(188) Olesińska, M.; Wu, G.; Gómez-Coca, S.; Antón-García, D.; Szabó, I.; Rosta, E.; Scherman, O. A. Modular Supramolecular Dimerization of Optically Tunable Extended Aryl Viologens. *Chem. Sci.* **2019**, *10*, 8806−8811.
(189) Wu, G.; Bae, Y. J.; Olesińska, M.; Antón-García, D.; Szabó, I.; Rosta, E.; Wasielewski, M. R.; Scherman, O. A. Controlling the Structure and Photophysics of Fluorophore Dimers Using Multiple Cucurbit[8]uril Clampings. *Chem. Sci.* **2020**, *11*, 812−825.
(190) Wu, G.; Huang, Z.; Scherman, O. A. Quantitative Supramolecular Heterodimerization for Efficient Energy Transfer. *Angew. Chem., Int. Ed.* **2020**, *59*, 15963−15967.
(191) Zhang, X.; Sun, T.; Ni, X.-L. Fluorescence Visualization of Cucurbit[8]uril-Triggered Dynamic Host−Guest Assemblies. *Org. Chem. Front.* **2021**, *8*, 32−38.
(192) Wang, H.; Ji, X.; Li, Z.; Huang, F. Fluorescent Supramolecular Polymeric Materials. *Adv. Mater.* **2017**, *29*, 1606117.
(193) Li, D.; Wang, J.; Ma, X. White-Light-Emitting Materials Constructed from Supramolecular Approaches. *Adv. Optical Mater.* **2018**, *6*, 1800273.
(194) Lou, X.-Y.; Yang, Y.-W. Aggregation-Induced Emission Systems Involving Supramolecular Assembly. *Aggregate* **2020**, *1*, 19−30.
(195) Huang, Z.; Ma, X. Tailoring Tunable Luminescence via Supramolecular Assembly Strategies. *Cell Rep. Phys. Sci.* **2020**, *1*, 100167.
(196) Wang, X.-H.; Song, N.; Hou, W.; Wang, C.-Y.; Wang, Y.; Tang, J.; Yang, Y.-W. Efficient Aggregation-Induced Emission Manipulated by Polymer Host Materials. *Adv. Mater.* **2019**, *31*, 1903962.
(197) Chen, C.; Ni, X.; Tian, H.-W.; Liu, Q.; Guo, D.-S.; Ding, D. Calixarene-Based Supramolecular AIE Dots with Highly Inhibited Nonradiative Decay and Intersystem Crossing for Ultrasensitive Fluorescence Image-Guided Cancer Surgery. *Angew. Chem., Int. Ed.* **2020**, *59*, 10008−10012.
(198) Li, B.; He, T.; Shen, X.; Tang, D.; Yin, S. Fluorescent Supramolecular Polymers with Aggregation Induced Emission Properties. *Polym. Chem.* **2019**, *10*, 796−818.
(199) Kim, H.-J.; Nandajan, P. C.; Gierschner, J.; Park, S. Y. Light-Harvesting Fluorescent Supramolecular Block Copolymers Based on Cyanostilbene Derivatives and Cucurbit[8]urils in Aqueous Solution. *Adv. Funct. Mater.* **2018**, *28*, 1705141.
(200) Chen, X.-M.; Chen, Y.; Yu, Q.-L.; Gu, B.-H.; Liu, Y. Supramolecular Assemblies with Near-Infrared Emission Mediated in Two Stages by Cucurbituril and Amphiphilic Calixarene for Lysosome-Targeted Cell Imaging. *Angew. Chem., Int. Ed.* **2018**, *57*, 12519−12523.
(201) Wu, H.; Chen, Y.; Dai, X.; Li, P.; Stoddart, J. F.; Liu, Y. In situ Photoconversion of Multicolor Luminescence and Pure White light Emission Based on Carbon Dot-Supported Supramolecular Assembly. *J. Am. Chem. Soc.* **2019**, *141*, 6583−6591.
(202) Shen, F.-F.; Chen, Y.; Xu, X.; Yu, H.-J.; Wang, H.; Liu, Y. Supramolecular Assembly with Near-Infrared Emission for Two-Photon Mitochondrial Targeted Imaging. *Small* **2021**, *17*, 2101185.
(203) Tian, J.; Wang, H.; Zhang, D.-W.; Liu, Y.; Li, Z.-T. Supramolecular Organic Frameworks (SOFs): Homogeneous Regular 2D and 3D Pores in Water. *Natl. Sci. Rev.* **2017**, *4*, 426−436.
(204) Yang, W.; Greenaway, A.; Lin, X.; Matsuda, R.; Blake, A. J.; Wilson, C.; Lewis, W.; Hubberstey, P.; Kitagawa, S.; Champness, N. R.; et al. The Construction of a Two-Dimensional Supramolecular Organic Framework with Parallelogram Pores and Stepwise Fluorescence Enhancement. *J. Am. Chem. Soc.* **2010**, *132*, 14457−14469.
(205) Xu, S.-Q.; Zhang, X.; Nie, C.-B.; Pang, Z.-F.; Xu, X.-N.; Zhao, X. The Construction of a Two-dimensional Supramolecular Organic Framework with Parallelogram Pores and Stepwise Fluorescence Enhancement. *Chem. Commun.* **2015**, *51*, 16417−16420.
(206) Li, Y.; Dong, Y.; Miao, X.; Ren, Y.; Zhang, B.; Wang, P.; Yu, Y.; Li, B.; Isaacs, L.; Cao, L. Shape-Controllable and Fluorescent Supramolecular Organic Frameworks Through Aqueous Host-Guest Complexation. *Angew. Chem., Int. Ed.* **2018**, *57*, 729−733.
(207) Li, Y.; Li, Q.; Miao, X.; Qin, C.; Chu, D.; Cao, L. Adaptive Chirality of an Achiral Cucurbit[8]uril-Based Supramolecular Organic Framework for Chirality Induction in Water. *Angew. Chem., Int. Ed.* **2021**, *60*, 6744−6751.
(208) Bai, H.; Liu, Z.; Zhang, T.; Du, J.; Zhou, C.; He, W.; Chau, J. H. C.; Kwok, R. T. K.; Lam, J. W. Y.; Tang, B. Z. Multifunctional Supramolecular Assemblies with Aggregation-Induced Emission (AIE) for Cell Line Identification, Cell Contamination Evaluation, and Cancer Cell Discrimination. *ACS Nano* **2020**, *14*, 7552−7563.
(209) Liu, H.; Pan, Q.; Wu, C.; Sun, J.; Zhuang, T.; Liang, T.; Mu, X.; Zhou, X.; Li, Z.; Zhao, Y. Construction of Two-dimensional Supramolecular Nanostructure with Aggregation-Induced Emission Effect via Host−Guest Interactions. *Mater. Chem. Front.* **2019**, *3*, 1532−1537.
(210) Zhang, Y.; Zhan, T.-G.; Zhou, T.-Y.; Qi, Q.-Y.; Xu, X.-N.; Zhao, X. Fluorescence Enhancement Through the Formation of a Single-Layer Two-dimensional Supramolecular Organic Framework and Its Application in Highly Selective Recognition of Picric Acid. *Chem. Commun.* **2016**, *52*, 7588−7591.
(211) Li, Y.; Qin, C.; Li, Q.; Wang, P.; Miao, X.; Jin, H.; Ao, W.; Cao, L. Supramolecular Organic Frameworks with Controllable Shape and Aggregation-Induced Emission for Tunable Luminescent Materials Through Aqueous Host-Guest Complexation. *Adv. Opt. Mater.* **2020**, *8*, 1902154.
(212) Ma, X.-K.; Zhang, Y.-M.; Yu, Q.; Zhang, H.; Zhang, Z.; Liu, Y. A twin-Axial Pseudorotaxane for Phosphorescence Cell Imaging. *Chem. Commun.* **2021**, *57*, 1214−1217.
(213) Shen, F.-F.; Chen, Y.; Dai, X.-Y.; Zhang, H.-Y.; Zhang, B.; Liu, Y.-H.; Liu, Y. Purely Organic Light-Harvesting Phosphorescence Energy Transfer by β-Cyclodextrin Pseudorotaxane for Mitochondria Targeted Imaging. *Chem. Sci.* **2021**, *12*, 1851−1857.
(214) Ma, X.-K.; Zhang, W.; Liu, Z.; Zhang, H.; Zhang, B.; Liu, Y. Supramolecular Pins with Ultralong Efficient Phosphorescence. *Adv. Mater.* **2021**, *33*, 2007476.
(215) Liu, F.; Chowdhury, S.; Rosas, R.; Monnier, V.; Charles, L.; Karoui, H.; Gigmes, D.; Ouari, O.; Chevallier, F.; Bucher, C.; et al. Triple Stack of a Viologen Derivative in a CB[10] Pair. *Org. Lett.* **2021**, *23*, 5283−5287.
(216) Liu, S.; Shukla, A. D.; Gadde, S.; Wagner, B. D.; Kaifer, A. E.; Isaacs, L. Ternary Complexes Comprising Cucurbit[10]uril, Porphyrins, and Guests. *Angew. Chem., Int. Ed.* **2008**, *47*, 2657−2660.
(217) Hu, X.; Liu, F.; Zhang, X.; Zhao, Z.; Liu, S. Expected and Unexpected Photoreactions of 9-(10-)Substituted Anthracene Derivatives in Cucurbit[*n*]uril hosts. *Chem. Sci.* **2020**, *11*, 4779−4785.
(218) Liu, C.; Wu, Y.; Han, X.; Liu, S. Emission Enhancement of Cationic Tetraphenylethylene Derivatives by Encapsulation in a Cucurbit[10]uril Host in Water. *New J. Chem.* **2020**, *44*, 3185−3188.
(219) Wang, H.; Yang, Y.; Yuan, B.; Ni, X.-L.; Xu, J.-F.; Zhang, X. Cucurbit[10]uril-Encapsulated Cationic Porphyrins with Enhanced Fluorescence Emission and Photostability for Cell Imaging. *ACS Appl. Mater. Interfaces* **2021**, *13*, 2269−2276.
(220) Xu, W.-T.; Luo, Y.; Zhao, W.-W.; Liu, M.; Luo, G.-Y.; Fan, Y.; Lin, R.-L.; Tao, Z.; Xiao, X.; Liu, J.-X. Detecting Pesticide Dodine by Displacement of Fluorescent Acridine from Cucurbit[10]uril Macrocycle. *J. Agric. Food Chem.* **2021**, *69*, 584−591.
(221) Liu, M.; Yang, M.; Yao, Y.; Zhang, Y.; Zhang, Y.; Tao, Z.; Zhu, Q.; Wei, G.; Bian, B.; Xiao, X. Specific Recognition of Formaldehyde by a Cucurbit[10]uril-Based Porous Supramolecular Assembly

https://doi.org/10.1021/acs.chemrev.1c01050
Chem. Rev. XXXX, XXX, XXX−XXX

Incorporating Adsorbed 1, 8-Diaminonaphthalene. *J. Mater. Chem. C* **2019**, *7*, 1597−1603.
(222) Zhang, W.; Luo, Y.; Zhou, Y.; Liu, M.; Xu, W.; Bian, B.; Tao, Z.; Xiao, X. A Highly Selective Fluorescent Chemosensor Probe for Detection of Fe^{3+} and Ag^{+} Based on Supramolecular Assembly of Cucurbit[10]uril with a Pyrene Derivative. *Dyes and Pigm.* **2020**, *176*, 108235.
(223) Luo, Y.; Zhang, W.; Liu, M.; Zhao, J.; Fan, Y.; Bian, B.; Tao, Z.; Xiao, X. A Supramolecular Fluorescent Probe Based on Cucurbit[10]uril for Sensing the Pesticide Dodine. *Chin. Chem. Lett.* **2021**, *32*, 367−370.
(224) Fan, G.; Yu, X.; Han, X.; Zhao, Z.; Liu, S. Tunable White-Light Emissions of Azapyrene Derivatives with Cucurbit[*n*]uril Hosts in Aqueous Solution. *Org. Lett.* **2021**, *23*, 6633−6637.
(225) Alrawashdeh, L. R.; Day, A. I.; Wallace, L. Strong Enhancement of Luminescence from an Iridium Polypyridyl Complex via Encapsulation in Cucurbituril. *Dalton Trans.* **2013**, *42*, 16478−16481.
(226) Alrawashdeh, L. R.; Cronin, M. P.; Woodward, C. E.; Day, A. I.; Wallace, L. Iridium Cyclometalated Complexes in Host−Guest Chemistry: A Strategy for Maximizing Quantum Yield in Aqueous Media. *Inorg. Chem.* **2016**, *55*, 6759−6769.
(227) Yu, Y.; Li, Y.; Wang, X.; Nian, H.; Wang, L.; Li, J.; Zhao, Y.; Yang, X.; Liu, S.; Cao, L. Cucurbit[10]uril-Based [2]Rotaxane: Preparation and Supramolecular Assembly-Induced Fluorescence Enhancement. *J. Org. Chem.* **2017**, *82*, 5590−5596.
(228) Yao, Y.-Q.; Zhang, Y.-J.; Zhang, Y.-Q.; Tao, Z.; Ni, X.-L.; Wei, G. Multiple Efficient Fluorescence Emission from Cucurbit[10]uril-$[Cd_4Cl_{16}]^{8-}$-Based Pillared Diamond Porous Supramolecular Frameworks. *ACS Appl. Mater. Interfaces* **2017**, *9*, 40760−40765.
(229) Liu, M.; Chen, L.; Shan, P.; lian, C.; Zhang, Z.; Zhang, Y.; Tao, Z.; Xiao, X. Pyridine Detection Using Supramolecular Organic Frameworks Incorporating Cucurbit[10]uril. *ACS Appl. Mater. Interfaces* **2021**, *13*, 7434−7442.
(230) Lee, T.-C.; Scherman, O. A. Formation of Dynamic Aggregates in Water by Cucurbit[5]uril Capped with Gold Nanoparticles. *Chem. Commun.* **2010**, *46*, 2438−2440.
(231) Appel, E. A.; del Barrio, J.; Dyson, J.; Isaacs, L.; Scherman, O. A. Metastable Single-Chain Polymer Nanoparticles Prepared by Dynamic Cross-Linking with Nor-seco-Cucurbit[10]uril. *Chem. Sci.* **2012**, *3*, 2278−2281.
(232) Hüsken, N.; Taylor, R. W.; Zigah, D.; Taveau, J.-C.; Lambert, O.; Scherman, O. A.; Baumberg, J. J.; Kuhn, A. Electrokinetic Assembly of one-Dimensional Nanoparticle Chains with Cucurbit[7]-uril Controlled Subnanometer Junctions. *Nano Lett.* **2013**, *13*, 6016−6022.
(233) Taylor, R. W.; Lee, T.-C.; Scherman, O. A.; Esteban, R.; Aizpurua, J.; Huang, F. M.; Baumberg, J. J.; Mahajan, S. Precise Subnanometer Plasmonic Junctions for SERS within Gold Nanoparticle Assemblies Using Cucurbit[*n*]uril "Glue. *ACS Nano* **2011**, *5*, 3878−3887.
(234) Coulston, R. J.; Jones, S. T.; Lee, T.-C.; Appel, E. A.; Scherman, O. A. Supramolecular Gold Nanoparticle−Polymer Composites formed in Water with Cucurbit[8]uril. *Chem. Commun.* **2011**, *47*, 164−166.
(235) Cao, M.; Lin, J.; Yang, H.; Cao, R. Facile Synthesis of Palladium Nanoparticles with High Chemical Activity Using Cucurbit[6]uril as Protecting Agent. *Chem. Commun.* **2010**, *46*, 5088−5090.
(236) Tao, C.; An, Q.; Zhu, W.; Yang, H.; Li, W.; Lin, C.; Xu, D.; Li, G. Cucurbit[*n*]urils as a SERS Hot-Spot Nanocontainer Through Bridging Gold Nanoparticles. *Chem. Commun.* **2011**, *47*, 9867−9869.
(237) Lu, X.; Masson, E. Formation and Stabilization of Silver Nanoparticles with Cucurbit[*n*]urils (n = 5−8) and Cucurbituril-Based Pseudorotaxanes in Aqueous Medium. *Langmuir* **2011**, *27*, 3051−3058.
(238) Lee, T.-C.; Scherman, O. A. A Facile Synthesis of Dynamic Supramolecular Aggregates of Cucurbit[*n*]uril (n = 5−8) Capped with Gold Nanoparticles in Aqueous Media. *Chem.—Eur. J.* **2012**, *18*, 1628−1633.
(239) Zhang, L.; Liu, S.; Wang, Y.; Zhang, H.; Liang, F. Controllable Synthesis and Catalytic Performance of Gold Nanoparticles with Cucurbit[*n*]urils (n= 5−8). *Nanomaterials* **2018**, *8*, 1015.
(240) Li, Q.-L.; Sun, Y.; Sun, Y.-L.; Wen, J.; Zhou, Y.; Bing, Q.-M.; Isaacs, L. D.; Jin, Y.; Gao, H.; Yang, Y.-W. Mesoporous Silica Nanoparticles Coated by Layer-by-Layer Self-Assembly Using Cucurbit[7]uril for in Vitro and in Vivo Anticancer Drug Release. *Chem. Mater.* **2014**, *26*, 6418−6431.
(241) Yue, L.; Sun, C.; Kwong, C. H. T.; Wang, R. Cucurbit[7]uril-Functionalized Magnetic Nanoparticles for Imaging-Guided Cancer Therapy. *J. Mater. Chem. B* **2020**, *8*, 2749−2753.
(242) Ma, N.; Wang, W.-J.; Chen, S.; Wang, X.-S.; Wang, X.-Q.; Wang, S.-B.; Zhu, J.-Y.; Cheng, S.-X.; Zhang, X.-Z. Cucurbit[8]uril-Mediated Supramolecular Photoswitching for Self-preservation of Mesoporous Silica Nanoparticle Delivery System. *Chem. Commun.* **2015**, *51*, 12970−12973.
(243) Qiu, X.-L.; Zhou, Y.; Jin, X.-Y.; Qi, A.-D.; Yang, Y.-W. One-pot Solvothermal Synthesis of Biocompatible Magnetic Nanoparticles Mediated by Cucurbit[*n*]urils. *J. Mater. Chem. C* **2015**, *3*, 3517−3521.
(244) Zhang, Q.; Qu, D.-H.; Wang, Q.-C.; Tian, H. Dual-Mode Controlled Self-Assembly of TiO_2 Nanoparticles Through a Cucurbit[8]uril-Enhanced Radical Cation Dimerization Interaction. *Angew. Chem., Int. Ed.* **2015**, *54*, 15789−15793.
(245) Cao, M.; Wu, D.; Gao, S.; Cao, R. Platinum Nanoparticles Stabilized by Cucurbit[6]uril with Enhanced Catalytic Activity and Excellent Poisoning Tolerance for Methanol Electrooxidation. *Chem.—Eur. J.* **2012**, *18*, 12978−12985.
(246) Yue, L.; Yang, K.; Lou, X.-Y.; Yang, Y.-W.; Wang, R. Versatile Roles of Macrocycles in Organic-Inorganic Hybrid Materials for Biomedical Applications. *Matter* **2020**, *3*, 1557−1588.
(247) Özkan, M.; Hadi, S. E.; Tunç, İ.; Midilli, Y.; Ortaç, B.; Tuncel, D. Cucurbit[7]uril-Capped Hybrid Conjugated Oligomer-gold Nanoparticles for Combined Photodynamic-Photothermal Therapy and Cellular imaging. *ACS Appl. Polym. Mater.* **2020**, *2*, 3840−3849.
(248) Jiang, T.; Qu, G.; Wang, J.; Ma, X.; Tian, H. Cucurbiturils Brighten Au Nanoclusters in Water. *Chem. Sci.* **2020**, *11*, 3531−3537.
(249) Cao, S.; Wang, P.; Zeng, X.; Tao, Z.; Ni, X.-L. Cucurbituril-Assisted Formation of Tunable Carbon Dots from Single Organic Precursors in Water. *Org. Chem. Front.* **2021**, *8*, 224−230.
(250) Krämer, J.; Kang, R.; Grimm, L. M.; Cola, L. D.; Picchetti, P.; Biedermann, F. Molecular Probes, Chemosensors, and Nanosensors for Optical Detection of Biorelevant Molecules and Ions in Aqueous Media and Biofluids. *Chem. Rev.* **2022**, *122*, 3459−3636.
(251) Yu, G.; Jie, K.; Huang, F. Supramolecular Amphiphiles Based on Host−Guest Molecular Recognition Motifs. *Chem. Rev.* **2015**, *115*, 7240−7303.
(252) Dong, S.; Zheng, B.; Wang, F.; Huang, F. Supramolecular Polymers Constructed from Macrocycle-Based Host−Guest Molecular Recognition Motifs. *Acc. Chem. Res.* **2014**, *47*, 1982−1994.
(253) Xue, M.; Yang, Y.; Chi, X.; Yan, X.; Huang, F. Development of Pseudorotaxanes and Rotaxanes: From Synthesis to Stimuli-Responsive Motions to Applications. *Chem. Rev.* **2015**, *115*, 7398−7501.
(254) Shen, H.; Liu, C.; Zheng, J.; Tao, Z.; Nie, H.; Ni, X.-L. Cucurbit[8]uril-Assisted Nucleophilic Reaction: A Unique Supramolecular Approach for Cyanide Detection and Removal from Aqueous Solution. *ACS Appl. Mater. Interfaces* **2021**, *13*, 55463−55469.
(255) Wang, H.; Xue, K.-F.; Yang, Y.; Hu, H.; Xu, J.-F.; Zhang, X. In Situ Hypoxia-Induced Supramolecular Perylene Diimide Radical Anions in Tumors for Photothermal Therapy with Improved Specificity. *J. Am. Chem. Soc.* **2022**, *144*, 2360−2367.
(256) Yu, J.; Wang, H.; Dai, X.; Chen, Y.; Liu, Y. Multivalent Supramolecular Assembly Based on a Triphenylamine Derivative for Near-Infrared Lysosome Targeted Imaging. *ACS Appl. Mater. Interfaces* **2022**, *14*, 4417−4422.

https://doi.org/10.1021/acs.chemrev.1c01050
Chem. Rev. XXXX, XXX, XXX−XXX

(257) Han, X.; Sun, D.; Tang, S.; Wu, Y.; Wang, L.; Zhang, X.; Liu, S. Host−guest Interaction-Directed Strategy for Managing Mechanochromic Luminescence Behavior by Modulating Molecular Packing and Conformation. *J. Mater. Chem. C* **2021**, *9*, 17307−17312.
(258) Ma, X.; Cao, J.; Wang, Q.; Tian, H. Photocontrolled Reversible Room Temperature Phosphorescence (RTP) Encoding β-cyclodextrin Pseudorotaxane. *Chem. Commun.* **2011**, *47*, 3559−3561.
(259) Xu, C.; Lin, X.; Wu, W.; Ma, X. Room-Temperature Phosphorescence of a Water-Soluble Supramolecular Organic Framework. *Chem. Commun.* **2021**, *57*, 10178−10181.
(260) Ding, B.; Ma, X. A Simple, Easy Preparation and Tunable Strategy for Preparing Organic Room-Temperature Phosphorescence. *Langmuir* **2021**, *37*, 14229−14236.
(261) Chen, Q.; Lei, Y.; Wu, G.; Li, Q.; Pan, Y.; Li, H. Ultramacrocyclization in Water via External Templation. *Chem. Sci.* **2022**, *13*, 798−803.
(262) Rabbani, R.; Saeedi, S.; Nazimuddin, M.; Barbero, H.; Kyritsakas, N.; White, T. A.; Masson, E. Enhanced Photoreduction of Water Catalyzed by a Cucurbit[8]uril-Secured Platinum Dimer. *Chem. Sci.* **2021**, *12*, 15347−15352.
(263) Biedermann, F.; Scherman, O. A. Cucurbit[8]uril Mediated Donor−Acceptor Ternary Complexes: a Model System for Studying Charge-Transfer Interactions. *J. Phys. Chem. B* **2012**, *116*, 2842−2849.
(264) Yu, H.-J.; Zhou, Q.; Dai, X.; Shen, F.-F.; Zhang, Y.-M.; Xu, X.; Liu, Y. Photooxidation-Driven Purely Organic Room-Temperature Phosphorescent Lysosome-Targeted Imaging. *J. Am. Chem. Soc.* **2021**, *143*, 13887−13894.
(265) Xu, C.; Yin, C.; Wu, W.; Ma, X. Tunable Room-Temperature Phosphorescence and Circularly Polarized Luminescence Encoding Helical Supramolecular Polymer. *Sci. China Chem.* **2022**, *65*, 75−81.
(266) Baryshnikov, G.; Minaev, B.; Ågren, H. Theory and Calculation of the Phosphorescence Phenomenon. *Chem. Rev.* **2017**, *117*, 6500−6537.
(267) Zhang, K. Y.; Yu, Q.; Wei, H.; Liu, S.; Zhao, Q.; Huang, W. Long-Lived Emissive Probes for Time-Resolved Photoluminescence Bioimaging and Biosensing. *Chem. Rev.* **2018**, *118*, 1770−1839.
(268) Zhang, M.; Yue, J.; Cui, R.; Ma, Z.; Wan, H.; Wang, F.; Zhu, S.; Zhou, Y.; Kuang, Y.; Zhong, Y.; et al. Bright Quantum Dots Emitting at ∼ 1,600 nm in the NIR-IIb Window for Deep Tissue Fluorescence Imaging. *Proc. Natl. Acad. Sci. U.S.A.* **2018**, *115*, 6590−6595.
(269) Chinnathambi, S.; Shirahata, N. Recent Advances on Fluorescent Biomarkers of Near-Infrared Duantum Dots for in Vitro and in Vivo imaging. *Sci. Technol. Adv. Mater.* **2019**, *20*, 337−355.
(270) Feng, Z.; Bai, S. Y.; Qi, J.; Sun, C. W.; Zhang, Y. H.; Yu, X. M.; Ni, H. W.; Wu, D.; Fan, X. X.; Xue, D. W.; et al. Biologically Excretable AIE dots for Visualizing Through the Marmosets Intravitally: Horizons in Future Clinical Nanomedicine. *Adv. Mater.* **2021**, *33*, 2008123.
(271) Li, Y. Y.; Liu, S. J.; Ni, H. W.; Zhang, H. K.; Zhang, H. Q.; Chuah, C.; Ma, C.; Wong, K. S.; Lam, J. W. Y.; Kwok, R. T. K.; et al. ACQ-to-AIE Transformation: Tuning Molecular Packing by Regioisomerization for Two-photon NIR Bioimaging. *Angew. Chem., Int. Ed.* **2020**, *59*, 12822−12826.
(272) Xu, W.-W.; Chen, Y.; Lu, Y.-L.; Qin, Y.-X.; Zhang, H.; Xu, X.; Liu, Y. Tunable Second-Level Room-Temperature Phosphorescence of Solid Supramolecules Between Acrylamide-Phenylpyridium Copolymers and Cucurbit[7]uril. *Angew. Chem., Int. Ed.* **2022**, *61*, No. e202115265.
(273) Zhang, Y.; Su, Y.; Wu, H.; Wang, Z.; Wang, C.; Zheng, Y.; Zheng, X.; Gao, L.; Zhou, Q.; Yang, Y.; et al. Large-Area, Flexible, Transparent, and Long-Lived Polymer-Based Phosphorescence Films. *J. Am. Chem. Soc.* **2021**, *143*, 13675−13685.
(274) Berezin, M. Y.; Achilefu, S. Fluorescence Lifetime Measurements and Biological Imaging. *Chem. Rev.* **2010**, *110*, 2641−2684.
(275) Zhang, D.-W.; Li, M.; Chen, C.-F. Recent Advances in Circularly Polarized Electroluminescence Based on Organic Light-Emitting Diodes. *Chem. Soc. Rev.* **2020**, *49*, 1331−1343.
(276) Gan, S.; Zhou, J.; Smith, T. A.; Su, H.; Luo, W.; Hong, Y.; Zhao, Z.; Tang, B. Z. New AIEgens with Delayed Fluorescence for Fluorescence Imaging and Fluorescence Lifetime Imaging of Living Cells. *Mater. Chem. Front.* **2017**, *1*, 2554−2558.
(277) Yang, X.; Zhao, Z.; Zhang, X.; Liu, S. Probing Guest Compounds Enabling the Facile Isolation of Cucurbit[10]uril. *Sci. China Chem.* **2018**, *61*, 787−791.
(278) Liu, Q.; Li, Q.; Cheng, X.-J.; Xi, Y.-Y.; Xiao, B.; Xiao, X.; Tang, Q.; Huang, Y.; Tao, Z.; Xue, S.-F.; et al. A Novel Shell-Like Supramolecular Assembly of 4,4′-Bipyridyl Derivatives and a Twisted Cucurbit[14]uril Molecule. *Chem. Commun.* **2015**, *51*, 9999−10001.
(279) Li, Q.; Qiu, S.-C.; Chen, K.; Zhang, Y.; Wang, R.; Huang, Y.; Tao, Z.; Zhu, Q.-J.; Liu, J.-X. Encapsulation of Alkyldiammonium ions within Two Different Cavities of Twisted Cucurbit[14]uril. *Chem. Commun.* **2016**, *52*, 2589−2592.
(280) Zhang, J.; Xi, Y.-Y.; Li, Q.; Tang, Q.; Wang, R.; Huang, Y.; Tao, Z.; Xue, S.-F.; Lindoy, L. F.; Wei, G. Supramolecular Recognition of Amino Acids by Twisted Cucurbit[14]uril. *Chem.—Asian J.* **2016**, *11*, 2250−2254.
(281) Gao, Z.; Zhang, J.; Sun, N.; Huang, Y.; Tao, Z.; Xiao, X.; Jiang, J. Hyperbranched Supramolecular Polymer Constructed from Twisted Cucurbit[14]uril and Porphyrin via Host−Guest Interactions. *Org. Chem. Front.* **2016**, *3*, 1144−1148.
(282) Li, Q.; Sun, J.; Zhou, J.; Hua, B.; Shao, L.; Huang, F. Barium Cation-Responsive Supra-Amphiphile Constructed by a New Twisted Cucurbit[15]uril/Paraquat Recognition Motif in Water. *Org. Chem. Front.* **2018**, *5*, 1940−1944.
(283) Li, Q.; Zhou, J.; Sun, J.; Yang, J. Host−Guest Interactions of a Twisted Cucurbit[15]uril with Paraquat Derivatives and Bispyridinium Salts. *Tetrahedron Lett.* **2019**, *60*, 151022.
(284) Zhang, J.; Tang, Q.; Gao, Z.-Z.; Huang, Y.; Xiao, X.; Tao, Z. Stimuli-Responsive Supramolecular Assemblies between Twisted Cucurbit[14]uril and Hemicyanine Dyes and Their Analysis Application. *J. Phys. Chem. B* **2017**, *121*, 11119−11123.
(285) Wang, C.-H.; Tang, Q.; Zhang, J.; Yao, Y.-Q.; Xiao, X.; Huang, Y.; Tao, Z. Alkaline Earth Cation-Mediated Photoluminescent Complexes of Thioflavin T with Twisted Cucurbit[14]uril. *New J. Chem.* **2018**, *42*, 9244−9251.
(286) Fan, Y.; Gao, R.-H.; Huang, Y.; Bian, B.; Tao, Z.; Xiao, X. Supramolecular Fluorescence Probe Based on Twisted Cucurbit[14]uril for Sensing Fungicide Flusilazole. *Front. Chem.* **2019**, *7*, 154.

https://doi.org/10.1021/acs.chemrev.1c01050
Chem. Rev. XXXX, XXX, XXX−XXX